Estimation of rainfall using METEOSAT TIR data for the Naivasha catchment

Mesfin Alemu Tessema

February, 2001

Estimation of rainfall using METEOSAT TIR data for the Naivasha catchment

By

Mesfin Alemu Tessema

Thesis submitted to the International Institute for Aerospace Survey and Earth Sciences in partial fulfilment of the requirements for the degree of Master of Science in Water Resource and Environmental Management.

Degree Assessment Board

Prof. Dr. A.M.J. Meijerink (chairman of the examination board, and supervisor)

Dr. D.I.F. Grimes (Examiner)

Dr.A.S.M.Geiske (Supervisor)

INTERNATIONAL INSTITUTE FOR AEROSPACE SURVEY AND EARTH SCIENCES

ENSCHEDE, THE NETHERLANDS

ACKNOWLEDGEMENT

First and foremost praise be to the living, almighty and ever-loving God for all what He has done, He is doing and will continue to do in my life. Not forgetting his presence, protections and solutions whenever I call to him in my distress.

I wish to express my unbounded sincere thanks to the Netherlands Government for awarding me a scholarship to come to ITC to study, and the Ethiopian Government (through commission for sustainable agriculture and environmental rehabilitation) for granting me to make use of this opportunity.

I would like to express my profound heart-felt gratitude and appreciation to my supervisor Prof.Dr.A.M.J. Meijerink, for his invaluable guidance, advice, reviews and comments during the writing of this thesis as well as for his kindness, patient, wonderful assistance and encouragement. I will ever remain grateful to him.

I would like to express my sincere gratitude to my supervisor Dr.A.S.M.Geiske for his precious assistance in the writing of the thesis.

Many thanks go to all my lecturers for their willingness to patiently reveal their knowledge, and their friendly attitudes they displayed. Endless thanks to my Director of studies, Ir.A.M Van Lieshout for his Friendliness and support throughout my stay in ITC.

I would like to extend my thanks to Drs.R.Becht and Drs. D. Kovacs who were willing to help whenever I need advise.

I would also wish to express my deep appreciation to Dr.R.Bonifacio for his priceless assistance in the writing of the thesis. I am also grateful to Dr.D.I.F.Grimes for his kindness, good hospitality besides his precious advice through out my stay in the University of Reading UK.

My acknowledgement should also go to the Dean office of ITC, Mrs. Allessie for her cordiality and efforts in making a comfortable journey to UK

My biggest thanks go to my be loved families for their caring, warm affection and curiosity to see my success all the time. All my friends in Ethiopia deserve the top hand appreciation for their concern and keeping in touch through out the entire time I am away.

I wish to thank all my classmates for the co-operation, togetherness and friendly sprit kept among us.

I would like to take this opportunity to express my sincere thanks to my best friends, Wondmu Tekle, Sene Solomon and Teferra Seleshi for their precious friendship and kind help. In fact, they have shown me that friendship is not just another word.

ABSTRACT

Areal rainfall computed by kriging from point data measured with the available rain gauge network over the Naivasha catchment were used to calibrate a satellite rainfall algorithm using TIR METEOSAT data, through TAMSAT method approach.

The TAMSAT technique uses infrared images and depends on the assumption that convective clouds are the main source of rain.

Cold Cloud Duration at different thresholds and gauge data from 1994 to 1998 were compared in this study, it was shown that CCD 30 is an optimum threshold which shows the highest level of agreement with the gauge data in this region.

The correlation between precipitation ground measurement and convective clouds derived from METEOSAT TIR data were computed for daily and decadal scales, the relation between precipitation and cold cloud field notably improved in decadal scale.

Some of the statistical techniques have been utilized for the determination of the best relationship between rainfall and satellite data.

The response of the runoff at the outlet of Malewa catchment to the event CCD and the kriged rainfall has been discussed briefly for two short periods during 1997 and 1998.

TABLE OF CONTENT

LIST OF FIGURES, TABLES AND ABBREVIATIONS

List of Figures

List of Tables

List abbreviations

ADMIT	Agricultural Drought Monitoring Interactive Technique
BIAS	Bristol Inter Active Scheme
CCD 30	Cold Cloud Duration at a temperature of -30°C
EUMETSAT	European METorological SATellite
FAO	Food and Agriculture Organisation (UN)
GOES	Geostationary Operational Environmental Satellites
GPI	Goes Precipitation Index
KR	Kriged rainfall
METEOSAT	METEOrological SATellite
NOAA	National Oceanic and Atmospheric Administration
NASA	National Aeronautics and Space Administration
PERMIT	Polar Orbiter Effective Rainfall Monitoring Interactive Technique
PR	TRMM Precipitation Radar
TAMSAT	Tropical Applications of Meteorology using SATellite
TMI	TRMM Microwave Imager
TIR	Thermal Infra-Red radiation
TRMM	Tropical Rainfall Measuring Mission
TSDIS	TRMM Data and Information System
VIRS	Visible and Infra-red Radiometer System
VIS	VISibleradiation

CHAPTER 1

1. INTRODUCTION

1.1 Problem Definition

Because of the need for better management of the scarce water resource, we need better data on water budgets. Rainfall is of course the first major component of the water budget.

Rainfall occurs over time periods from minutes to days and weeks and over areas of a few kilometers to hundreds of kilometers. Hence to measure space/time averaged rainfall a dense net work of rain gauge is needed. However, the distribution density of rain gauges is often too low to cope with the extreme spatial and temporal variations of rainfall, especially in arid and semi-arid regions and through much of the tropics (Barrett and Martin, 1981).

See Fig 3.5, the spatial variation of decadal rainfall over the Naivasha catchment, the correlation between distance and rainfall is less than 50% after 5 km. (data obtained from Kenya Meteorology office). Further, rain gauge data are often inaccurate and /or untimely.

It is well known that rainfall observations from relatively isolated rain gauges are rarely representative of rainfall over wider areas. (The World Meteorological Organization, 1974) recommended the minimum gauge density of precipitation networks in various geographical regions. For temperate, Mediterranean, and tropical mountainous region 100 – 250km^2 per gauge is recommended (Ward, 1974). The over all rain gauge density in Naivasha catchment is 290 km^2 per gauge, but large parts have a much lower density.

Understanding rainfall in the tropics is important because of its influence on large-scale atmospheric dynamics and its relevance to human life (Barrett and Martin, 1981).

Real time rainfall data is needed to assess and monitor the water budget, to signal short falls in crop growth, and to provide warning for floods. In Africa the scarcity of ground based data means that the only feasible approach to real-time area estimation is the use of satellite imagery. Thus, satellite remote sensing could play a significant role in improving knowledge of rainfall distribution and quantification in areas like Naivasha.

Therefore this thesis is devoted to find a relation between METEOSAT thermal infrared imagery (CCD) based on temperature thresholding (to identify potential rain clouds) and actual rainfall over the Naivasha catchment.

1.2 Objective

The main objective of the research is

- To work out areal rainfall estimates using *TAMSAT* method as developed from the *GOES* precipitation index *(GPI)* which is widely used for climatological studies of global precipitation, for the Naivasha area.
- To analyze deviation of predicted and observed rainfall
- To study whether the result yields improved rainfall-runoff relationships in the Naivasha catchment.

1.3 Research Methodology

The Cold Cloud Duration (CCD) daily image taken by satellite over the whole African continent is used as an input data (supplied by TAMSAT group, University of Reading, Department of Meteorology), the following is based on their method.

First the entire area is divided in to grid square map (latitude, longitude), then the satellite images overlay with grid square map, the grid squares are identified as " gauge cells" (those containing the gauge stations) and "satellite cells" (those lacking stations)

Then a contingency table, which contains both satellite derived (CCD) and conventional data will be prepared to select an appropriate cold cloud top temperature threshold, to determine whether or not the cloud produced rain and the rainfall estimated from the period during which the cloud remained over a site, using the above "gauge cell".

By using Kriging the areal rainfall based on the rain gauge data is estimated for the corresponding period of CCD images.

After merging of CCD and gauge data, evaluation of the result will be analyzed by examining events, which deviate much from the expectations.

Regression analysis is used to define the relation between CCD and the kriged rainfall; the result is used to make a prediction of rainfall for the full catchment.

River gauging records are utilized to verify how well the discharge responses to the event CCD estimated rainfall and kriged rainfall.

1.4 Study area

The Lake Naivasha basin, stretching over an area of 3200 km^2, lies in the East African Rift Valley, about 100 km Northwest of Nairobi. Its geographical coordinates are 0^0 00' to 1^0 00' S and 36^0 00' to 36^0 45' E. Administratively, it is situated in the Naivasha division, Nakuru district, Rift Valley province of Kenya.

It receives an average of 1000 mm of rain per year and it exhibits smooth to very high relief. The area has two rainy season short rainy season (mid October to mid December) and long rainy season (March to June), During the rain season the major rain bearing system is the squall line: a convective system and moving from east to west.

The cumulonimbus clouds have a low cloud base and very high cloud tops. For this reason, on the METEOSAT image these clouds appear very cold in the thermal infrared and very bright in the visible domain. This offers a possibility to discriminate them from other clouds. (Ears and Rosema, 1988)

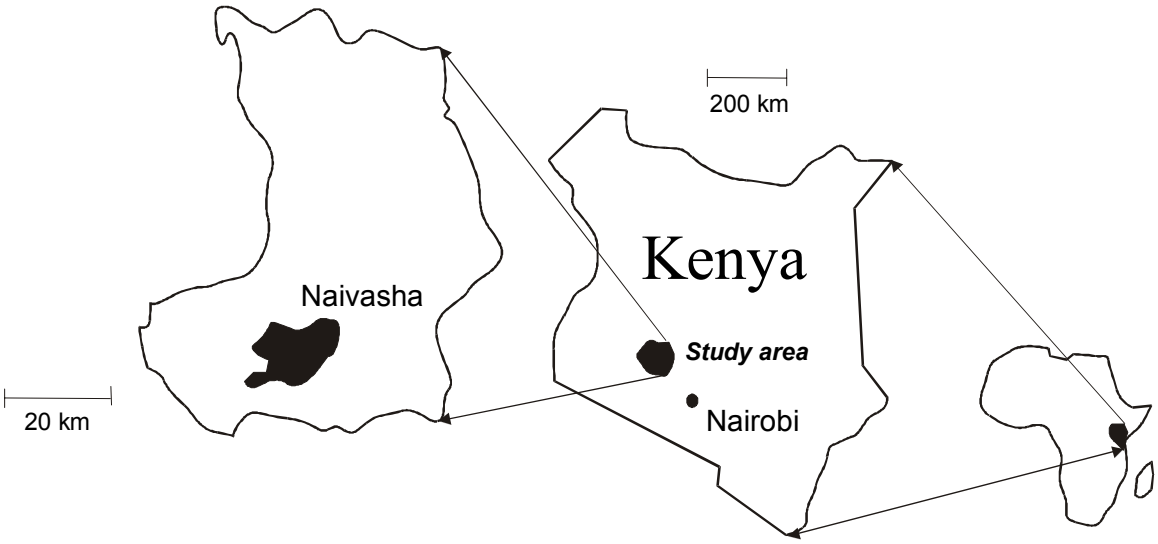

Figure 1.1 The study area in international, national, and regional contexts.

1.4.1 Meteosat data

Windowing of Study Area:

This is a method to define (windowing out) the above area from the whole African continent CCD image in METEOSAT projection. The Latitude-Longitude co-ordinate of the catchment is defined using the Atlas GIS. These co-ordinates convert to METEOSAT co-ordinates using the program LL2METXY (Rogerio, 1996).

Each degree Latitude is about 20 METEOSAT pixels, and the rectangular area covering entire Kenya is 200*200 METEOSAT pixels.

Windowing by convention and to give some margin for further trimming, following re-projection, a square region is defined in METEOSAT coordinates of 256x256 pixels.

This window is extracted from the original whole continent imagery and then re-projected to Latitude-Longitude co-ordinates to derive the original region.

Hence the " Real-time window rectified daily CCD image", data which is based on half hour image is utilized for this study (1994 -1998).

1.4.2 Rain gauge network description

The network stations inside and around the catchment are composed of more than 200 manual recording raingauges. 11 raingauge stations within the catchment and an additional 19 stations in the area around the catchment with daily rainfall data for the period 1994 to 1998 are available, see Fig 1.3, out of 32101 available data 3647 data are missed.

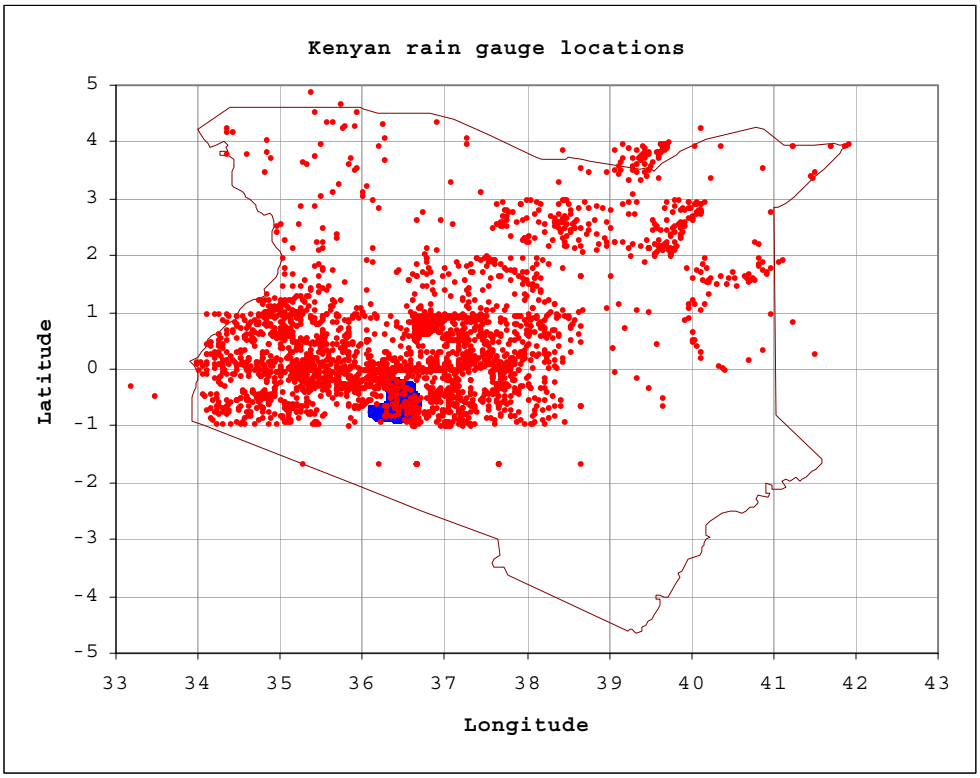

Figure 1.2 Map of Kenya with Naivasha catchment outline and rain gauge locations (source: Kenya meteorology department).

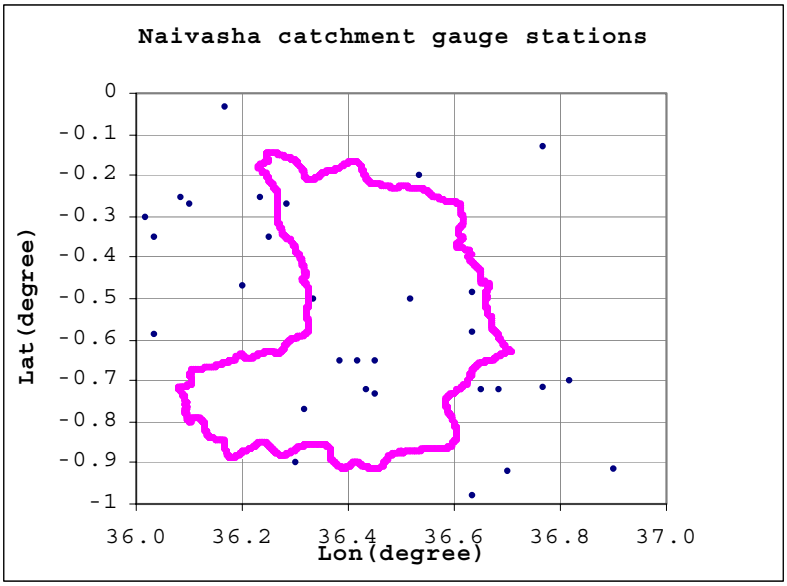

Figure 1. 3 Map showing Naivasha catchment and rainfall gauge stations which have recorded values for the year 1994 to 1998.

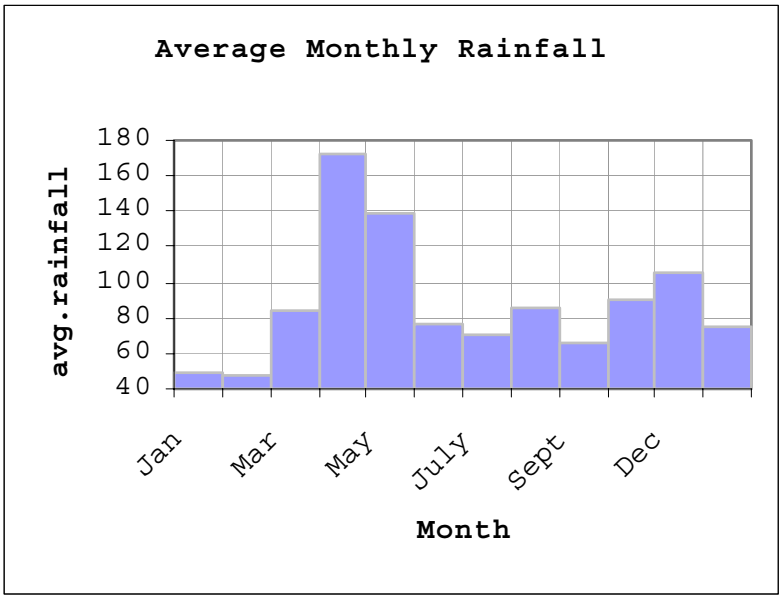

Figure 1.4 Graph, showing the average monthly rainfall pattern for the Naivasha catchment using the above 30 stations (1994 to 1998).

CHAPTER 2

2. REVIEW OF TECHNIQUES IN QUANTITATIVE RAINFALL ESTIMATION

2.1 Measurement of rain with standard rain gauges

Even if the measurement of rainfall by rain gauges is fraught with some problems, that relatively simple instrumentation will long continue to provide the data against which rainfall assessments by other means must be adjusted.

The advantage of using rain gauges to monitor rainfall is (Grimes, Bonifacio and Loftie, 1998).

- *Comparability:* rainfall amounts can be compared through out a region or over a period of time if standardized gauges is used. Correction factors can be used to take account of differences in design.

- *Simplicity:* rain gauges are easily manufactured from local materials and do not require specialized maintenance. Observers can easily be trained.

The disadvantage using rain gauges are (Grimes, Bonifacio and Loftie,1998).

- *Point measurements:* rain gauges measure rainfall at a point but most often the information required is the rainfall average over a large area.

- *Distribution of gauges:* because gauges usually need to be read at once per day, gauge sites are often dictated by ease of access. This means that there are few gauges in uninhabited areas. Thus the distribution may not be representative of the area as a whole.

- *Time delay:* rain gauges are typically read at 6 AM to give the previous days rain. Data are rarely available in a central location on the same day and weeks or even months may elapse before sufficient data are assembled to give a meaningful overview.

Of the disadvantages, the first mentioned is the most significant. Particularly in the tropics, rainfall is often localized and a single gauge may only be representative of a very small area in its immediate vicinity, on a particular day.

As stated in (Barrett and Martin, 1981), (Woodley et al., 1974) found relatively small differences 5 to 10% in the measurements of heavy convective rainfall by pairs of co-located, unshielded rain gauges. (Rodda, 1971) stated similarly discouraging findings: catch deficiencies for rain collected in standard gauges were found to vary from 3% to 30% for annual totals and over a wider range for individual storms.

2.2 Areal rainfall estimation from Point data

The accuracy of areal rainfall estimation is depends on the spatial variability of precipitation; thus more gauges would be required in those area where rainfall is highly variable, Naivasha is of course one of the area where the rain fall is highly variable with space and time.

Many interpolation schemes have been proposed in the literature for the estimation of areal rainfall. The most familiar and simple scheme is the well-known Thissen polygons and the isohyetal methods, whereby the isohyets are often based on simple linear interpolation.

The statistical methods first require an examination of the spatial correlation structure of the data set, such as the analysis of the semi-variogram for the kriging method. This method is described in chapter three in more detail, since it is applied in this study.

The general form of the equation for interpolation at a point is:

$$\hat{Z} = \hat{Z}o = \sum_{i=1}^{n} W_i Z_i \quad \text{.....(2.1)}$$

Where: $\hat{Z}o$ is the estimated value of the process at any point with coordinates x_0,y_0;
W_i the weight of the sampling point i
Z_i the observed value of the attribute (or process) at a point i with coordinates x_i,y_i
n the number of sampling points considered, i = 1,2,n.

The various interpolation technique differ only in evaluating the weight W.

Interpolation uses the principle that for the estimation of unknown values, the known values in the locality, surrounding or neighborhood is more relevance than those further away and weights may be given to the surrounding points.

Generally, a fairly large number of reference points (stations) are required, which restricts the application of the method. Even with an adequate density of the gauge network, the analysis of the spatial correlation structure may take so much time that one would be reluctant to use a stochastic (statistical) method when many rainfall pattern have to analyzed, for example for Studying daily rainfall patterns and runoff (Meijerink,de Brouwer, Mannaerts and Valenzuela, 1994).

2.3 Areal rainfall estimation using Satellite Remote Sensed data

(Griffth et al., 1978) recognized the transient evolution and extent of cloud-top temperature as a tool to infer convective activity. (Dugdale and Milford, 1986) developed the concept of cold cloud duration (CCD), using the thermal channel of Meteosat, to generate time series of cloud temperature for tropical altitudes, where most rainfall comes from large convective storms. They suggested that the duration above a threshold temperature value is representative of the amount of rain that is generated. Although there is an essential amount of empiricism included in this methodology, it helps to interpret rainfall intensities at unsampled locations between gauges in a network of rain gauges. As stated in (Bastiaanssen, 1998).

2.3.1 Satellite Remote Sensing Systems

It has become fashionable and convenient to differentiate between two groups of earth observation satellites, namely "Earth Resource" and "Environmental" satellites. In more general terms, the differences between the two groups arise from design capabilities for the frequency, and spatial resolution on the ground, of the data they provide. These capabilities are inversely related to each other largely because of data-flow constraints (Barrett and Martin, 1981). Since Earth Resource satellites provide a low temporal resolution (low imaging frequency) they only provide indirect rainfall through vegetation response (Meijerink, deBrouwer, Mannaerts and Valenzuela, 1994).

Environmental satellites have commonly occupied two types of orbits, and may be grouped in (Barrett and Martin, 1981).

(A) Polar-orbiting, and

(B) Geostationary satellite families

Polar-orbiting Satellites

The satellites occupy relatively low-level orbits (usually between 500-1500 km above the surface of the earth), crossing the equator at high angles so that each orbit takes such a satellite close to the north and South Pole. These satellites are usually sun-synchronous, i.e. their orbits are so organized that, as the earth rotates on its polar axis, within the orbital ellipses, each new orbit results in the presentation of a new strip of the global target to the satellite in such away that the relationship between earth surface and sun angle is kept relatively constant.

The speed of the satellite is determined by its height above the earth. United States NOAA (National Oceanic and Atmospheric Administration) satellites, which are widely used for vegetation monitoring, orbit at a height of around 800km.This means they complete an orbit roughly every 90 minutes. The NOAA AVHRR (Advanced Very High-Resolution Radiometer) sensor scans the entire Earth's surface in about 12 hours. In this way most points on the Earth are viewed at least twice per day. Because of their low orbits, polar orbiters can give relatively high spatial resolution images.

Examples of polar orbiting satellite include NOAA, TIROS, ESSA, Molniya and Meteor (Russian), DMSP.

Geosynchronous satellites

The satellites are placed in to orbit at approximately 36000km in the plane of the equator, and advance in the same direction as the rotation of the Earth. This type of orbit is geosynchronous, the satellite keeping pace with the rotation of the earth on its polar axis, and geostationary in that it ensures that any satellite occupying it appears to be fixed or stationary above a given point on the surface. Such a satellite is able to record the same geographic field of view very frequently through the diurnal cycle, commonly at interval of 30 minutes.

Thus a geostationary satellite sees the same view of the full Earth disc all the time. Because a geosynchronous satellite has the same view of the Earth at all times; it is possible to build up a more detailed picture of how the scene is changing over time with in the field of view.

METEOSAT produces imagery every 30 minutes giving a total of 48 images per day. These factors are very important in estimating tropical rainfall. In contrast, a polar orbiting satellite, which may pass over the same spot at the same time only once or twice per day, will obtain a very biased view of the strong daily cycle of rainfall in the tropics.

Most convective storms build up in the late afternoon and evening so an overpass in the afternoon will exaggerate the rain, while an overpass in the morning will tend to underestimate it. For this reason, a geostationary satellite is much more useful than polar orbiters particularly when estimating rainfall on short time scales.

Examples include Applications Technology Satellite (ATS); The American Geostationary Operational Environmental Satellites (GOES-1, 2); GOES-10, an American satellite located over the Indian Ocean and controlled by ESA-European Space Agency satellite; METEOSAT (over west Africa controlled by ESA). The METOSAT satellite is positioned above 0° latitude, 0° longitude off the coast of West Africa. It is ideally positioned for looking at Africa); and a Japanese satellite, GMS-1, located over Borneo.

In this study METEOSAT is used to produce the image.

2.3.2 Satellite sensors and The Electromagnetic Spectrum

All sensor measure radiation in particular range of the electromagnetic spectrum. The electromagnetic spectrum is the term used to describe a whole family of types of radiation, which consist of electromagnetic wave motions.

Electromagnetic sensors and limitations

Sensors, which are sensitive to different wavelength bands in the electromagnetic spectrum, give us different information about the earth and its atmosphere. The wavelengths in common uses, which are relevant to rainfall estimation, are summarized below (Grimes, Bonifacio and Loftie, 1998).

(A) Visible sensor (0.4 – 0.7μm)

A sensor in the visible region of the spectrum measures reflected sunlight, of clouds and earth surface.

Thicker clouds are more opaque, i.e. less sunlight passes through them than through thin clouds and more light is reflected back into space. This means that, seen from below, the base of the cloud is very dark, but seen from the satellite's point of view, the reflected light makes the cloud appear very bright. Therefore, it is supposed that as cloud thickness increases precipitation is more probable and its intensity is likely to be greater. Thinner clouds (which may be either at a low altitude or a high altitude) allow through more light and so reflect less. Therefore they appear less bright to the visible sensor on the satellite.

(B) Thermal Infra-Red (TIR) sensor (10.5 – 12.5 μm)

The temperature of the atmosphere decreases with height in a regular way throughout the troposphere (the bottom 10-15 km of the atmosphere) depending on weather conditions and the amount of the moisture present.

The emission of infrared radiation is less at lower temperature and greater at higher temperatures. The infrared sensor therefore acts as a remote thermometer, which can estimate the temperature of the cloud tops. *Cirrus* is also identified as very cold and lower, inactive cumulus show up at higher temperature of between 0°C to -20°C.

The infrared sensor can identify storm clouds by their low temperature although they may be confused with cirrus.

(C) Microwave sensor (5000 - 300000μm)

C.1. Passive sensor:

At wavelength of about 1.5 cm (15000μm), rainy areas show up very well over the oceans as bright against a dark background. Over the land, however, the background emission from the surface is very variable. The wetness of the surface as well as its roughness and the kind of vegetation all cause variations in the emitted radiation. Making quantitative estimates of rainfall against this continually changing background is a difficult task.

A further problem is that, because the micro wavelengths are so long, the energy available is quite small compared to the above wavelengths. Thus, the fields of view must be large to detect enough energy to record a signal; consequently, the spatial resolution in the microwave band is much coarser than in the other wavebands mentioned above. Hence, microwave sensor on a geostationary satellite would give images with a pixel size of several kilometers, which is far too coarse a scale for rainfall estimation.

C.2. Active sensor

TRMM sensor package:

The TRMM (Tropical Rainfall Measuring Mission) is designed to measure tropical rainfall from a low-inclination orbit using a suite of sensors, including the first spaceborn application of the precipitation radar. It covers the tropics between 35°N and 35°S. The primary rainfall instruments on TRMM are the precipitation radar (PR), the TRMM Microwave Imager (TMI) and the visible and Infrared Radiometer system (VIRS) (Kidd, 1998).

Table 2.1 TRMM sensors complementarity (Meneghini and Kozu, 1990)

	TMI	*PR*	*VIRS*
Advantage	• Quantitative measure of rain wide swath	• Quantitative measure of rain • Better spatial resolution • Rain type vertical profile of rain • Can provide layer thickness • works well over land	• Best spatial resolution distinguish between convective and stratiform precipitation • Transfer standard to geosynchronous to polar orbital
Limitation	• Less quantitative over land for low rainfall • Moderate spatial resolution	• Narrow swath width • Largely untested in space	• Less quantitative measure • Obscuration by cirrus shields

Many algorithms exist for calculating rainfall from infrared or visible images from geostationary satellites.

The approach in this thesis is the TAMSAT method for rainfall estimation in Africa, which only uses information from the infrared sensor on the METEOSAT satellite.

The reason for this is according to (Grimes, Bonifacio and Loftie, 1998):

- In most of Africa a significant fraction of rain falls at night. The visible sensor has no use during the night.
- Calculations based on a single sensor have the great merit of simplicity, which is important for automatic operational procedures. Marginally better results might be achievable by including visible imagery for daytime storms, but this would be at the expense of a more complicated algorithm, which is more difficult to automate.
- It is difficult to verify small improvements that might be expected from the inclusion of visible images because of the sparseness of rain gauges in Africa.

2.3.3 General approach in rainfall estimation

The approaches discussed here pertain to making quantitative estimates of rainfall by using satellites visible and infrared techniques.

Visible and infrared techniques

There are three dominant approaches: the cloud indexing approach, the thresholding approach, and the life-history approach (Quanwei, 1996).

1.Cloud-indexing methods:

It is time independent, and it identifies different types of rain clouds and estimates the rainfall from the number and the duration of clouds of their area.

The techniques rely on visible and infrared data to characterize a cloud type or temperature, which is then related to rainfall via empirical relationships. Different methods have been used to calibrate the indices to give rainfall estimates.

The Earthsat method, (Moses and Barrett., 1986) is an operational rainfall estimation scheme that has been developed to provide input to crop yield models and commodity forecasting systems. *The Earthsat method* uses a regression approach to estimate 6-hour precipitation from cloud temperature and empirical information for the major crop-growing regions of the world.

The manual Bristol method uses an empirical relationship between satellite-determined cloud indices, climatic indices dependent on the mean monthly rainfall, and 12-hour rainfall totals. *The Bristol method* has been further developed into an interactive method known as *BIAS (Bristol/NOAA Interactive System)* originally for the *USDA agRISTARS* program (Schultz and Barrett, 1989). *BIAS* uses the following relationship:

$$R = f(C_t, C_a, C_d, C_c, S_w) \quad \text{.....(2.2)}$$

Where: **R** is the 6-12 or 24-hour rainfall, $\mathbf{C_t}$ is a rain cloud type, $\mathbf{C_a}$ is the fraction of rain-cloud-type area and $\mathbf{C_d}$ is the duration. The product of $\mathbf{C_t}$, $\mathbf{C_a}$ and $\mathbf{C_d}$ is the cloud index, which is translated into rainfall estimates through the regression equations. Each pixel is assigned a climate category, $\mathbf{C_c}$, in order to select the proper cloud index/rainfall regression equation to be used in the absence of surface measurements of rainfall. However, if the surface measurements are available, the synoptic weather term, $\mathbf{S_w}$, may be used to provide more accurate results.

2. Thresholding methods:

Consider that all clouds with low upper-surface temperature and clouds often brighter than others are likely to be rain clouds. So, there exist two types of thresholding methods, one is based on cloud top brightness, and the other is based on cloud top temperatures.

The cloud brightness techniques: depend on the assumption that precipitating clouds are often brighter than others, so that automatic brightness thresholding can be used to map rainfall from satellite visible imagery, and that calibration of rainfall amounts can be achieved using rain gauge and/or radar observations.

The cloud temperature technique: is based on temperature thresholding of thermal infrared imagery analyzed by computer to identify potential rain clouds and considers that all clouds with low upper-surface temperatures are likely to be rain clouds.

Examples of this technique include the TAMSAT and the PERMIT methods.

• The TAMSAT approach:

The use of Cold Cloud Duration (CCD) as a surrogate for rainfall has its roots in the work of (Arkin and Meissner, 1987) who showed that rainfall in the tropical could be related to the fractional coverage of cloud with satellite-measured temperature below 235K (-38°C). This work has lead to the development of the GOES precipitation index (GPI) which is widely used for climatological studies of global precipitation.

$$\mathbf{GPI = 3f\Delta t} \quad \text{.....(2.3)}$$

Where: **GPI** is the mean rain rate estimate in an area, **f** is the fraction of the area covered with clouds colder than 235K and $\mathbf{\Delta t}$ is time in hours between successive images.

The **GPI** works well for rainfall over the ocean but generally tends to underestimate rainfall over land. This is unsurprising as no allowance is made for the effect of land surface characteristics such as topography.

The TAMSAT method will be described in more detail in the next chapter since it is applied in this study

• PERMIT:

The PERMIT method (Polar-orbiter Effective Rainfall Monitoring Integrative Technique) uses a TIR threshold for the discrimination of rain cloud areas. The main objective of this discrimination is to identify rainy days, not cold cloud duration. The relation between rainy days and rainfall is therefore not based on regression analysis using meteorological data, but instead on climatological data of mean rain-per-rainy-day (Snijders, 1991).

The relationship used in PERMIT can be expressed as:

$$R = f\ (C_T, C_d, M_c, S_w) \quad \text{.....(2.4)}$$

Where: **R** is the estimated rainfall for periods of 10 days or longer, $\mathbf{C_T}$ is the cloud top temperature, $\mathbf{C_d}$ is the number of satellite observed rain cloud days, $\mathbf{M_c}$ is an empirical term that describes the combined climate/terrain effect and $\mathbf{S_w}$ is a synoptic weight related to surface measurements.

3. Life-history methods

Some life-cycle methods are designed to provide rain estimates from any type of convectional clouds by taking into objective consideration of the growth or dissipation of individual clouds with time. This approach implicitly recognizes that convective clouds exhibit different rainfall intensities during their growth and dissipation cycle.

The *Woodley-Griffith techniques* were developed initially to predict rainfall over south Florida as part of the Florida area cumulus experiment. (Griffith et al., 1978). This method uses an empirically derived relationship between calibrated ground-based radar echoes and geostationary satellite imagery of cloud areas. A time-cycle relationship between the radar echo area and the cloud area is developed for discrete time intervals during the lifetime of the cloud.

$$R_v = IA_e \sum q_i b_i \Delta t \quad \text{.....(2.5)}$$

Where: $\mathbf{R_v}$ is the rain volume in mm, **I** is the rain rate in $m^3\ km^{-2}h^{-1}$, $\mathbf{A_e}$ is the inferred radar echo in square kilometers, **I** is the temperature index, **q** is the fraction of pixels at each threshold within the cloud, **b** is a temperature-dependent weighting factor and $\mathbf{\Delta t}$ is the time interval between successive satellite images.

Table 2.2 Summary of Several Visible/Infrared Satellite Rainfall monitoring Techniques. (Schultz and Barrett, 1989) as discussed in (Adegu, 1999).

Model	Analysis Type	Parameters/equation	Characteristics
Earthsat	Cloud indexing	R=[a+b(C*V*0 .6)]M	Empirical. Uses a regression approach to estimate 6h rainfall from cloud temp. and empirical information.
BIAS	Cloud indexing	R= f (Ct, Ca, Cd ,Cc, Sw)	Design for unsual events, 12h rainfall total. Uses satellite determined cloud indices dependent on mean monthly rainfall and 12h rainfall totals. (fully interactive)
GPI	Cloud indexing	*R=f(CT)*	Give monthly rainfall estimates for 2.50 squares. It is a global hyd. model.Temperature statistics of cloud top required.
NESS	Cloud indexing	R=(K1A1+K2A2+K3A3)/A0	gives 24h period av. rain across the area
PERMIT	Threshhold	R=f(CT,Cd,Mc,Sw)	Estimates rainfall for, >=10days. Based on T thresholding of thermal IR imagery for potential rain cloud.
ADMIT/ (FAO)	Threshhold	Rv=f(CB,CT,Cd,Mc ,Sw).	An extension of PERMIT .Uses daytime visible and IR images to establish rain/no-rain threshold.
TAMSAT Method	Threshhold	$R=f(C_T)$	IR based cloud-top temperature technique. Uses hourly imagery, to displays regional regressions to translate CCD into rainfall estimates for time frames of 1,5,10 & 30 days
CST	Threshold	$R=f(C_T,T_S)$	Estimates both convective and stratiform rainfall

f-function, a*, b*-rainfall coefficients, *R*-rainrate, *S*w-synoptic weather term
C -local cloud brightness category, *Ct*-rain cloud type, *CT*-cloud top temp.
V-vertical motion class, *Cd*-sat. obs. rain cloud days, *M*-weighting factor
Cc-climate category, *CB* -cloud brightness
A0-total area, *A1*, *A2* ... areas covered by the 3 most rain-producing clouds(cumulonimbus, cumulocongestus, nimbostratus), *K1,K2* ..- empirical coefficients.

CHAPTER 3

3. APPLICATION OF THE TAMSAT METHOD FOR RAINFALL ESTIMATION.

3.1 General

The TAMSAT rainfall estimation is one of a number of approaches developed from the GPI application in Africa (Milford and Dugdale, 1990). It was devised in response to the needs of some African countries for rapid identification of regions with rainfall deficits and likely shortfall in crop yields. The method uses cloud-top temperature calculated from METEOSAT TIR radiance and utilizes more frequent images (every half an hour), needed to monitor the highly variable rainfall of a region.

The basic assumptions inherent in the TAMSAT rainfall estimation procedure are, (Grimes, Bonifacio and Loftie, 1998):

1. Rainfall comes mainly from convective storm clouds.

2. These clouds only rain when their tops have reached a certain minimum height (the height threshold).

3. The cloud top height can be identified by its temperature on the thermal infrared (TIR) image. This temperature is referred to as threshold temperature T_t.

4. At a given location, the quantity of rainfall can be calculated from the length of time the cloud top has been above the height threshold (or colder than the corresponding temperature threshold T_t). This length of time is the *Cold Cloud Duration or CCD*.

A further assumption is that the relationship between *rainfall quantity* and *CCD* is *linear* provided there is adequate averaging of the data either in space or in time. Thus we can write

$$R = a_0 + a_1 \times CCD \quad \text{for } CCD > 0$$

$$R = 0 \quad \text{for } CCD = 0 \qquad (3.1)$$

Where: **R** is rainfall, **CCD** is Cold Cloud Duration, $\mathbf{a_0}$,$\mathbf{a_1}$ are respectively the offset and the slope (or coefficient) of the straight line graph represented by equation 3.1.
a_0,a_1 and T_t depend on local climate conditions and hence vary both in space and time.

3.2 Overview of rainfall estimation procedure

The steps involved in the production of the rainfall estimates are as follows: (Grimes, Bonifacio and Loftie, 1998):

- Generation of **CCD** images at a number of temperature thresholds.
- Determination of the optimum threshold $\mathbf{T_t}$ for the calibration zone
- Determination of optimum calibration parameters $\mathbf{a_0}$ and $\mathbf{a_1}$ for the zone.

- Calculation of rainfall estimates.
- Evaluation (geostatistical approach) of rainfall estimates.

3.2.1 Generation of CCD images

Thermal Infrared Red (TIR) images

TIR images are transmitted by METEOSAT every 30 minutes. It is from these that CCD images are derived. The row data are in the form of radiometer counts, which are related to the radiance of the observed surface by the equation

$$L = \alpha(C - C_0) \quad (3.2)$$

Where: **L** is radiance ($Wm^{-2}s^{-1}$), **C** is the radiometer count, α and $\mathbf{C_0}$ are calibration coefficients, which depend on the radiometer. $\mathbf{C_0}$ is known as the space count. To allow the calibration drift, the values of α and $\mathbf{C_0}$ are adjusted with a calibration system on the satellite and transmitted with the imagery twice per day (usually 8.a.m and 8.p.m). The radiance can be converted to temperatures by a look-up table or alternatively the following relationship between radiance and temperature **T** (k) can be applied.

$$L = \exp\{A + B/T\} \quad (3.3)$$

The value of **A** and **B** depend on the radiometer used. Values for Meteosat 2 to 7 are given in table 3.1 below.

Table 3.1 Values of coefficients A and B in the radiance-temperature relationship provided by EUMETSAT.

Metosat	M2	M3	M4	M5	M6	M7-1	M7-2
A	6.1401	6.1694	6.7300	6.7348	6.7615	6.9676	6.9618
B	-1267.00	-1262.70	-1272.20	-1272.20	-1267.20	-1255.61	-1255.55

Radiometer counts **C** in terms of radiance is obtained by rearranging equation (3.2)

$$C = (C_0 - L/\alpha) \quad (3.4)$$

An equation relating temperature to digital counts or vice versa for any date and Meteosat satellite can be obtained by combining (3.3) and (3.4)

$$C = C_0 + 1/\alpha(\exp(A + B/T)) \quad (3.5)$$

or

$$T = B/\ (-A + \ln[\alpha(C - CO)]) \quad (3.6)$$

Thus, from a table of **T** and **C,** one can know the **T** corresponding to any count.

Derivation of CCD (CCU) images

To begin generation of CCD images, a temperature threshold is selected which is converted to a radiometer count via the calibration relationship. After that the procedure is (Grimes, Bonifacio and Loftie, 1998):

The threshold $\mathbf{T_t}$ is applied to each individual TIR image. This means that the pixels within temperature value below a threshold $\mathbf{T_t}$ (assumed 'rainy') is assigned value **1** and those with **T** above $\mathbf{T_t}$ (assumed 'dry') are assigned **0**. This forms a Boolean image (as a secondary image).

The thresholding is repeated for 48 half hourly TIR images to obtain 48 Boolean images.
The 48 Boolean images are added up-the result is a daily CCD image. Each pixel value is the number of hours that the pixel was under rain-bearing cloud.

To produce a decadal CCD image, the daily CCU images in slots are totaled over the appropriate number of days and divided by 2 to give the cold cloud duration in hours for that decade.

3.2.2 Determination of optimum threshold T_t for the calibration zone

In order to determine the optimum temperature threshold for the zone, the CCD images at a number of different thresholds are compared with contemporaneous rain gauge data. The optimum threshold is the one, which shows the highest level of agreement with the gauge data as to whether or not rainfall has occurred within pixels containing gauges. This can be done most conveniently using contingency table as shown below

	CCD = 0	CCD > 0
Gauge = 0	N_{11}	N_{12}
Gauge > 0	N_{21}	N_{22}

Where:

- N_{11} is the number of occasions when both gauge records zero rain and CCD is zero.
- N_{12} is the number of occasions when gauge records zero but there is some CCD.
- N_{21} is the number of occasions when gauge records some rain but CCD is zero.
- N_{22} is the number of occasions when gauge records and CCD values are non-zero.

(N_{11} and N_{22}) represent agreement between the gauge and the satellite while (N_{12} and N_{21}) represent disagreement.

For the optimum temperature threshold, we would like the number of occasions on which the satellite and gauge agree to be much greater than the number of disagreement. Also the number of occasions for which the gauge register rain but there is zero CCD should just be roughly balanced by the number of occasions for which the gauge registers no rain but there is some CCD. Thus the two conditions for the optimum temperature threshold are:

$$\mathbf{N_{11} + N_{22} >> N_{12} + N_{21}}$$

$$\mathbf{N_{12} \cong N_{21}}$$

The most important parameters that should be seen to choose optimum threshold temperature are:

1.Percent correctness→ $P_C = (N_{11} + N_{22}) / (N_{11} + N_{22} + N_{21} + N_{12})$ to check the accuracy

2.Bias = $(N_{12} + N_{22}) / (N_{21} + N_{22})$ = (estimated rainy day/no of rain day), desired value = 1 to check un biasdnes.

3.HIT RATE→ $HR = (N_{22}) / (N_{22} + N_{21})$ = (fraction of observed rainy day that are correctly estimated), desired value = 1

4.FAR (false alarm rate) = $(N_{12}) / (N_{11} + N_{12})$ = (fraction of observed dry day that estimated as wet), desired value = 0

5.Kuipers skill score→ $KSS = (HR - FAR)$, desired value = 1

Success → corresponds to **CCD=0, R=0 or/and CCD>0, R>0**
Too cold → corresponds to **CCD=0, R>0**
Too warm → corresponds to **CCD>0, R=0**

For too cold (if CCD = 0, R>0), then some warmer threshold would likely give the correct classification, hence the temperature threshold is too cold for discrimination. The reverse is true for too warm.

In this study CCD30 and CCD40 decadal data are compared, it is shown that CCD 30 is an optimum threshold which shows the highest level of agreement with the gauge data in this region. See appendix C-1

The result of the analysis of the daily CCD30/Rain data pairs for Naivasha based on the above five conditions, including the contingency table are shown below, for decade see appendix C-1

Table 3.2 Determination of CCD30 slot for best estimation of daily rainfall for the Naivasha catchment.

			March							April				
			Ir=0	Ir=1						Ir=0	Ir=1			
		Ic=0	2551	597					Ic=0	1275	658			
R >	0mm	Ic=1	596	586			R >	0mm	Ic=1	346	837			
h =	0	2	4	6	8	10	h=	0	2	4	6	8	10	
PC	0.72	0.74	0.75	0.75	0.74	0.74	PC	0.68	0.66	0.64	0.62	0.59	0.60	
Bias	1.00	0.74	0.55	0.46	0.37	0.31	Bias	0.79	0.61	0.49	0.40	0.32	0.27	
HR	0.50	0.39	0.31	0.27	0.22	0.19	HR	0.56	0.45	0.36	0.31	0.25	0.22	
FAR	0.19	0.13	0.09	0.07	0.06	0.05	FAR	0.21	0.14	0.11	0.09	0.06	0.05	
KSS	0.31	0.26	0.22	0.20	0.16	0.14	KSS	0.35	0.31	0.25	0.22	0.19	0.17	

			May							June				
			Ir=0	Ir=1						Ir=0	Ir=1			
		Ic=0	2063	1124					Ic=0	2015	846			
R >	0mm	Ic=1	431	753			R >	0mm	Ic=1	321	466			
h=	0	2	4	6	8	10	h =	0	2	4	6	8	10	
PC	0.64	0.64	0.63	0.62	0.60	0.60	PC	0.68	0.68	0.68	0.67	0.65	0.65	
Bias	0.63	0.44	0.32	0.24	0.17	0.13	Bias	0.60	0.44	0.32	0.21	0.13	0.09	
HR	0.40	0.30	0.23	0.18	0.14	0.10	HR	0.36	0.28	0.21	0.14	0.09	0.06	
FAR	0.17	0.10	0.06	0.05	0.03	0.02	FAR	0.14	0.09	0.06	0.04	0.02	0.01	
KSS	0.23	0.20	0.17	0.14	0.11	0.08	KSS	0.22	0.19	0.15	0.10	0.07	0.05	

			October							November				
			Ir=0	Ir=1						Ir=0	Ir=1			
		Ic=0	1614	789					Ic=0	1458	1282			
R >	0mm	Ic=1	267	289			R >	0mm	Ic=1	396	794			
h=	0	2	4	6	8	10	h =	0	2	4	6	8	10	
PC	0.64	0.65	0.65	0.64	0.64	0.64	PC	0.57	0.55	0.53	0.52	0.49	0.50	
Bias	0.52	0.28	0.14	0.07	0.04	0.02	Bias	0.57	0.41	0.29	0.21	0.15	0.10	
HR	0.27	0.15	0.08	0.05	0.03	0.01	HR	0.38	0.28	0.20	0.15	0.11	0.08	
FAR	0.14	0.07	0.03	0.01	0.01	0.00	FAR	0.21	0.15	0.09	0.07	0.04	0.03	
KSS	0.13	0.08	0.05	0.03	0.02	0.01	KSS	0.17	0.13	0.11	0.08	0.06	0.05	

			December			
			Ir=0	Ir=1		
		Ic=0	2752	712		
R >	0mm	Ic=1	174	258		
h=	0	2	4	6	8	10
PC	0.77	0.78	0.77	0.76	0.75	0.75
Bias	0.45	0.24	0.13	0.08	0.06	0.04
HR	0.27	0.17	0.10	0.06	0.04	0.02
FAR	0.06	0.02	0.01	0.01	0.00	0.00
KSS	0.21	0.15	0.09	0.06	0.04	0.02

The above contingency table reveal a problem with the satellite data, for most months the bias is nearly always below 1.0. December is the worst, when bias = 0.45 for rainfall>0, using CCD>0. This means more than half of the rainfall events are not detected by the satellite.

3.2.3 Calibration of parameters

The choice of approach in determining the parameter $\mathbf{a_0}$ and $\mathbf{a_1}$ in the equation 3.1 depends to a large extent on the application.

Three approaches described by include: (Grimes et al., 1993) as described in (Adegu, 1999)

(A) Days are classified according to CCD values. Regressing the median gauge in each class against the mid-class CCD carries out the calibration. The choice of the median as the representative rainfall value prevents abnormally large events from having an undue influence on the calibration.

(B) Mean rain gauge values are regressed against mean CCD for the pixels containing rain gauges, with the assumption that the gauge pixels are representative of the rainfall/CCD relationship for the area.

(C) Mean gauge value is regressed against mean CCD for the area, with the assumption that the gauge pixels are representative of the area rainfall.

Since the ultimate goal of this thesis is to estimate rainfall for hydrological purposes, method **B** and **C** are adopted in the analysis.

3.2.4 Evaluation (geostatistical approach) of rainfall estimates.

Interpolation (Kriging)

There is a difficulty in comparing data from gauges with those from satellites in that they provide two different kinds of information. Satellite estimates are essentially average of the area of the satellite pixel, where as gauges provides measurement made at a point (Grimes and Rogerio, 1998).

For meaningful comparison between the two data sets, one must be either derive point value from the satellite pixel or compute pixel areal average from rain gauge data. Here we choose the latter approach; this can be conveniently carried out by using **block kriging** *(Journel and Huijbregts, 1978).* As discussed in, (Grimes and Rogerio, 1998).

We are interested in the mean rainfall, $\mathbf{P_{At}}$ over area **A** at time **t**. This can be found by first determining rainfall estimate $\mathbf{P_{rt}}$ at any other point at distance ***r*** in the area under study from the available rain gauge data. Then, the area rainfall estimate, can be integrated numerically from the equation:

$$\mathbf{p_{At}} = 1/A \int_A P_{rt}\, dr \qquad \text{.....(3.7)}$$

This quantity $\mathbf{p_{At}}$ obviously unknown, since the rainfall depth is accessible only at finite number (say, n) of scattered point wise observations. It is therefore common practice in hydrology to estimate $\mathbf{p_{At}}$ using linear estimator of the form:

$$\mathbf{p_{At}} = \sum_{j=1}^{n} \lambda_j\, p(x_j) \qquad \text{.....(3.8)}$$

That is as weighted mean of the random variables P (X_1), P (X_2), P (Xn) observed at the rain gauges.

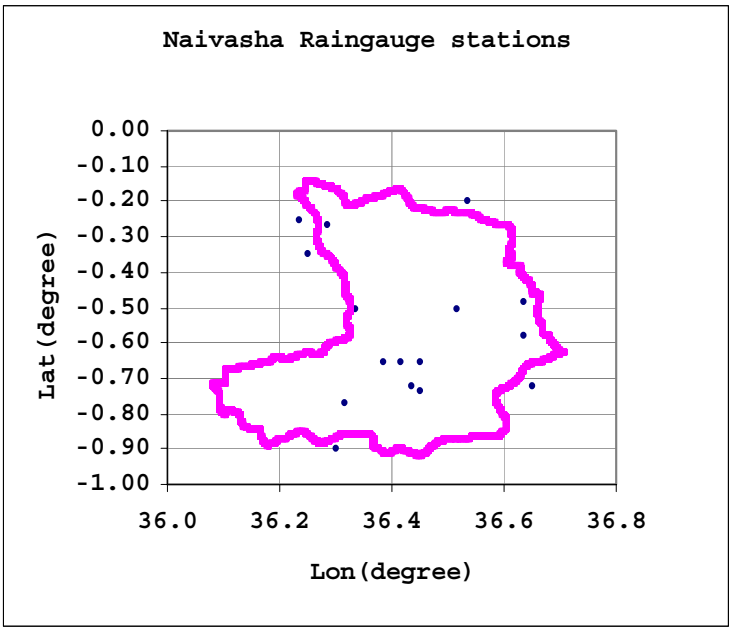

Figure 3.1 Map of Naivasha catchment and rain gauge stations, which are selected for kriging, year 1994 to 1998.

The linear estimates should satisfy two main conditions; these are

- Estimate is Unbiased

$$\sum \lambda_j = 1 \qquad (3.9)$$

- Estimate has minimum error. (Journel and Huijbregts, 1978)

$$\epsilon^2 = \sum_{j=1}^{n} \lambda_j \gamma(x_i - x_j) + \mu \qquad (3.10)$$

Where μ is a LaGrange multiplier, $\gamma(X_i,X_j)$ is the rainfall variogram function (matrix) among **n** measuring points, and $\gamma(X_i,X_0)$ is variogram values between each measurement point and estimation point. Therefore, if the variogram function is known, two matrices can be built to find the unknown weights and LaGrange multiplier.

Variogram

The variogram $\gamma(X_i,X_j)$ describes the variation of the correlation of rainfall field with distance. It is defined as (Jobard and Desbois,1992).

$$\gamma(h) = \gamma(X_i - X_j) = 1/2n(h) \sum_{i=1}^{n(h)} \{P[X+h] - P[X]\}^2 \quad \text{.....(3.11)}$$

where **h** is the vector separating X_i and X_j and **n(h)** is the number of gauge pairs with separating vector **(h).** This is on the assumption of a constant mean and infinite variance (intrinsic hypothesis), the mean and variance of the first order increments are independent of the actual locations and dependent only on the vector difference **(h).**

Where gauges are sufficiently close that their observed rainfalls are well correlated, **γ(h)** will have a **small** value. Where the gauges are further apart, **γ(h)** is **large**, eventually reaching a limiting value equal to the spatial variance of the rainfall field. The inclusion of **γ(h)** in equation **(3.9)** and **(3.10)** means that both the rainfall estimates and their associated errors take account of the distribution of the gauges relative to the spatial structure of the rainfall.(Clark, 1979).

Here in the above equation if we use $P^*(x) = (P_i - P_{mean})/\sigma P$ then the variogram becomes *standardized.*

$$\gamma^*(h) = 1/2n(h) * \sum_{i=1}^{n(h)} [P^*(x) - P^*(x+h)]^2 \quad \text{.....(3.12)}$$

Where:

$$\gamma^*(h) = \gamma(h)/\sigma^2 \quad \text{.....(3.13)}$$

Climatological variogram

In application to real-time estimation of areal rainfall, previous studies (Bastin et al.,1984, Label and Bastin, 1985) have lead to the development of "climatological kriging" i.e., kriging with a "climatological Variogram" as the covariance function. As described in, (Lebel et al.,1987)

We have, n points and t time steps, if we look at variogram at t-steps we will have t variograms, but the number of gauge stations (n) is very small. Hence, apart from being laborious, the t-variogram will have poor quality. The idea of climatological variogram is then to obtain a single variogram from all (n*t) points.

The same as the above is applied with a little modification

$$\gamma^*(h) = 1/2(t*n) \sum_{j=1}^{t} \sum_{i=1}^{n(h)} [P^*(x) - P^*(x+h)]^2 \quad \text{.....(3.14)}$$

Where: $P^*(x) = P_i - P_{mean}/\sigma P$

Monthly variogram:

For the Naivasha catchment, variograms were determined on the basis of months (grouping wet season months data together), for the period 1994-1998. The variogram function was standardized by spatial mean and variance (σ^2) of each data set. Illustrations of the variograms obtained are shown in Figure 3.2.

Model

The main types of the theoretical variogram models commonly used are.(Delhomme, 1978):

- Exponential model**:-**

$$\gamma(d) = C0+C1\{1-\exp[-(d/a)2]\}$$

- Spherical model**:-**

$$\gamma(d) = C_0+C_1[(3/2)(d/a)-(1/2)(d/a)^3] \quad \text{for } d < a$$

$$\gamma(d) = C_0+C_1 \quad \text{for } d \Rightarrow a$$

where **d** = denotes the length of the vector **d**, $\mathbf{C_0}$ is the *nugget* effect, $\mathbf{C_0+C_1}$ is the *sill* and **a** is the *range*. The variogram approaches the sill when the distance approaches the range.

Range:

It is the distance at which the model reaches its maximum value or sill. The larger the range, the stronger the spatial correlation. The variance of the estimation error decreases with increase of range.

Sill:

The upper limit of any variogram model which has such a limit. If the variogram goes beyond the sill then it is an indication of a trend.

Nugget:

This is a discontinuity at the origin. It is variance at very low distances. It caused by small-scale variations or by measurement error. With the nugget effect the kriging weights become more similar and the variance of the estimation error increases.

Model fitting

There are two type of model fitting, these are:

1.interactively (Visual) if only for smooth variograms

2.statistical fitting : these are least square and maximum likelihood

Generalized least square fitting method and exponential model is applied here, since most of the time rainfall varies exponentially with space and time. See Fig 3.2 and 3.3

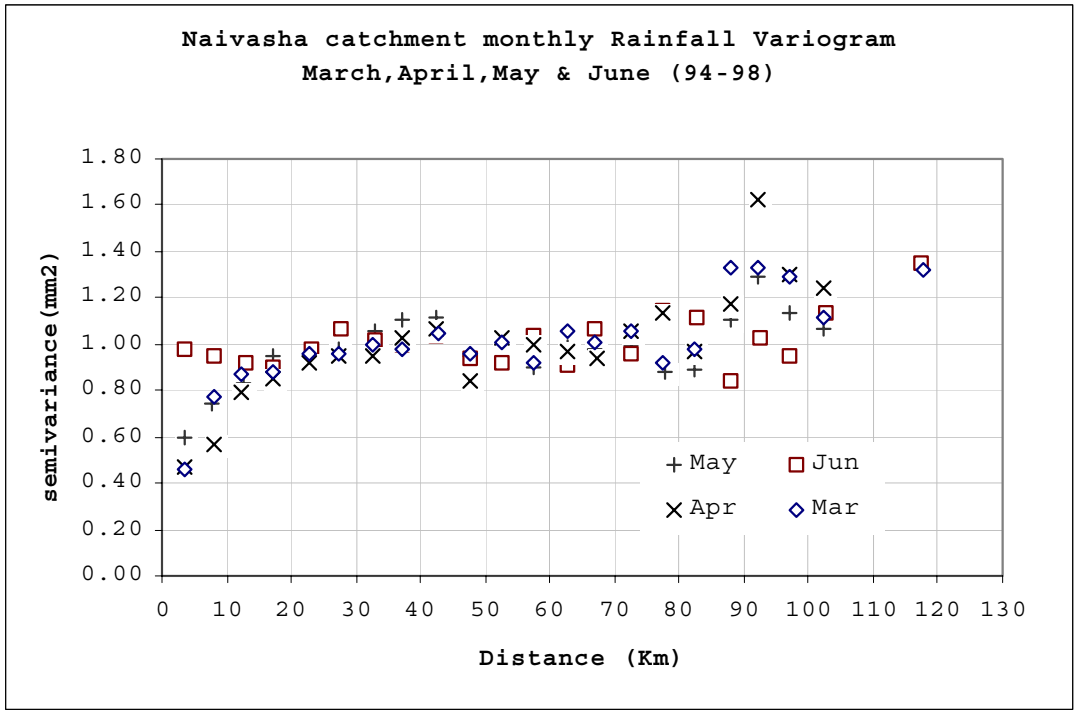

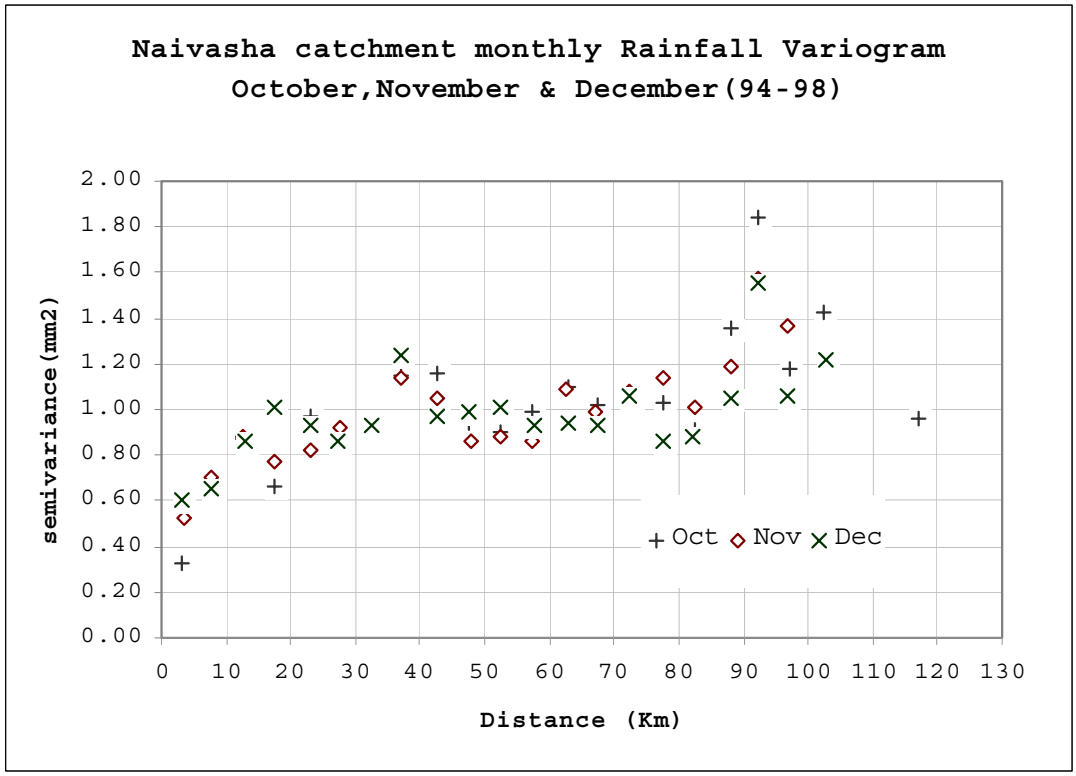

Figure 3.2 Graphical illustration of monthly variograms for rainfall data (1994-1998), with lag spacing of 5km for the above 30 station.(for daily data) before combining the long and short rainy season months.

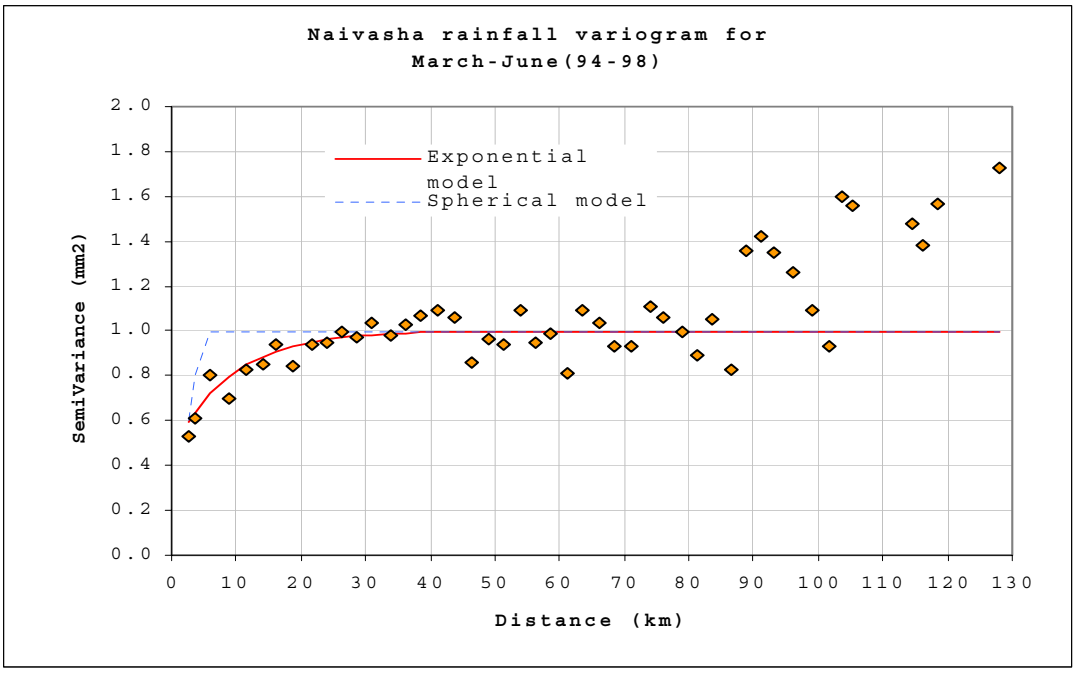

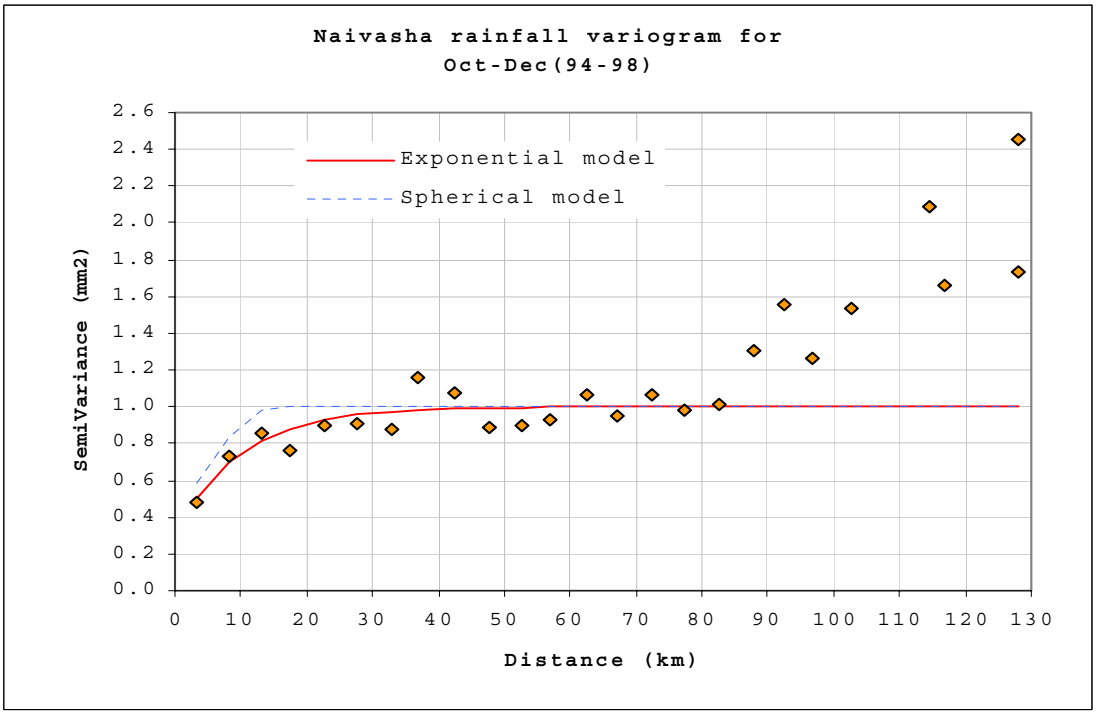

Figure 3.3 Graphical illustration of variograms for March-June and October-November rainfall data (1994-1998), with lag spacing of 2.5Km and 5km respectively for the above 30 stations. (For daily data).

All the variograms for the months are fairly close to each other and consistent between themselves, hence only two variograms one for Oct, Nov and Dec and another for the other months can be used. The only month outside is June because of strange rainfall values and less data points than the other months.

The big advantage in putting several months together is that it is possible to get more data to use a smaller lag, in this case it is very important since the data is so noisy.

After combining the months we use lag spacing 2.5km and 5 km for the derivation of variograms, for the long and short rainy season respectively, because the variograms at this spacing are not too noisy and not too smooth. (See appendix D, for decadal scale)

Table 3.3 Summary result of fitted theoretical variograms to the experimental variograms for the wet season of the year (Naivasha rainfall data 1994-1998).

	MONTH	Range	Sill	Nugget
Daily	MAR to June	9	0.54	0.46
	October to December	10	0.68	0.32
Decadal	MAR to June	14	0.92	0.08
	October to December	14	0.95	0.05

The range for the Naivasha catchment varies between 9-14km (for both daily and decade scale) this is generally a low value, the sill values γ are always greater than 0.5 for both daily and decadal scale and the nugget effect is high for daily data this is may be an indication that the spatial variability of the rainfall in this region is high, this can be supplemented by the following two graphs.

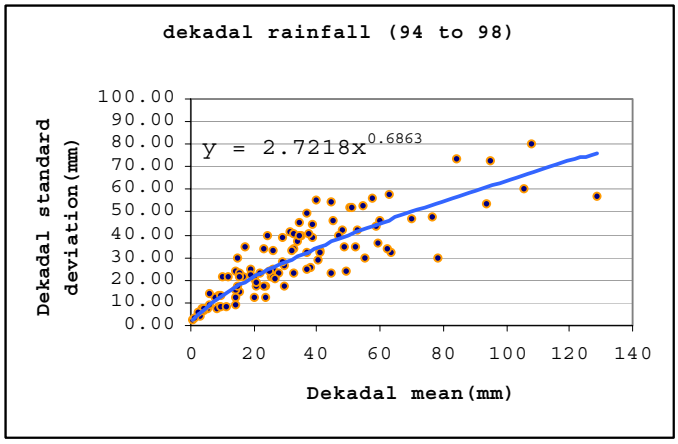

Figure 3.4 Plot of standard deviation against mean rainfall for decadal data (1994 to 1998) for the above 30 station.

From the plot above, the standard deviation of decadal rainfall for the area is comparable to the decadal mean rainfall, besides the standard deviation increase as the rainfall value increase, which is called heteroscedasticity which causes a problem to plot a regression line between rainfall and CCD.

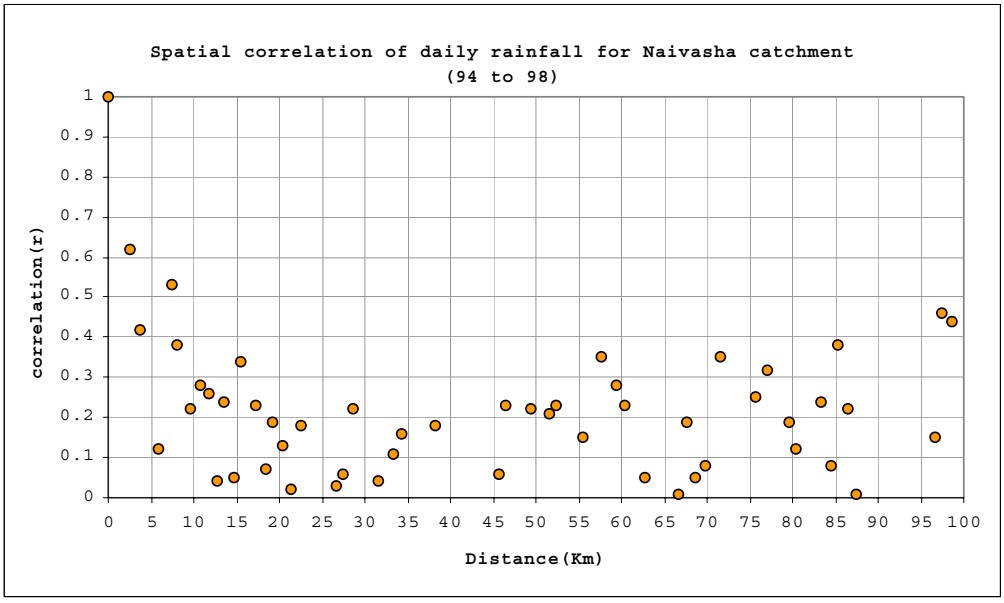

Figure 3.5 Graph, showing the spatial correlation of daily rainfall for the Naivasha catchment using 30 stations for the year 1994 to 1998.

The spatial correlation of the daily rainfall data is less than 50% after 5km.

Remarks: Due to the high nugget effect in almost all the variograms, the high spatial variation of the rainfall and low density of gauge in the region, arithmetic mean and Thiessen polygon can be used to find the area rainfall, see appendix G.

Note: because the variogram shows us the spatial characteristics of the rainfall around the area we use all the 30 stations inside and around the catchment to derive the variogram. But for kriging, we used only 16 stations. 11 stations inside and 5 stations around the catchment. see Fig 3.1.

3.2.5 Calibration for hydrological monitoring

In the hydrological case, the greatest importance is attached to successful estimation of heavy rainfall. Furthermore, for short-medium term flow forecasting daily or decadal data is usually required.(Grimes, Bonifacio and Loftie, 1998):

Preliminary preparation of the CCD images involved the conversion of Meteosat images to Longitude-Latitude projection by the AWK program.

The following scheme was devised to allow decadal or daily estimation on a catchment basis,

• A mask image is created for which each pixel within the catchment is assigned the value 1; each pixel outside the catchment is assigned the value zero. In this study IDRISI, modules INITIAL and POLYRAS were used to create the mask image.

• The decadal (daily) CCD image is multiplied by the mask, and the average value of CCD within the Catchment, $\mathbf{D_{av}}$ calculated. (achieved through Meanpol prog).

• A decadal (daily) average area rainfall value for the catchment $\mathbf{R_{av}}$ is calculated (kriged).

• A linear regression is performed of $\mathbf{R_{av}}$ against $\mathbf{D_{av}}$ to determine the calibration parameter $\mathbf{a_0}$ and $\mathbf{a_1}$ from the relation,

$$R_{av} = a_0 + a_1 \times D_{av} \quad , \text{for } R_{av} > 0,\ D_{av} > 0. \qquad \text{.....(3.14)}$$

Once the parameter $\mathbf{a_0}$ and $\mathbf{a_1}$ are found, rainfall estimates can be calculated from equation (3.14) for any other period. Because the calibration has been performed on non-zero CCD days only, the relationship only applies to the fraction of the catchment with non-zero cold cloud. Thus, if the average CCD over the area covered by cold cloud (the rainy area) is $\mathbf{D'_{av}}$, the average rainfall over the same area is:

$$R'_{av} = a_0 + a_1 \times D'_{av} \qquad \text{.....(3.15)}$$

However for hydrological purposes, (Grimes, Bonifacio and Loftie, 1998): it is convenient to calculate the average rainfall over the whole catchment rather than the average over the rainy area. If the area covered by CCD is **f**, then the average rainfall over the whole catchment is,

$$\begin{aligned} R_{av} &= f(R'_{av}) \\ &= f(a_0 + a_1 \times D'_{av}) \\ &= fa_0 + a_1 fD'_{av} \end{aligned}$$

But $\mathbf{fD'_{av}}$ is the average CCD over the whole catchment (including the zero CCD fraction). Then $\mathbf{R_{av}}$ is,

$$R_{av} = fa_0 + a_1 D_{av} \qquad \text{.....(3.16)}$$

Where: $\mathbf{D_{av}}$ is the average CCD over the whole catchment. Figure3.10 illustrates this procedure.

Derivation of the above constants a_o and a_1 using only area covered by CCD (wet) is preferable, provided that the area is very big in size. In this study, it doesn't matter much which approach is used, since, the Naivasha catchment is very small in size.

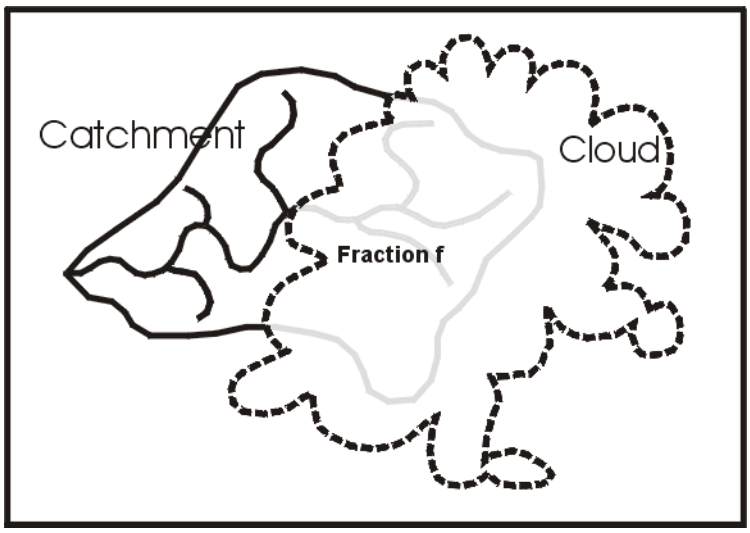

*Figure 3.6 Cold Cloud over the catchment. The intersection of the cloud area and the catchment is the fraction **f** of the catchment covered by cloud. (Modified from NRI-TAMSAT).*

To obtain **f** (the area cover) the following procedure is followed,

- A mask image of each CCD image (already converted to Longitude/Latitude projection) is created. By the module RECLASS in IDRISI, all pixel values of the CCD image greater than 0 (in this case, 1-48), are assigned the value 1.

- The daily CCD image is then multiplied by the catchment mask image, and the mean value of the resultant image is obtained. This gives the daily mean fraction of catchment covered by cold cloud, **f**. (Executed through "Meanpol program").

The calibration is carried out for the wet season of Naivasha. The results of the calibration procedure for the Naivasha catchment is shown in graphical illustration in figure 3.11 and appendix E.

Note: pixel calibration is also carried out for the decadal data just to have some idea of the distribution of rainfall within the catchment. Averaging the resulting rainfall estimate image with a catchment mask would give us a mean amount over the catchment.See, appendix H for the plot.

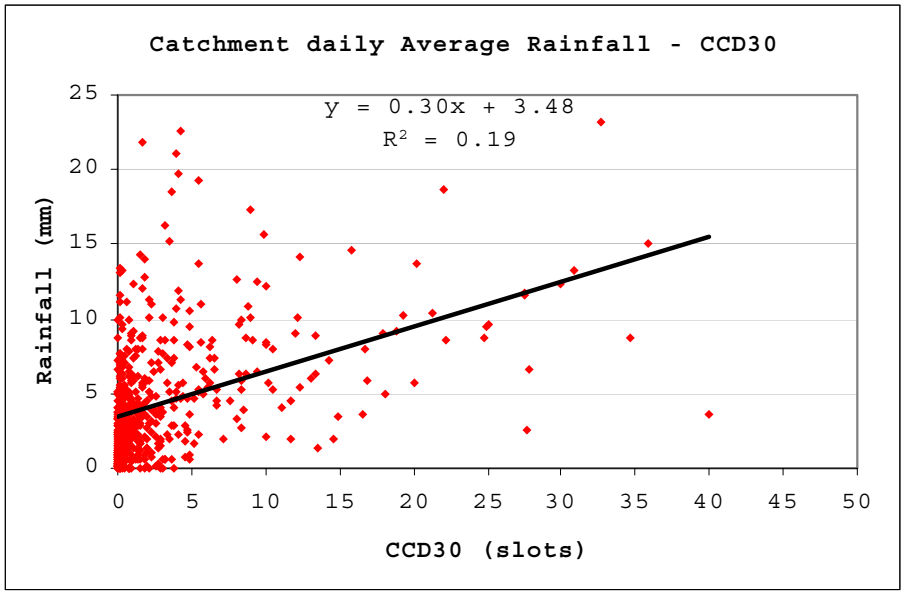

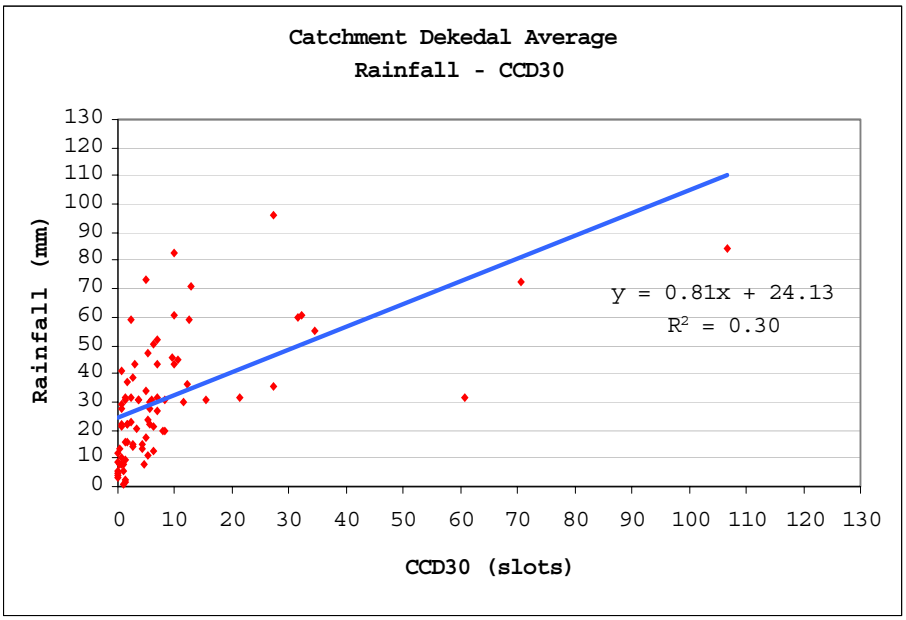

Figure 3.7 Graph showing relation between CCD and rainfall, for daily and decadal rainfall data (1994 to 1998).

CHAPTER 4

4. PRECIPITATION AND CCD CORRELATION ANALYSIS

4.1 Introduction

Besides the sparse distribution of gauges inside the Naivasha catchment, large variation in precipitation over relative short distance contributes to poor correlation.

In the table daily rainfall for a few selected stations are listed.

Table 4. 1 Daily rainfall for a few selected stations, which have large variation as compared to nearby stations.

Date	Station	Recorded value	Near by stations(5-25km) recorded value
07/10/97	9036308	148.5mm	0-5mm
21/04/98	9036308	100.5mm	0-10mm
15/05/95	9036072	93.5mm	0-10mm
12/03/95	9036323	104.6mm	0-10mm

This may show that either the gauge recording may not be very good or that strong convectional rainfall occurs. This causes problem to the calibration (makes it noisy).

As seen in the bias and accuracy presented in chapter three, in this region the cloud produces rain without reaching enough in to the atmosphere to register as "cold" clouds. In such cases rainfall would indeed occur but would not appear in the satellite rainfall estimate image.

All the above problem from CCD image and rainfall data lead us to treat the data in a more detailed statistical approach.

Daily and decadal CCD data for the year 1994 to 1998; the corresponding rainfall data from 30 stations in and around the catchment is also available. Out of 32101 available rainfall data 3647 data are missed, the daily raingauge data is found in the xls file, the decadal data is attached to appendix B.

Using the above data set, it is tried to do the univariate statistics for the raw data. Since the data is not normally distributed.Transformation of the data is executed through Box-Cox transformation.

The regression analysis is applied for the transformed data since in this stage the data already satisfies the regression assumption. It is also shown that there is a significant relation ship between the CCD and rainfall transformed data, then the CCD and kriged rainfall relationship established.

4.2 Univariate statistics on the CCD and rainfall data

It is generally risky to assume the distribution of the data is normal without actually examining some statistical parameters of the data..

The normal distributions provide good models for some distributions of real data In this study it is tried to judge whether the row data is normally distributed or not, by constructing a histogram for both CCD and rainfall data set. (see Fig 4.1) all the data set are not normally distributed.

Table 4.2 Summary result of some descriptive parameters for the raw CCD and rainfall data.

	data type	Mean	Median	Skewness	standard deviation	Maximum	Minimum	Kurtosis
Daily	CCD	3.16	0.91	3.29	5.76	39.94	0.02	12.31
Data	rainfall	4.43	3.48	1.59	4.01	23.16	0.00	3.24
Decadal	CCD	9.42	4.79	3.83	16.56	106.60	0.09	17.45
data	rainfall	32.27	29.68	1.57	24.06	136.14	0.86	3.75

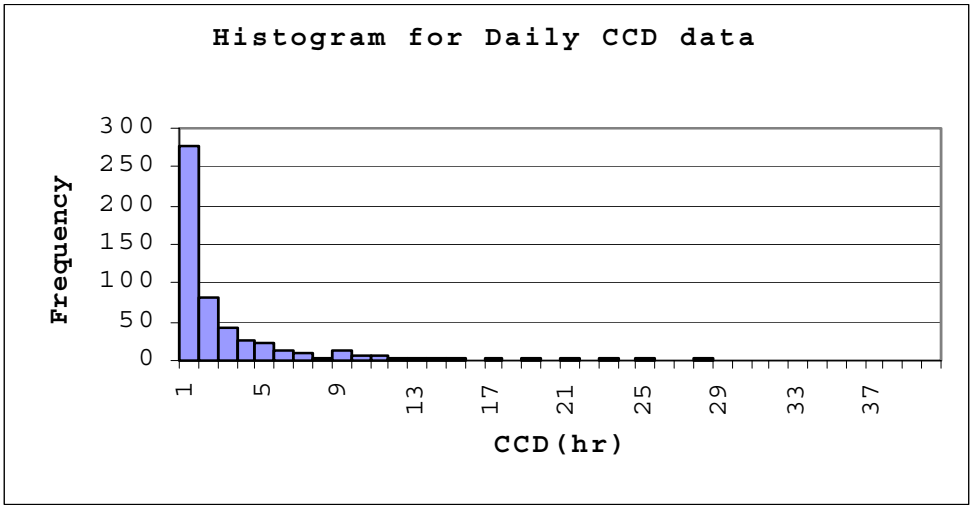

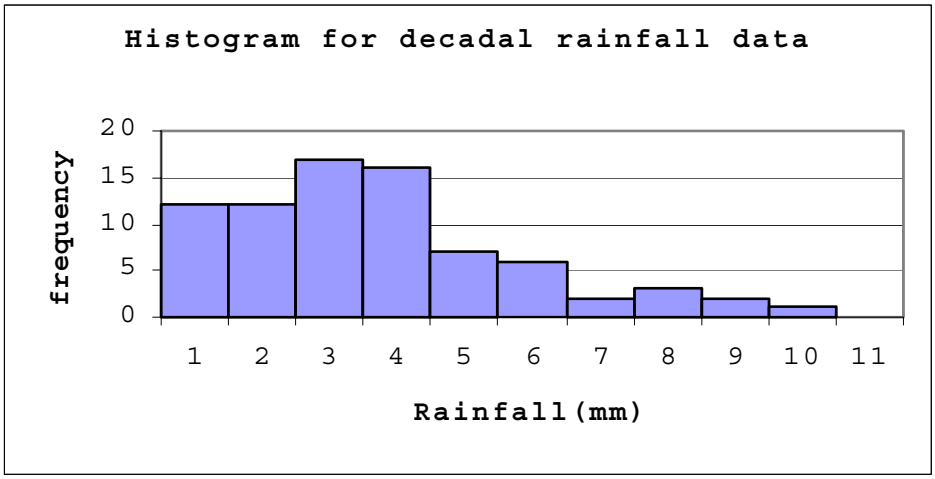

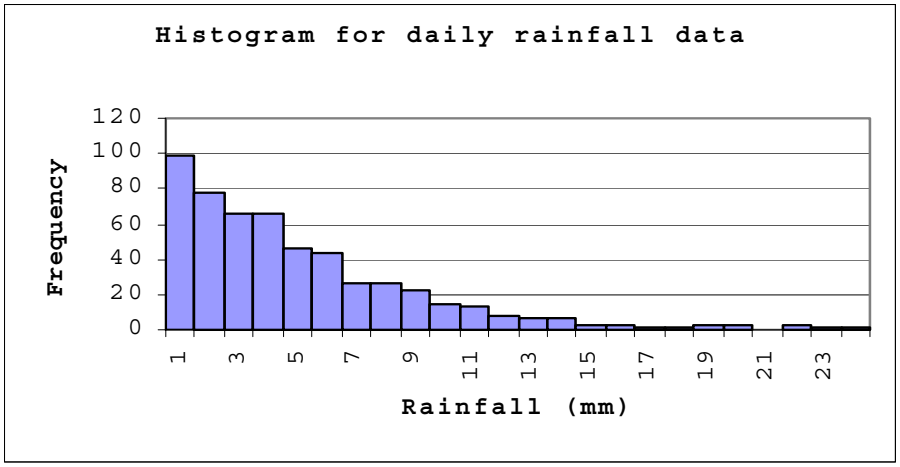

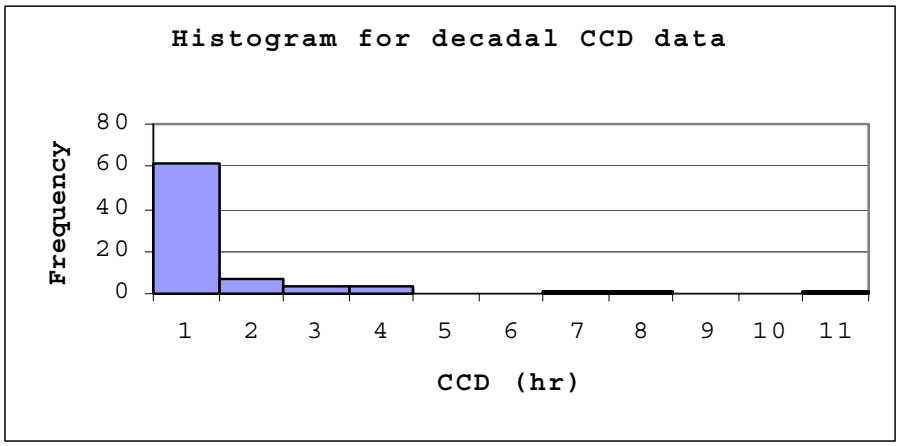

Figure 4.1 Histogram plot which shows that the above data sets are not normally distributed.

4.2.1 Normal Quantile plot

If x is an observation from a distribution that has mean μ and standard deviation σ, the standardized value of x is

$Z = (x-\mu)/\sigma$

A standardized value is often called a z- score

The most useful tool for assessing whether the data is normally distributed or not is the normal quantile plot; it is a plot, which shows the data points x against the corresponding Z score.

Fig 4.2 shows normal quantile plots for decadal rainfall and CCD data, it is shown that there is a deviation from a straight line which indicates that the data are not normally distributed,

the skewness of the distribution on the above summary table indicate that the distribution is right-skewed. In a right-skewed distribution, the largest observations fall distinctly above a line drown through the main body of points.

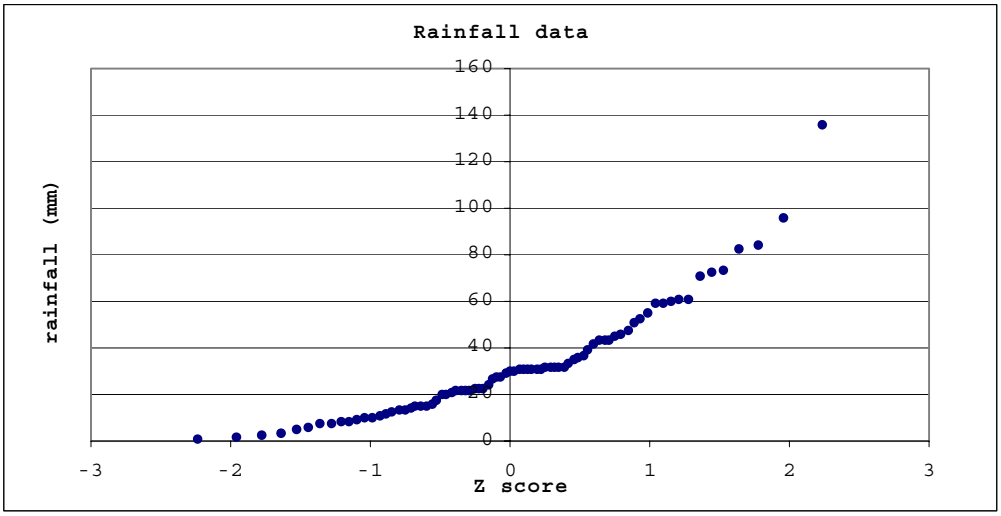

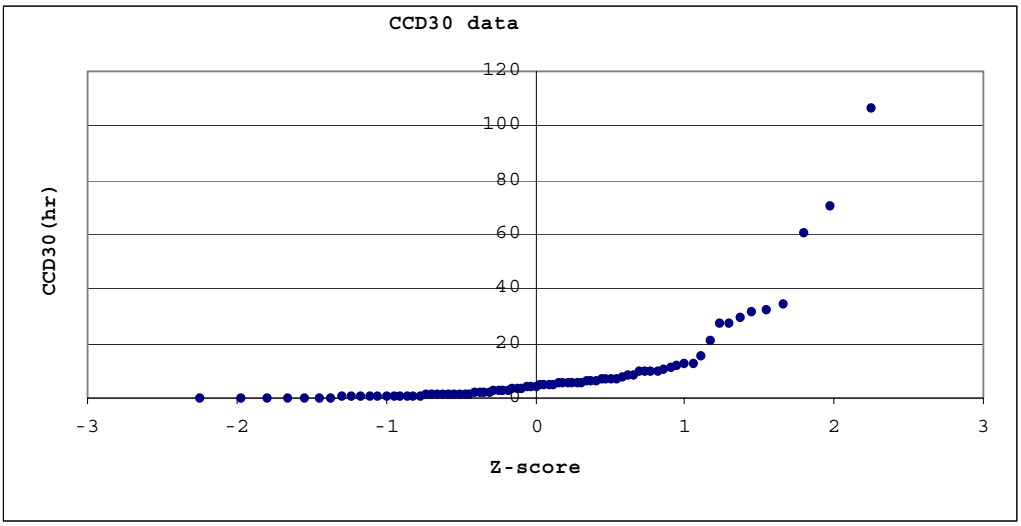

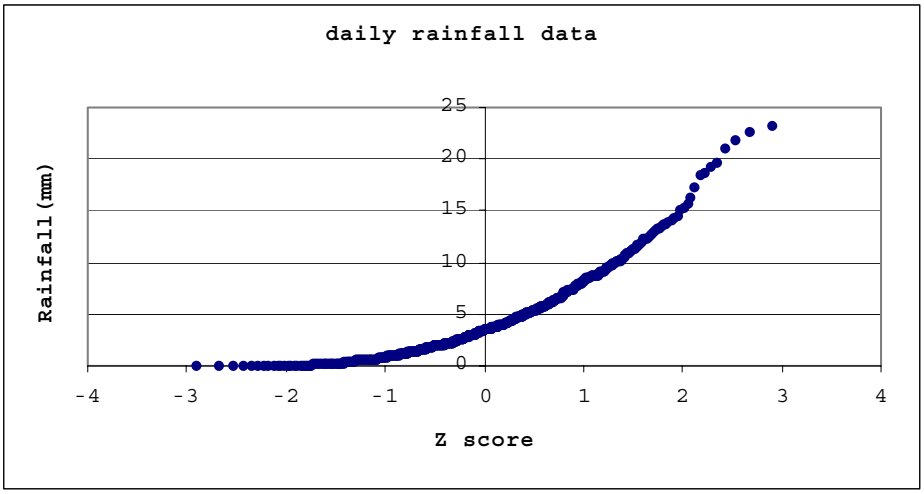

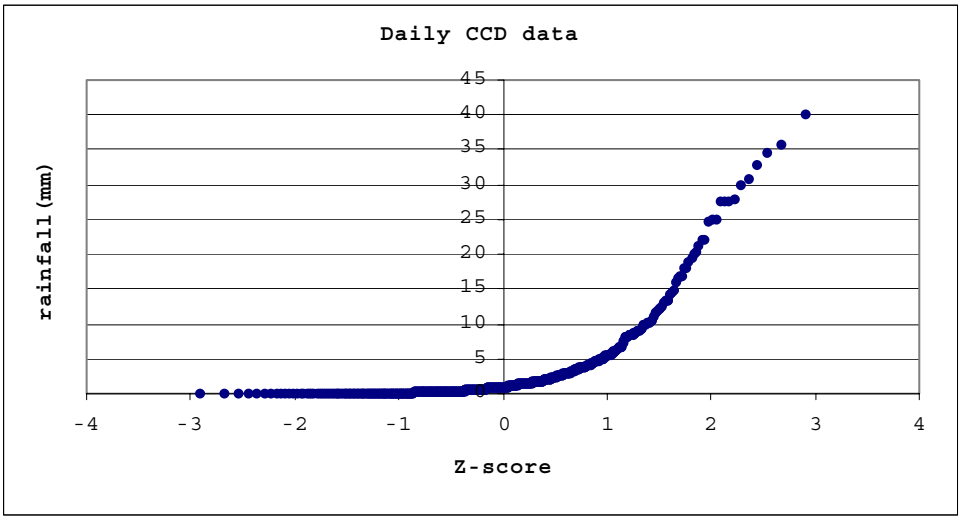

Figure 4.2 Normal probability plots of the data, the pattern bends up at the right for all data type, showing the right skewness of the data.

The distributions are different from normal distribution and positively skewed. This indicates that the assumption of constant standard deviation, or homogeneity of variances is violated, this can cause regression difficult between the two data set.

4.3 BOX-COX transformations

It is possible to improve the above model by applying transformations of the data.

There are really three situations in which transformation of the data may be appropriate in regression analysis. (Cook and Weisberg, 1982); these are: as discussed in (Clarke, 1994)

1.Where the response variable **Y** comes from a family of distributions known to be non-normal. A transformation is selected so that the distribution of the transformed responses is sufficiently near to normal to allow us to use standard methods, based on normal theory.

2. Where the expected response **E (Y)** is related to the explanatory variables **X** by a known non-linear function of the parameters. A transformation is selected to **linearise** this response function;

3.Where neither the distribution of error nor the functional form of the relationship between **E (Y)** and **X** is known. This situation is the most difficult to handle since a specific rationale for choosing a transformation is lacking. Generally, we would like a transformation to result in a model with constant error variance, approximately normal errors, and a systematic component $\mathbf{X\beta}$ which is easily interpreted in hydrological terms.

One method of proceeding in case 3 is to specify a family of transformation **R (P),** with parameter **P**. We then use the data to select which transformation **R (P)** of the family is most appropriate, in the sense that it yields a model $\mathbf{R(P) = X\beta+\varepsilon}$ having all the desirable properties. (Clarke, 1994).

One such family of transformation is the **Box-Cox** family; which finds transformation to **maximize correlation** between two variables; it is defined by,

$$R_T = (R^P-1)/P \quad \text{when P is non zero}$$
$$= \log R \quad \text{when P is zero}$$

In this case, **R** is rainfall, which is being transformed; R_T is the transformed variable.
P is transformation variable parameter, usually in the range between 2 and –2.

The transformation is carried out by varying **p** until the skewness of the transformed data becomes zero.

Table 4.3 The assumed values for the transformation variable parameter

	P for kriged rainfall	P for CCD
Decadal data	0.35	0.35
Daily data	0.21	0.21

The normal quantile plot is constructed between the transformed data and the
Z score including the histogram. The straight pattern for all the data shows that the distribution of the data after transformation is close to normal, the same is true for the histogram, which shows approximately normal distribution for the entire data set.

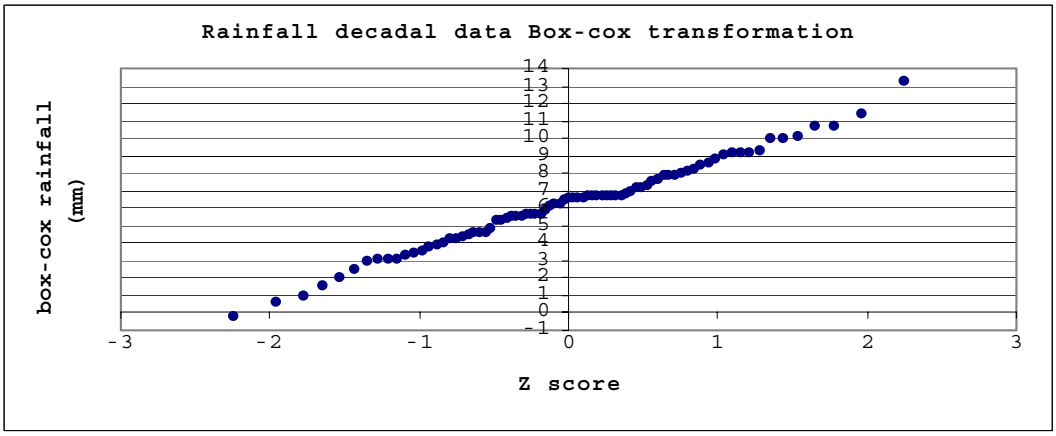
Rainfall decadal data Box-cox transformation
box-cox rainfall (mm)
Z score

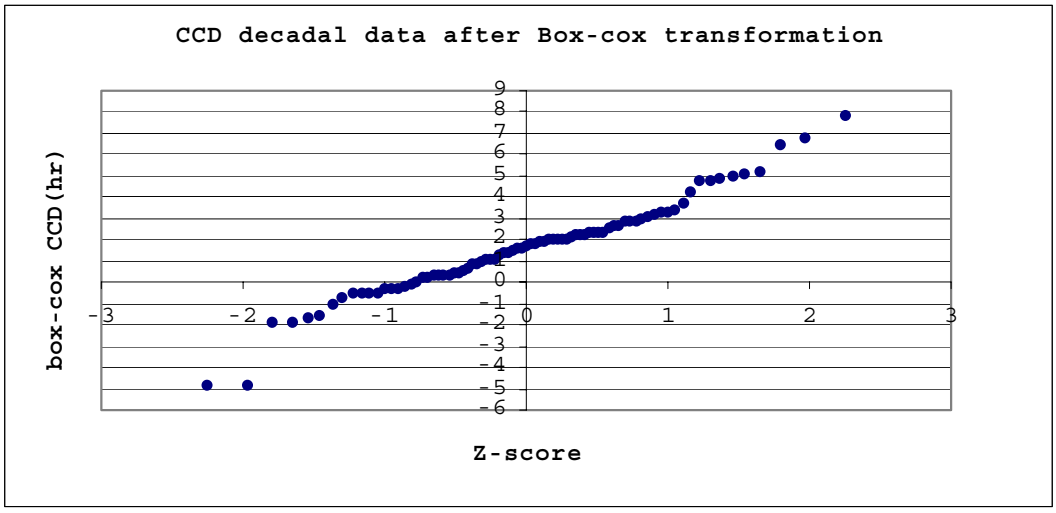
CCD decadal data after Box-cox transformation
box-cox CCD(hr)
Z-score

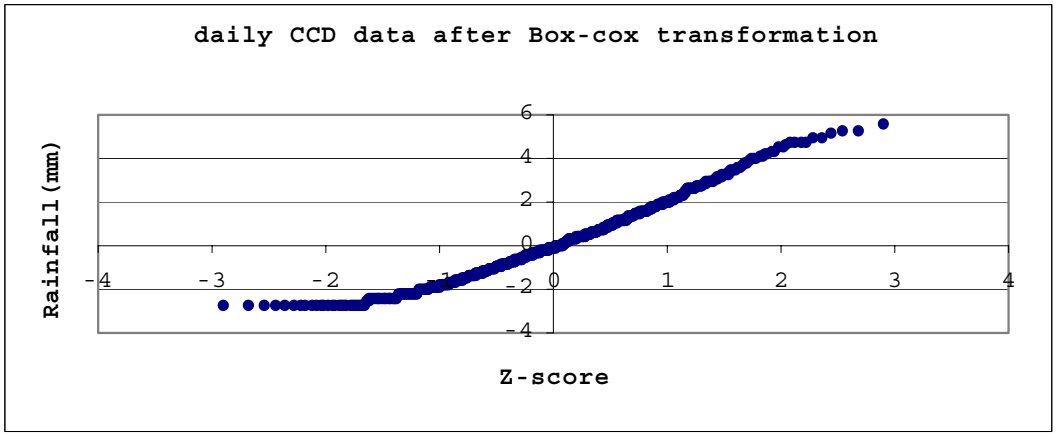
daily CCD data after Box-cox transformation
Rainfall(mm)
Z-score

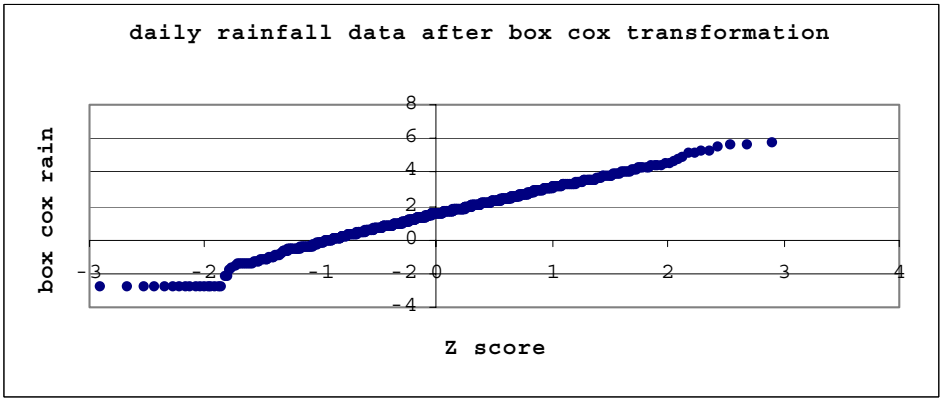

Figure 4.3 Normal probability plots of the rainfall and CCD data. The straight pattern shows that this distribution is close to normal. There are also low outliers in CCD and rainfall data plot.

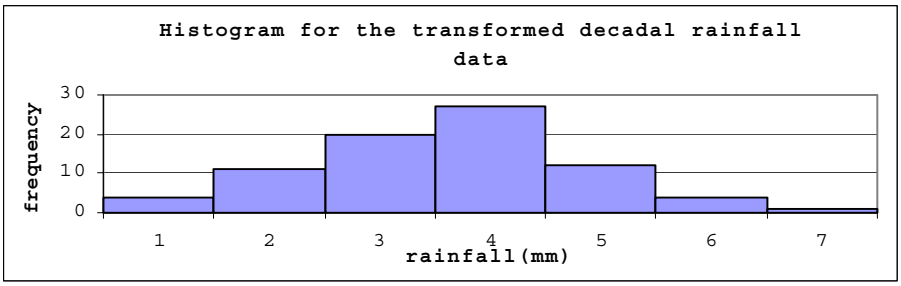

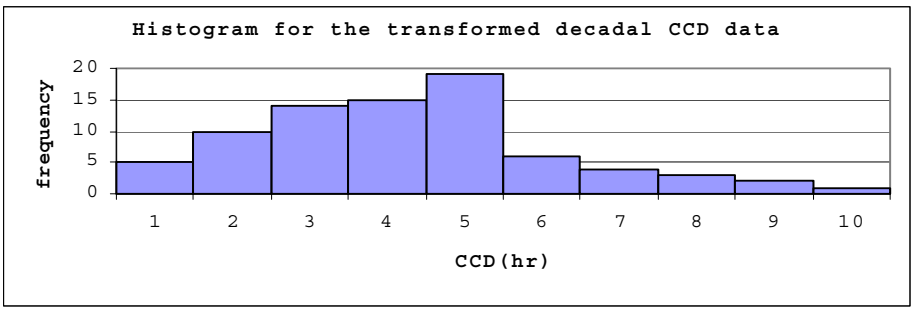

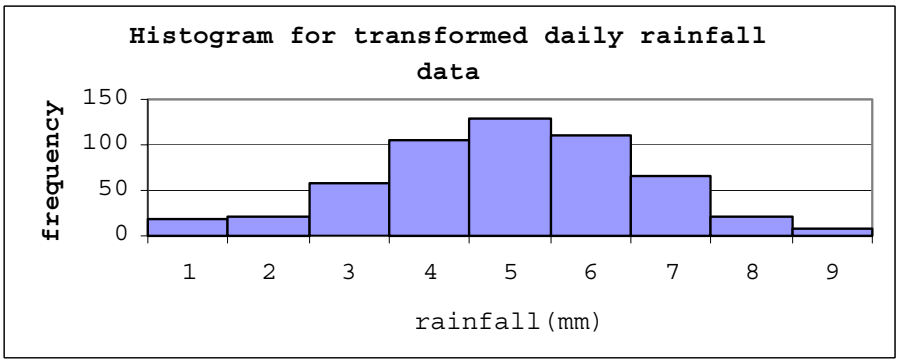

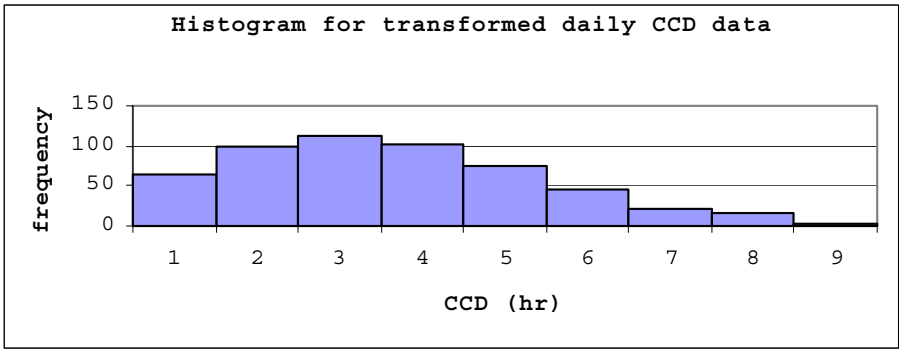

Figure 4.4 Histogram of the transformed data showing approximate normal distribution.

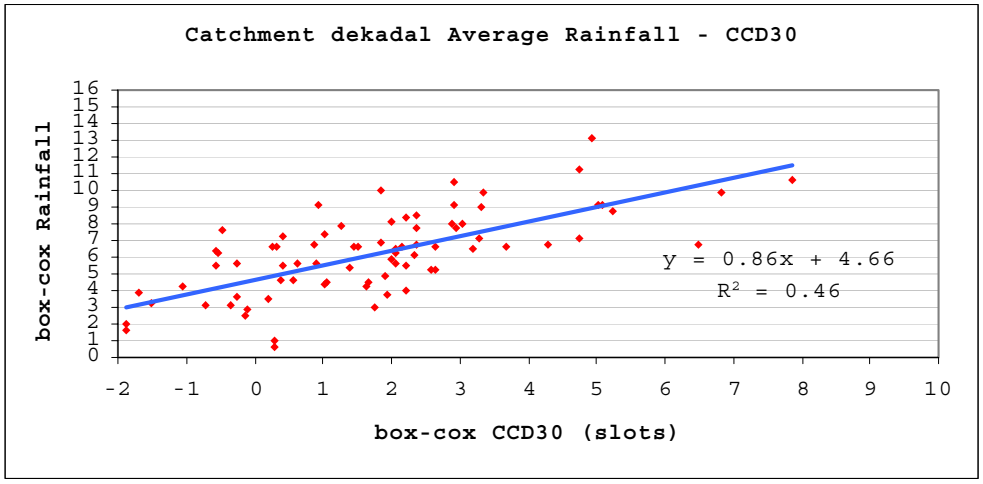

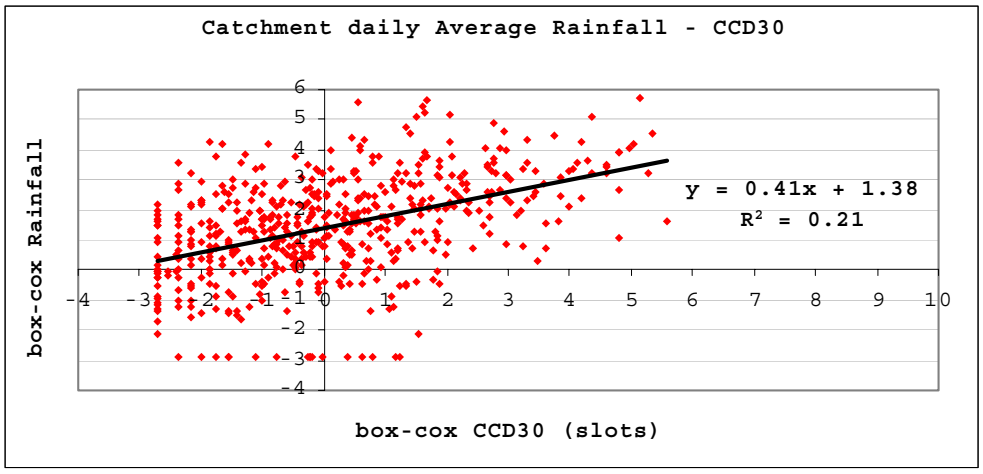

Figure 4.5 Graph showing the relation between CCD and rainfall data after Box-Cox transformation for decadal and daily data.

The plot of the transformed data indicates a better fit than the original data. In addition, the variability of the data across the horizontal range of the plot seems relatively constant, which satisfy the assumption of homogeneous variances.

4.4 Regression analysis and hypothesis testing

Using the Naivasha rainfall data set (30 stations, 1994 to 1998) and the CCD values extracted, regression analysis is applied for both daily and decadal transformed data.

Given **n** observations on the explanatory variable **x** and the response variable **y,**

$$(x_1,y_1),\ (x_2,y_2),(x_n,y_n)$$

The statistical model for simple linear regression states that the observed response y_i when the explanatory variable takes the value x_i is

$$Y_i = \beta o + \beta_1 x_i + \varepsilon_i \quad \text{.....4.1}$$

Here $\beta o+\beta_1 x_i$ is the mean response when $x = x_i$. The deviation ε_i are assumed to be independent and normally distributed with mean 0 and standard deviation σ.

The parameter of the model are βo, $\beta_1 x_i$ and σ. (David and Gorge, 1998).

From the equation for the regression line $\mu_y = \beta o + \beta_1 x$, βo is the mean response corresponding to x = 0. On the other hand, the test Ho: $\beta_1 = 0$ is useful, when we substitute $\beta_1 = 0$ in the model, the x term drops out and we are left with $\mu_y = \beta o$, this means that in this model the mean of y does not vary with x.

The hypothesis H_0: $\beta_1 = 0$ therefore says that there is no straight-line relationship between y and x and that linear regression of y on x is of no value for predicting y.

In this study it is tried to do the above hypothesis using t test statistics using 95% confidence interval.

A confidence interval for the intercept is $b_o \pm t^* SE_{b_0}$

A confidence interval for slope is equal to $b_1 \pm t^* SE_{b_1}$

In this expression t is the value for the t (n-2) density curve with area of the curve between -t and t, and can estimated as

SE_{b_1} is the standard error of the slope b_1

$$SE_{b_1} = \frac{S}{\sqrt{\sum (x_i - x)^2}} \quad \text{.....4.2}$$

SE_{b_0} is the standard error of the intercept b_o

$$SE_{b_0} = S\sqrt{\frac{1}{n} + \frac{x^2}{\sum (x_i - x)^2}} \quad \text{.....4.3}$$

To test the hypothesis Ho: $\beta_1 = 0$ we compute $\mathbf{t = b_1 / } SE_{b_1}$

Where:

S is estimated standard deviation

$$S = \sqrt{\frac{\sum e_i^2}{n-2}} \quad \text{.....4.4}$$

e_i = the residuals = $y_i - \hat{y}_i$

x and $\hat{y}$ are the mean of the data

n number of data

The degree of freedom is n-2. Interms of a random variable T having the t (n-2) distribution, the probability value for a test Ho against the two sided alternative is

Ha: $\beta_1 \neq 0$ is 2P ($T \geq |t|$)

The probability-value corresponding to t statistics in table 4.4 shows that there is strong evidence against the null hypothesis for the above transformed daily and decadal plot. So we may conclude that linear regression on CCD measure is useful for predicting rainfall for both daily and decadal data.

Table 4.4 Summary of t statistics for the transformed rainfall and CCD data.

Decadale Regression Statistics						
Multiple R	0.68					
R Square	0.46					
Adjusted R Square	0.46					
Standard Error	1.86					
Observations	79					
	Coefficients	*Standard Error*	*t Stat*	*P-value*	*Lower 95%*	*Upper 95%*
β_0	4.66	0.28	16.59	4.E-27	4.10	5.22
β_1	0.86	0.11	8.13	5.64E-12	0.65	1.07
Daily Regression Statistics						
Multiple R	0.45					
R Square	0.21					
Adjusted R Square	0.21					
Standard Error	1.48					
Observations	540					
	Coefficients	*Standard Error*	*t Stat*	*P-value*	*Lower 95%*	*Upper 95%*
β_0	1.38	0.06	21.61	5.13E-75	1.26	1.51
β_1	0.41	0.03	11.84	6.44E-29	0.34	0.48

4.5 Estimation of rainfall from CCD

It is clear that the relation between CCD and precipitation is poor for daily data The improvement in correlation coefficient in decadal data is quite notable. On decadal bases the correlation coefficient reaches 0.68. The standard error (the standard deviation of the rainfall about the regression line, and is given by equation 4.4) is 1.86mm on the average for the decade. For daily data the correlation coefficient is 0.45, the standard error is 1.48mm.See table 4.4, for the detail of regression analysis.

Finally the calibration plot is constructed between the rainfall and the CCD data after the rainfall is estimated in terms box-Cox transformed CCD data, See Fig 4.5 for decadal and daily calibration plot.

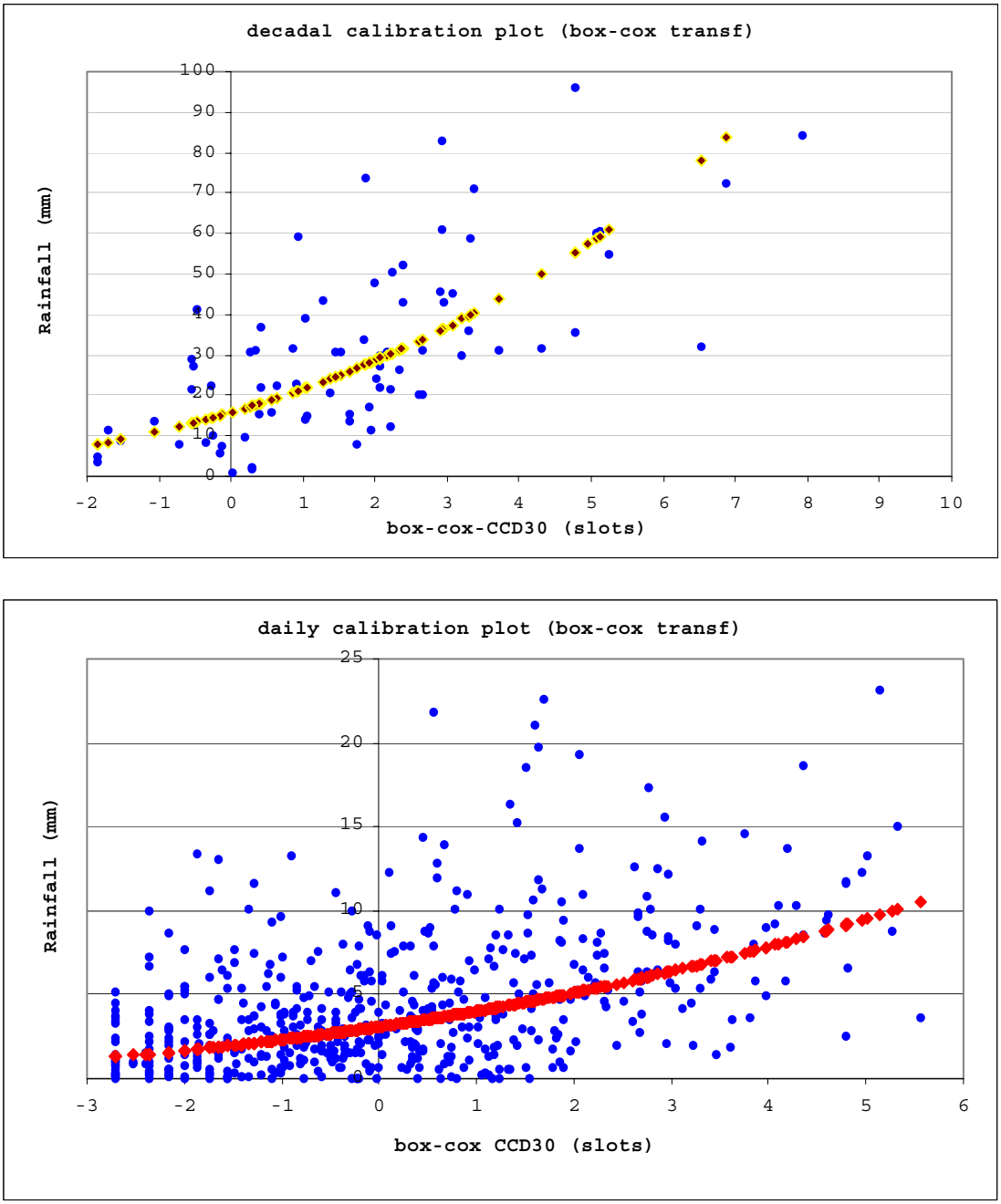

Figure 4.6 Calibration plot, the estimated rainfall is in terms of Box-Cox transformed CCD data.

In Fig4.5 the regression line between the already transformed CCD and rainfall data is presented, so the equation for these graphs have the form:

$$R^* = a_o CCD^* + a_1 \quad \text{.....4.5}$$

Where:

$\mathbf{R^*}$ is the transformed rainfall data, which is equal to

$$R^* = (R^{Pr} - 1)/P_r \quad \text{.....4.6}$$

R is the rainfall data before transformation (the raw data).

$\mathbf{P_r}$ is transformation variable parameter, is equals to **0.35** for both daily and decadal rainfall data.

$\mathbf{CCD^*}$ is the transformed CCD data, which is equals to

$$CCD^* = (CCD^{Pccd} - 1)/P_{ccd} \quad \text{.....4.7}$$

CCD is the Cold Cloud duration data before transformation (raw data), and here

$\mathbf{P_{ccd}}$ is equals to **0.21** for both daily and decadal CCD data.

Combining equation 4.4 and 4.5

$$(R^{P_r} - 1)/P_r = a_o CCD^* + a_1$$

The equation of the line for the calibration plot which is presented on Figure 4.4 become

$$R = \{[a_o CCD^* + a_1] * P_r + 1\}^{1/Pr} \quad \text{.....4.8}$$

We can further expand the above equation in the form of the following

$$R = [\{[a_o((CCD^{P_{ccd}} - 1)/P_{ccd}) + a_1]\} * P_r + 1]^{1/Pr} \quad \text{.....4.9}$$

Assume

$$[a_o((CCD^{P_{ccd}} - 1)/P_{ccd}) + a_1] = K$$

Estimated rainfall become:

$$R = [K * P_r + 1]^{1/P} \quad \text{.....4.10}$$

So before we estimate the rainfall from CCD, the CCD data has to be transformed, using Box-Cox transformation.

4.6 Deviation assessment

Following the poor correlation between CCD and rainfall some assessment is done just to have an overview of the deviation between actual and estimated rainfall and to discern where the maximum error occurs, see Fig 4.5 and 4.6 and see appendix F for the calculation.

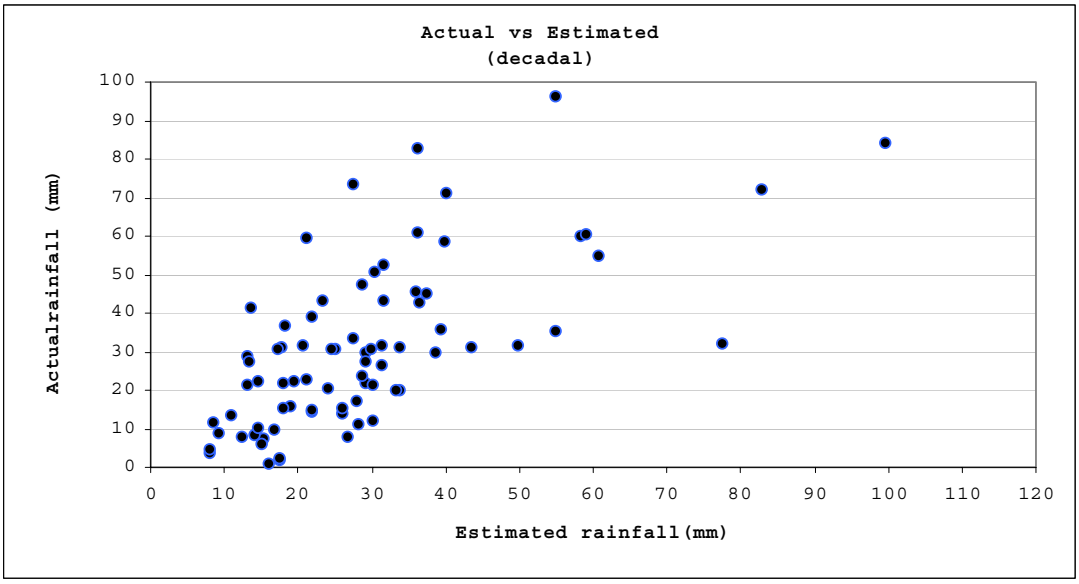

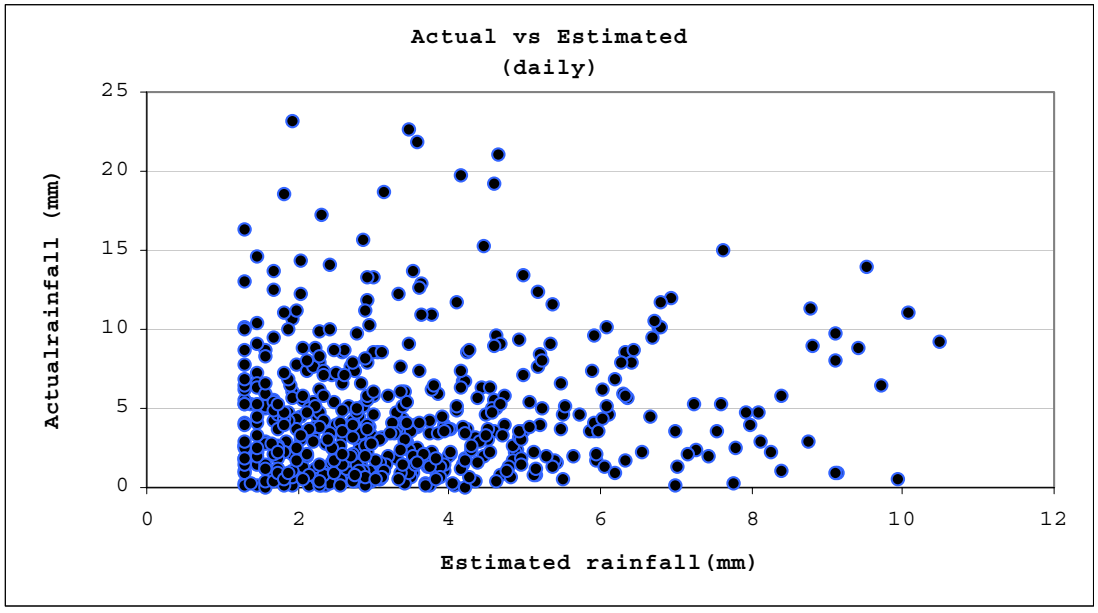

Figure 4.7 Graph showing actual rainfall Vs Estimated rainfall (decadal and daily data, 1994 to 1998).

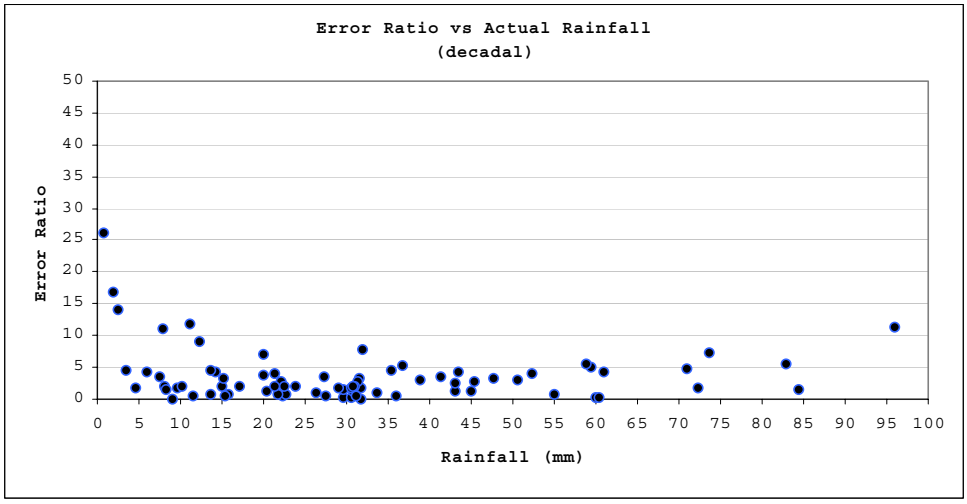

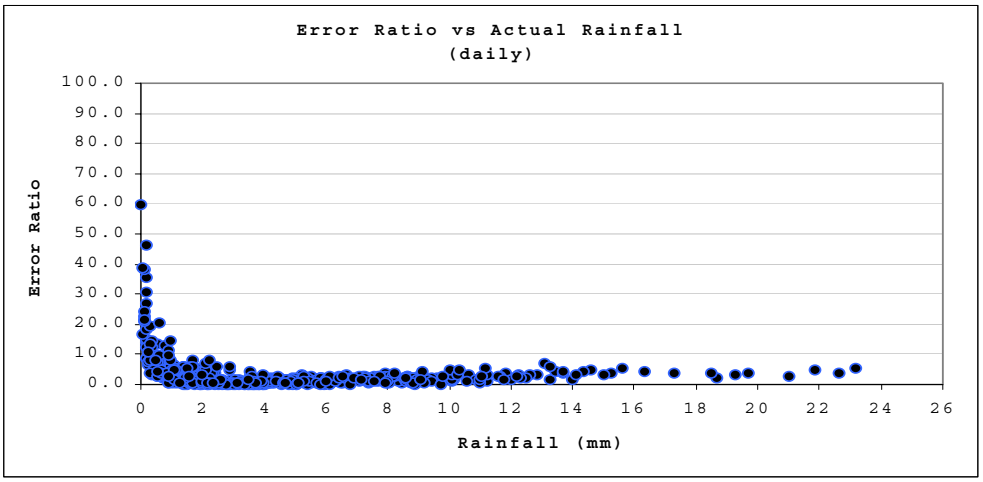

Figure 4.8 Graph showing error ratio (ratio between absolute and actual error) Vs actual rainfall (decadal and daily data, 94 to 98).

Absolute error = ABS (estimated rainfall-actual rainfall).
Actual error = error calculated by kriging.
If we draw a straight line Y = X on the scatter plot of fig 4.5, we find almost equal amount of underestimate and overestimate values showing the estimated rainfall is unbiased.

Actually notable error also occurs for the value between 0 to 1 mm for daily and 0 to 5mm for decadal data, otherwise the estimated value doesn't have notable error as compared to the actual rainfall.

4.7 Discussion of the result

It is shown that the CCD and rainfall data are not normally distributed. To satisfy the assumption of regression model between the two data points, the data were transformed using Box-Cox transformation. Consequently the correlation between rainfall and CCD data remarkably improved, the hypothesis testing also proves that linear regression on CCD measure is useful for predicting rainfall.

The calibration plot is constructed between the actual rainfall and the Box-Cox transformed CCD data and the equation of the line between these two data set is presented in equation 4.8.

As seen on the calibration plot which is presented above, there are data points which are deviated far away from the estimated rainfall line.The reasons for such discrepancies between ground based and estimated rainfall amounts may be manifold: among these, the following are common.

1. Raingauge do not always properly measure the actual rainfall amount reaching the ground. Differences up to 30% have been reported. (Huygen, 1989).

2. Because of the spatial and temporal variability of rainfall in the area, precipitation can not be determined accurately by means of interpolation (kriging). This error is caused by low density and heterogeneous distribution of rainfall stations as well as by inaccuracies in the measurement themselves. See Fig 1.3, 3.4, and 3.5. Moreover it is generally accepted that altitude is the main variable, governing the spatial distribution of rainfall in areas of complex topography. The area that has been selected for this study has a complex topography, but the daily or decadal rainfall data for the Naivasha catchment are not correlated with the altitude values. For this reason orographic effect were not considered in this study. See appendix H for annual rainfall and altitude relation.

3. Satellite TIR images are used to distinguish raining cloud from non- raining cloud on the basis of there observed cloud top temperature. This is because it is assumed that all rain comes from deep convective clouds with cold, high tops. However, even in the tropics there is some variability in the type of clouds, which produce rain. In particular, regions near the coast or in mountainous area (like, Naivasha) may experience rainfall from clouds, which have not formed from vigorous local convection. Consequently they do not reach high enough in to the atmosphere to register as "cold" clouds. In such cases rainfall would indeed occur but would not appear in the satellite rainfall estimate image. (Grimes, Bonifacio and Loftie, 1998). The contingency tables which is presented in chapter 3 reveals the above problem with the satellite data, for most months the bias is nearly always below 1.0. This means most of the time the rainfall events are not detected by the satellite.

The reverse is true for cirrus clouds; such clouds appear as very cold to the satellite and therefore would indicate the presence of rain, although infact the clouds are not enough for rainfall to develop.

4. Lack of a direct physical connection between the observed radiance and the precipitation-sized drops falling at the surface (indirect measurement of rain) also contributes to the discrepancies between CCD and rainfall.

CHAPTER 5

5. Runoff response to CCD, rainfall and estimated rainfall events

5.1 Introduction

After rainfall falls on the earth, it evaporates, infiltrates or lies in the depression storage. When these losses become surplus flows, and thresholds are exceeded, runoff is generated over the surface to the nearest stream channel.

With an adjusted and well-measured rating curve (curve between stage and discharge on the same section of the river) the daily gauge reading can be converted directly to runoff volume.

Daily runoff hydrographs including CCD30, kriged rainfall and estimated rainfall are presented in Fig 5.2 and 5.3.

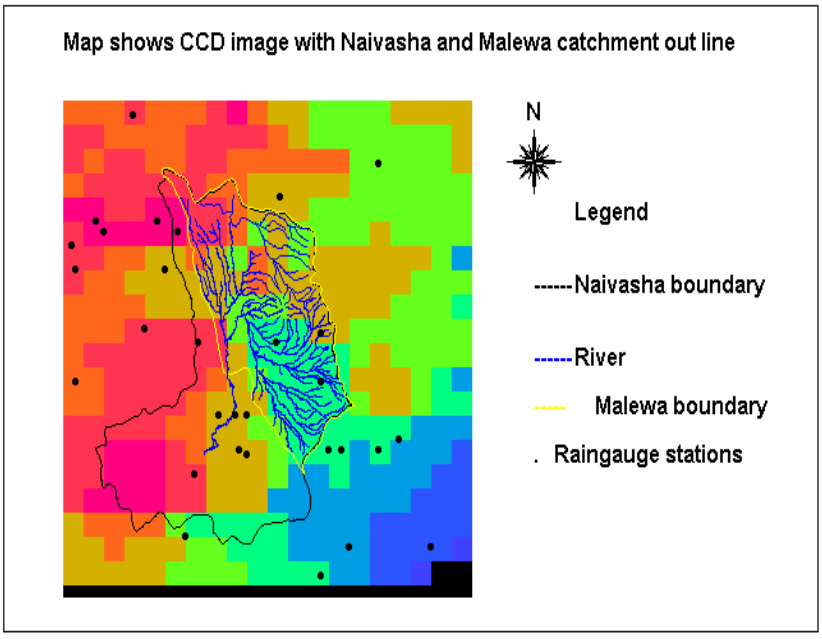

Figure 5.1 CCD image with Naivasha and Malewa catchment outlines including rain gauge stations.

5.2 Hydrology of the catchment

The main river in the Malewa catchment is the Malewa River; it has a number of tributaries, contributing to the discharge at the outlet of the catchment. (Fig 5.1).

The low relative humidity and the average daily temperature 24°C in the area combine to cause an annual potential evapotranspiration of 1500-1900mm/year (Trottman, 1998)

The rainfall pattern in this area is bimodal; the rainy seasons are typically from March to June (long rainy season) and from October to December (short rainy season).

5.3 Data analysis

5.3.1 Qualitative analysis

Due to the lack of discharge data for the period 1994 to mid 1997 for which the TAMSAT have been obtained, the analysis for this period could not be done.

Year 1997 short rainy season (October to December) and 1998 long rainy season (March to June) daily discharge data at the outlet of Malewa catchment and the corresponding CCD, rainfall data and estimated rainfall are used in the analysis of examining the cause and effect relationship between the events and the response. The result for the above two time periods is presented in the form of graphs below (Figs 5.2 and 5.3).

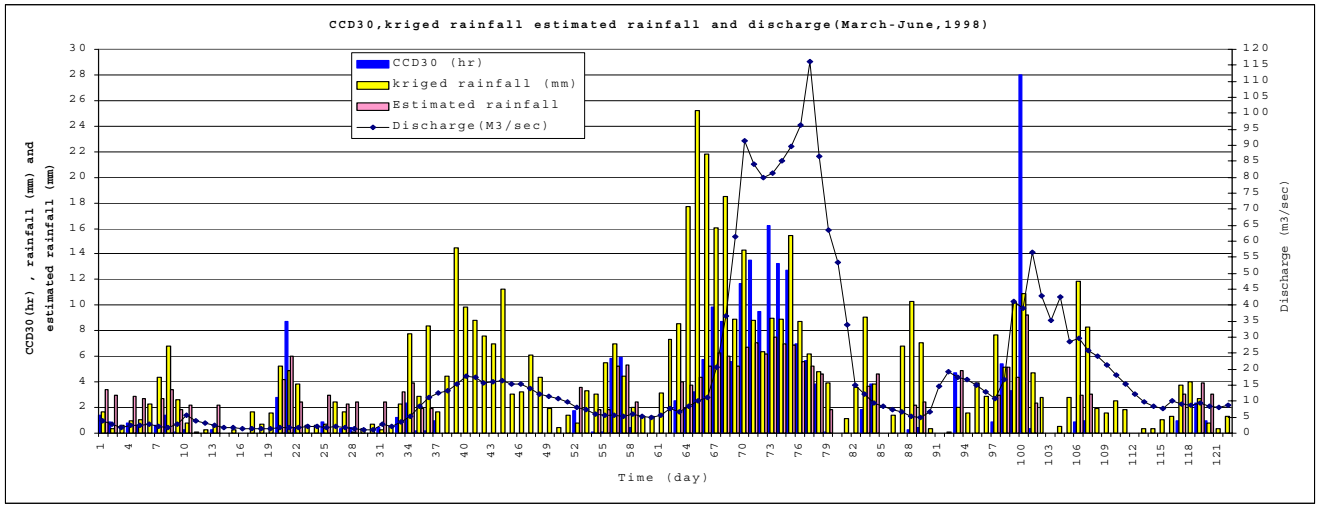

Figure 5.2 Runoff response at the outlet of Malewa for CCD, rainfall and estimated rainfall event (long rainy season 1998).

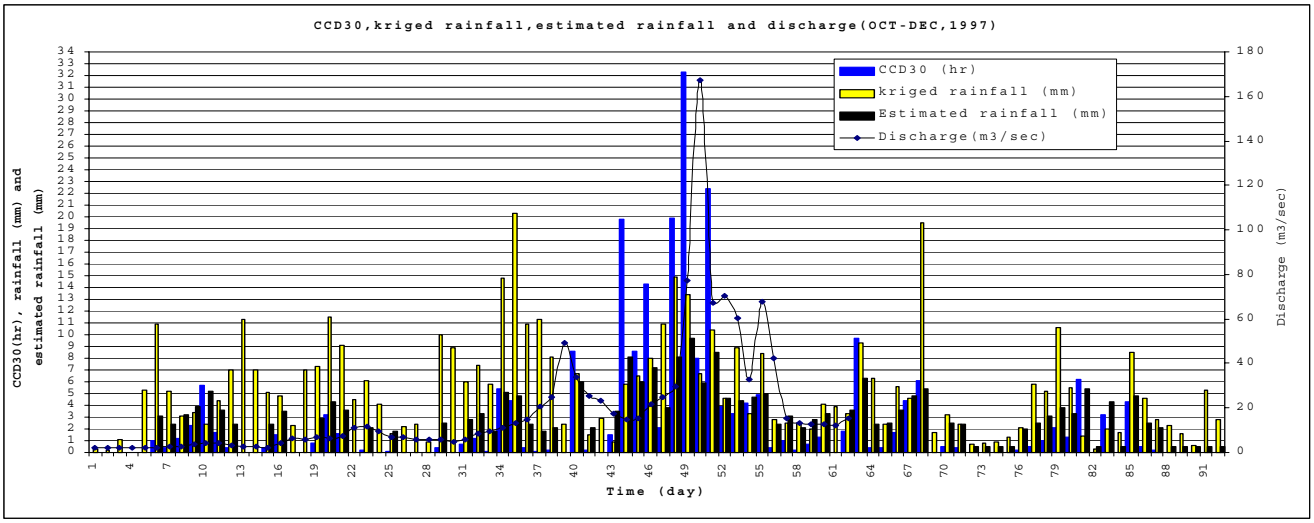

Figure 5.3 Runoff response at the outlet of Malewa for CCD, rainfall and estimated rainfall event (short rainy season 1997).

In fact it is difficult to evaluate the above graphs in this condition because most of the CCD data are missed and invalid, consequently it is difficult to say which event is best fit for the observed response. However, there is a cause and effect relationship between the events and the response even if it is difficult to know the exact lag between the events and the response.

There are also some discrepancies between the events and the response; it is tried to analyze these discrepancies by examining the CCD images on the date when these discrepancies occurred.

5.3.2 CCD image analysis

IMAGES: (refer to Table 5.1 and Figs 5.2, 5.3 and 5.4)

- L3L: it is the date when large CCD and very small response recorded. Large value of CCD are recorded at those pixels which are found at the most remote point of the catchment, so may be it takes time to see the corresponding response at the outlet of the catchment. The same may happened at KAA. (Fig 5.4).

- L68: large CCD small response. Those pixels, which are very near to the catchment, have small value of CCD and we may only see the response of these pixels with small lag time.

- L5C: CCD and large response, here most of the CCD pixels have average values.What this may show us is that possibly CCD has missed the rainfall event at this time, the opposite is happened at the date KBD is called False alarm rate.

Generally looking at the value of CCD on a pixel scale gives us a detailed overview distribution of rainfall within the catchment; the above daily images also indicate the problem of averaging CCD values over the area.

Table 5.1 Table showing naming convention with the corresponding dates.

Image	Julian day	Date
KAA	10	10/10/97
KBD	44	13/11/97
KBI	49	18/11/97
L3L	21	21/3/98
L5C	73	12/5/98
L68	100	8/6/98

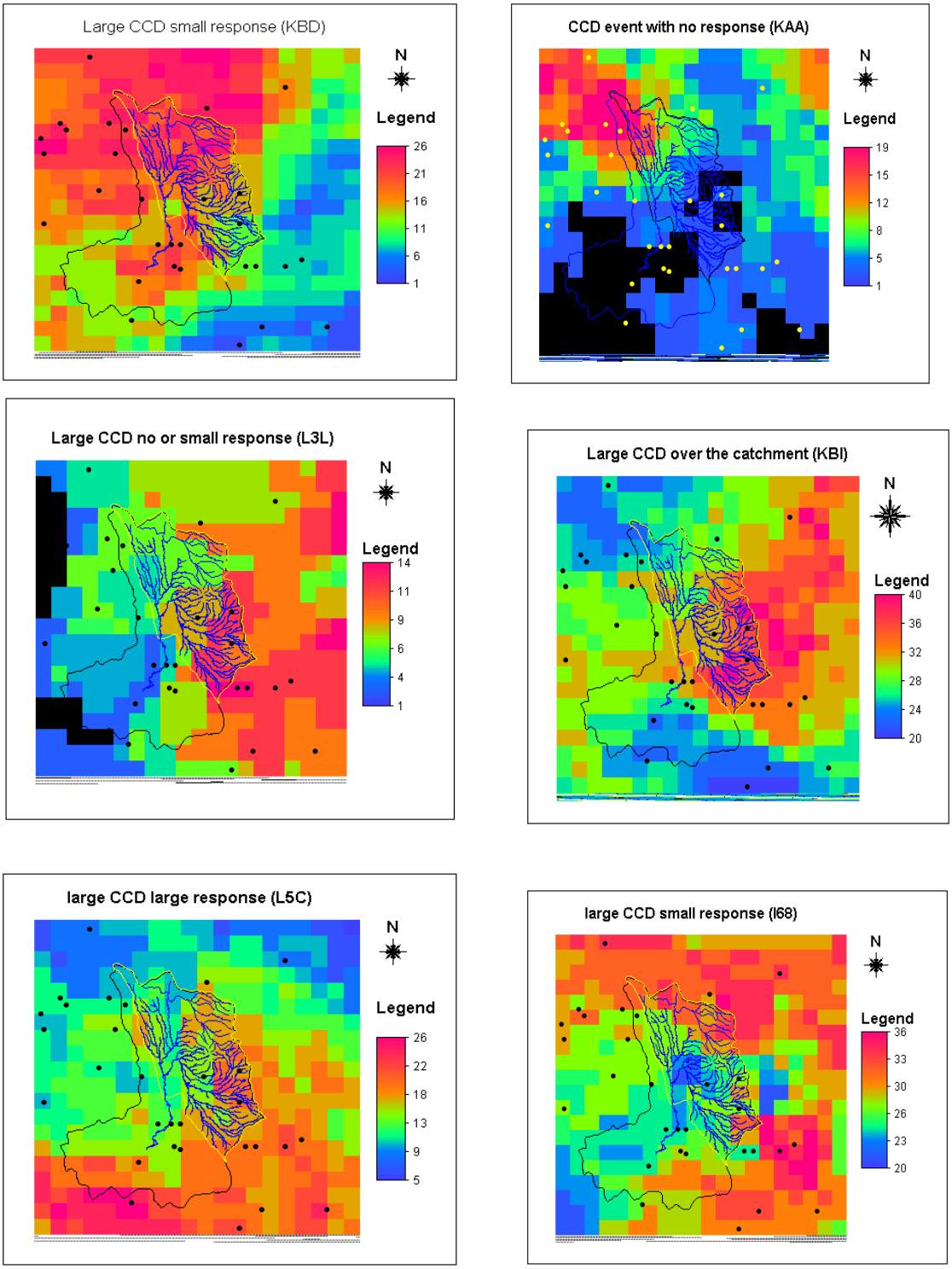

Figure 5.4 Daily CCD images for the date large discrepancies between the event and the response recorded.

5.4 Discussion of the result

In attempting to describe the rainfall event response process, one must keep in mind the possibilities that

- The water identified as the response to a given event may originate on only a portion of the watershed. That portion is called the contributing area.
- At least some of the water identified as the response to a given event may be "old water" that entered the watershed in a previous event. (Dingman, 1994).

Depending on the climate and the transmissivity of the aquifer bordering the stream, the lag between rainfall and runoff may extend to periods of days or weeks. (Wilsson, 1990).

Because the Malewa river is perennial it is always fed by base flow, even with a low dry season, and there may be a bank storage which flows into the river even in the absence of rain, that is why we may encounter a base flow throughout the season.

On the other hand there are dates when the CCD is high with very small response, this may be due to the high permeability of the soil in the catchment and high evaporation after rain to evaporate the water which is already available at a shallow depth below the surface.

There are also dates when there is quick responses to the event CCD this is may be due the presence of " old water " that entered in the watershed before this event.

CHAPTER 6

6. CONCLUSION AND RECOMMENDATION

6.1 Conclusions

In the thresholding technique the TAMSAT approach is a simple method to derive CCD within reasonable time scale. Moreover, it is automated and easy for operational application.

A statistical (Kriging) estimation technique for areal estimation is plausible, because this technique provides a mean rainfall over an area and an associated standard deviation. These values allow a better comparison of rainfall and satellite data.

The area of the Naivasha catchment is about 3200km^2 and the pixel size of the METEOSAT is 25km^2, only 128 pixels, nearly 11*11 pixel square area which is very small and very difficult to compare cloud and rain using only these pixels.

In the study area there are quite a few huge rainfall amount differences between even fairly nearby gauges. However, the bottom line is that in this region the satellite doesn't have much power to properly discriminate rainfall and in particular it misses a fair number of rainfall events, see the contingency table presented in chapter three, for most months the Bias is nearly always below 1.0. This means more than half of the rainfall events do not detected by the satellite. We would need a warmer threshold of CCD (say -20°C, which isn't available) to catch them.

It was shown that the relation between rain and CCD notably improved for the Box-Cox transformed variables, consequently the calibration plot has been carried out between rainfall and transformed CCD variables, this implies that the relation between rain and CCD is non-linear.

Hence trying to fit a linear relationship between the untransformed variables would be an error in this case.

Due to lack of CCD data for the year 1998 long rainy and 1997 short rainy season, it was difficult to compare the runoff response from CCD estimated rainfall and kriged rainfall events. Hence it is difficult to say the rainfall-runoff relation is improved in the case of CCD estimated rainfall.

The present study has shown that METEOSAT data and the TAMSAT method are valuable supplementary tools in assessing rainfall and runoff characteristics in remote areas where rainfall data are scarce.

6.2 Recommendations

If convective clouds can be identified with TIR data, and if there is a direct connection between the observed radiance and precipitation sized drop, a reasonable estimate (not measured) of rain could be made. So systematic attention should be paid to the refinement of existing technique so that general biases, special local regional factors, etc. may be recognized and accommodated.

A combination of satellite data and rainfall data will still be necessary for a comparison, since the constant a_o and a_1 depend on season.

It is better to test the method with more data (and a higher number of gauges) in the area to minimize the associated error in the estimation of areal rainfall. Averaging the data in space and time also improves the result; it is shown that the correlation for decadal values is not very much degraded as compared to daily data.

The method of merging rain gauges data and satellite data seems promising if it is applied to areas, which are flat and large in size.

Networks and methods for quality control, notably for point observation from surface station, should be designed to improve the reliability of the point data.

In collaboration with the TAMSAT group and other relevant organizations it is essential to improve the estimate by using the TAMSAT technique to test CCD20 threshold which is not done in this study.

REFERENCES

Adegu, D.B. 1999 Rainfall-Runoff Modeling of the Nyando Catchment (Kenya) using satellite (CCD) data. IHE, Msc Thesis, Delft, The Netherlands.

Arkin, P.A. and Meissner, B.N. 1987 The relationship between large-scale convective rainfall and cold cloud over Western Hemisphere during 1982-84 monthly weather review. vol.115, pp51-74.

Barrett, E.C. and Martin, D.W. 1981 The Use of Satellite Data in Rainfall Monitoring. Remote sensing unit, Department of Geography, University of Bristol, U.K.

Bastin, G., Lorent, B., Duque, C. and Gevers, M. 1984 Optimal estimation of the average rainfall and optimal selection of raingauge locations. Water Resources Research, 20(4), pp 463-470.

Cook, R.D. and Weisberg, S. 1982 Residual and influence in regression. Chapman and Hall, London.

David, S.M and Gorge, P.McC. 1998 Introduction to the Practice of Statistics. W.H.Freeman and Company, Newyork, pp. 670-675.

Delhomme, J.P. 1978 Kriging in the hydrosciences. Adv.Water Resour.,1(5), pp 251-256.

Dingman, S.L. 1994 Physical Hydrology. Prentice–Hall, Inc., Simon and Schuster/A Viacom Company, Upper saddle River, New Jersey 07458, pp 110-120.

Dugdale, G., and Milford. 1986 Rainfall estimation over the Sahel using Meteosat thermal infrared data. In ISLSCP. Parameterization of land-surface characteristics: Use of satellite data in climate studies, Department of meteorology, University of Reading UK.

Ears, B.V. and Rosema, A.. 1988 FAO detailed rain-mapping Experiment phase A Meteosat based rainfall mapping in the Sahel region. Final report project TO-1.7, report 88-11,The Netherlands remote sensing board (BCRS), pp.3.

Griffth, C.G., Woodly, W.L., Grube, P.G., Martin, D.W., Stout, J., and Skidar, D.N. 1978 Rain estimation from geosynchronous satellite imagery-visible and infra-red studies. Mon.Wea. pp,1153-1171.

Grimes, D.I.F. and Bonafico,R. 1998 Drought and flood warning in southern Africa.Thomas Telford Publishing, 1 Heron Quay, London E144JD.URL, UK, pp.2.13.

Grimes, D.I.F., Bonifacio, R. and Loftie, H.R.L. 1998 Rainfall Estimation Workbook. Natural Resources Institute. Chatham, UK.pp.A-3 to B-6.

Huygen, J. 1989 Estimation of Rainfall in Zambia using METEOSAT-TIR data. The Wnand Staring center for Integrated land, Soil and Water Research, Wageningen, The Netherlands, pp.100.

Jobard, I. and Desbois, M. 1992 Remote Sensing of Rainfall over Tropical Africa using Meteosat Infrared Imagery: Sensitivity to time and space averaging. Laboratory de Meteorology Dynamic/C.N.R.S., Ecole Polytechnic,91128 Palaiseau Cedex, France, pp.2689.
Journel, A.G. and Huijbregts, C.J. 1978 Mining Gostatistics. Academic Press, NewYork.

Kidd, C., 1998 Rainfall Estimates derived from the Tropical Rainfall Measuring Mission. School of Geography and Environmental Sciences, University of Birmingham, Edgbaston, Birmingham B152TT, pp.424.

Lebel, T., Bastin, G., Obled, C. and Creutin, J.D. 1987 Water Resources Research vol23. No11 on the accuracy of areal Rainfall Estmation: case study, pp 2123-2124.

Lebel, T. and Bastin, G. 1985 Variogram identification by the mean-square interpolation error method with application to hydrologic fields. Hydrol (77), pp 31-56.

Meijerink, A.M.J., DeBrouwer, Mannaerts, C.M. and Valenzuela, C.R. 1994 Introduction to the use of Geographic Information System for practical hydrology. ITC, The Netherlands, pp 108-110.

Meneghini, R. and T.Kozu, 1990 Spaceborn weather radar. Artech House Inc., Norwood, U.S.

Milford, J.R. and Dugdale G. 1990 Estimation of rainfall use geostationary satellite data. In application of remote sensing in agriculture.48th Easter Sch. In Agr.Science, university of Nottingham, London.

Moses, J.F., and Barret, E.C 1986 Interactive procedures for estimating precipitation from satellite imagery, In (Ed.) A.i.Johnson, Hydrological applications of space technology, Proc.Workshop, Cocoa Beach,FL, IHAS publication No160 pp25-39.

Quanwei, L.1996 The application of remote sensing in rainfall monitoring. University of Technology, Helsinki, pp.9-12.

Rodda, J.C 1971 The precipitation measurement paradox- the instrument accuracy problem. Reports on WMO/IHD projects no.16, WMO No.316,pp55.

Robin,T.C. 1994. Statistical Modeling in Hydrology. by John Willy & Sons Ltd, Baffins Lane, Chichester, West Sussex PO19 1UD, England, pp. 150-152.

Rosema, A. 1990. Comparison of Meteosat-based rainfall and evapotranspiration mapping in the Sahel region. International Journal of Remote Sensing11(12) pp 2299-2309.

Snijders, F.L. 1991 Rainfall monitoring based on METEOSAT data a comparison of techniques applied to the western Sahel. Remote sensing center, AGRT, Food and Agriculture Organization of the United Nations, Via delle Terme di Caracalla, 00100 Rome, Italy, pp.1336.

Schultz,G.A. and Barrett, E.C. 1989 Advances in remote sensing for hydrology and water resource management.

Trottman, D. K., 1998 Modelling ground water storage change in response to fluctuating levels of lake Naivasha, Kenya, pp 10.

Ward, R.C. 1974 Principles of Hydrology. McGraw-Hill Book Company (UK) Limited, Maidenhead, Berkshire, ENGLAND, A comparative analysis of techniques for spatial interpolation of precipitation. Water Resource Bulletin, pp 365-380.

Weiss, L.L. and Wilson, W.T. 1958 Precipitation gage shields. Int. Assoc. Sci. Hydrol.Pp,43,462-484.

Wilson, E.M., 1990. Engineering hydrology. MACMILLAN EDUCATION LTD, Houndmills, Basingstoke, Hampshire RG21 2XS and London, pp.151.

Woodley, W.L.,Olsen, A., Herndon,A and Wiggert,V.1974 Optimizing the Measurement of convective Rainfall in Florida.NOAA Technical Memorandum ERL WMPO-18, Boulder,Col., pp99.

APPENDICES

APPENDIX A Station names and Locations

Station name	Staton ID	longitude	Latitude
NAIVASHA D.O.	9036002	36.43	-0.72
N. KINANGOP FOREST STATION	9036025	36.63	-0.58
GILGIL RAILWAY STATION.	9036034	36.33	-0.50
KIRITA FOREST STATION	9036061	36.63	-0.98
MWEIGA ESTATE	9036072	36.25	-0.35
TECHNOLOGY FARM, NAKURU	9036076	36.02	-0.30
NAIVASHA VET.EXPT. STATION	9036081	36.42	-0.65
KARAMENO SHOPPING CENTRE N/MORU	9036085	36.77	-0.13
NAIVASHA MARULA ESTATE	9036109	36.38	-0.65
ELEMENTAITA,SOYSAMBU ESTATE	9036147	36.20	-0.47
SUBUKIA PYRETHRUM NURSERY	9036151	36.17	-0.03
S.KINANGOP NJABINI F.T.C.	9036152	36.65	-0.72
S. KINANGOP FOREST STATION	9036164	36.68	-0.72
DUNDORI FOREST STATION	9036243	36.23	-0.25
MENENGAI FOREST STATION	9036252	36.08	-0.25
EASTERN RIFT SAWMILL LTD.	9036257	36.70	-0.92
GATARE FOREST STATION	9036259	36.77	-0.72
NAKURU METEOROLOGICAL STATION	9036261	36.10	-0.27
OLARAGWAI FARM NAIVASHA	9036262	36.45	-0.65
N. KINANGOP MAWINGO SCHEME	9036264	36.52	-0.50
MUTUBIO GATE (A.N.PARK)	9036272	36.63	-0.48
NAIVASHA W.D.D.	9036281	36.45	-0.73
NGETHU WATER SUPPLY	9036308	36.90	-0.92
KAMIRITHU FANCY FARM	9036310	36.03	-0.35
CHAMATA GATE	9036312	36.53	-0.20
CRESCENT ISLAND	9036322	36.32	-0.77
KIANGANYE FARM ICHICHI	9036323	36.82	-0.70
TUMAINI N.Y.S. CAMP	9036336	36.28	-0.27
SURURU FOREST STATION	9036337	36.03	-0.58
OLKARIA GEOTHERMAL STATION	9036343	36.30	-0.90

1. Available rainfall stations which have daily rainfall data for the year 1994 to1998, the arranged daily data can be found in the xls Caliberation on the daily file.

Runoff station	Longitude	Latitude
2GB1	36.40	-0.56
2GB4	36.48	-0.28
2GB5	36.40	-0.49
2GC4	36.42	-0.48
2GC5	36.56	-0.55
2GC7	36.49	-0.57

2.Available runoff gauging stations in the Malewa catchment.Only 2GB1 has daily data for the year 1997 to 1998.

APPENDIX B Arranged decadal rainfall data

March	ID	LON	LAT	H3X	H3Y	H3Z	I3X	I3Y	I3Z	J3X	J3Y	J3Z	K3X	K3Y	K3Z	L3X	L3Y	L3Z
	9036002	36.43	-0.72	9.9	26	20.2	61	6	26.8	17.2	37.3	39	0	0	31	5.2	15	11.3
	9036025	36.63	-0.58	12.4	7.6	65.1	101	66.9	23.5	14	15.7	42	0	4.2	49	19	24.1	8.6
	9036034	36.33	-0.50	8.2	14	0	26	5.8	11.7	9.8	3.6	47	0	0	5.7	22	0	11.5
	9036061	36.63	-0.98	34.2	13.1	74.2	111	7	19.5	8.5	26.2	50	0	0	46	52	25	60.6
	9036072	36.25	-0.35	24.1	4.7	43.2	37	0	50.6	31.7	17.2	79	0	15	38	64	18.1	33.5
	9036076	36.02	-0.30	23.3	6.1	49.2	58	5.3	29.6	0	8.8	45	0	0	15	0	2	61.3
	9036081	36.42	-0.65	35.9	16.7	20	104	5	13.2	6.3	8.2	35	10	0	16	4.8	9.6	1
	9036085	36.77	-0.13	8	26.7	53.1	31	0	20.6	13	9	39	5.5	0	25	73	14	46
	9036109	36.38	-0.65	15.5	14.5	41.8	89	0	22.1	7.4	15.3	43	0.4	0	8.1	31	0	25
	9036147	36.20	-0.47	0	5.6	9	63	13.3	10.2	15.2	0	12	0	0	11	28	0	5.2
	9036151	36.17	-0.03	5.5	4.2	13.8	73	19	0	2.5	6.3	48	0	0	0	11	0	0
	9036152	36.65	-0.72	69.7	27.2	76.7	120	28.7	19.1	9.6	13.5	108	0	0	74	16	33	18.6
	9036164	36.68	-0.72	-99	-99	-99	-99	-99	-99	6.1	13	50	0	0	167	1	108	22
	9036243	36.23	-0.25	-99	-99	-99	45	26.7	10.3	4	18.8	47	0	0	0	0	0	0
	9036252	36.08	-0.25	17.5	10.1	53.7	68	16	21.6	4	10	54	0	0	26	50	0	8.5
	9036257	36.70	-0.92	11.1	5.9	75.6	91	26.7	17.1	9.3	19.5	86	0	0	89	0	7	19
	9036259	36.77	-0.72	19.6	28.7	87.8	126	1.5	50	29	36.7	86	0	0	127	55	11.3	137
	9036261	36.10	-0.27	22.9	9.3	41.7	64	14.5	24.5	5.9	10.3	54	0	0	22	36	0.8	15.5
	9036262	36.45	-0.65	27.8	8.1	13.1	56	1.4	12.1	3.5	10.2	28	0	0	15	18	4.3	6.2
	9036264	36.52	-0.50	23.1	12.2	22.4	55	5.3	10.8	5	11	25	0	0	23	13	1.5	0.3
	9036272	36.63	-0.48	24.7	14.8	75.5	74	3	91	0.8	27.4	144	0	9	92	28	19	55
	9036281	36.45	-0.73	0	30.6	1.9	70	8.3	32.5	5.1	34.6	40	0	0	51	13	13.6	8.4
	9036308	36.90	-0.92	3.5	5.2	47.8	93	2.6	20.2	7	42.3	106	0	0	25	96	51.6	96.2
	9036310	36.03	-0.35	6	5.6	61.9	31	16.9	11.6	11.8	9.5	68	0	0	7.5	34	0	10.2
	9036312	36.53	-0.20	0	19.6	11.3	0	0	20.1	9	1.5	24	2	3	16	13	6.2	12.6
	9036322	36.32	-0.77	12.7	7.7	17.4	65	0	24.6	6.4	37.1	23	2.5	0	47	3.6	14.7	7.7
	9036323	36.82	-0.70	6.5	27.8	52.9	0	114	40.6	18.2	38.3	67	0	0	88	77	3.5	102
	9036336	36.28	-0.27	5	9.4	25.4	-99	-99	-99	2.2	31.4	103	0	0	0.3	41	1	4.5
	9036337	36.03	-0.58	0	33	53	35	16	19.5	32.9	22.4	55	0	0	18	33	9	9
	9036343	36.49	-0.52	16.9	9	57.2	71	24.2	11.1	0.9	35.2	52	2.2	0	13	29	0	28.9

April	ID	LON	LAT	H4X	H4Y	H4Z	I4X	I4Y	I4Z	J4X	J4Y	J4Z	K4X	K4Y	K4Z	L4X	L4Y	L4Z
	9036002	36.43	-0.72	34.7	12.3	76.6	7.7	32.5	67.2	47.2	12	0	78	13	60	22	36.6	15.8
	9036025	36.63	-0.58	42.3	31.8	126	15	0	38.3	44.2	0	6.8	121	45	105	162	47.8	15.6
	9036034	36.33	-0.50	28.8	6.5	89.1	21	6.8	46.9	4.2	6.9	2	44	27	63	37	34.2	29.9
	9036061	36.63	-0.98	42.7	108	155	99	12.9	79.6	73.8	28	13	108	105	178	119	74.7	104
	9036072	36.25	-0.35	28.4	21.8	111	15	7.5	53.4	6.7	4.7	21	46	31	95	44	42.3	43.6
	9036076	36.02	-0.30	0	18.7	70.6	17	3.5	37.6	14.6	25.9	10	6.4	11	21	29	78	44.8
	9036081	36.42	-0.65	9	26.4	130	26	8.6	3.7	21.2	3.6	14	68	44	95	25	17.9	4.7
	9036085	36.77	-0.13	20.6	34.6	63.7	8	3	28	41	0.5	0	99	14	61	39	33.9	6
	9036109	36.38	-0.65	26.9	33	87.7	8.4	8.8	55.9	9	2.4	0	70	38	94	48	46.5	57.4
	9036147	36.20	-0.47	7.2	2.8	81.9	10	6.4	54.9	12	3.1	3.2	53	37	75	31	27.9	63.3
	9036151	36.17	-0.03	0	35.2	181	12	0	152.9	-99	-99	-99	201	10	160	30	4.5	2
	9036152	36.65	-0.72	77.3	48.3	121	24	21	11.5	95.9	13.7	8.7	179	83	186	110	60.3	28.8
	9036164	36.68	-0.72	-99	-99	-99	18	26.4	38.8	-99	-99	-99	149	82	176	163	84	31.3
	9036243	36.23	-0.25	0	9	91.5	30	20.2	102.4	9.6	0	0	85	40	187	0	0	28.7
	9036252	36.08	-0.25	3.9	18.5	90.2	20	8.5	82.4	15.2	12.8	28	80	64	80	23	48.6	43.5
	9036257	36.70	-0.92	82	39.2	83.4	7.3	16.7	84.6	33.2	8.5	1.2	168	51	90	10	9	10
	9036259	36.77	-0.72	112	126	322	162	52.9	127.8	210	37.1	55	213	161	305	179	165	97.4
	9036261	36.10	-0.27	13.2	12.1	89.7	16	9.5	45.6	14.7	25.3	6	85	56	66	18	52.8	19.7
	9036262	36.45	-0.65	18	12.5	106	12	2	31.6	14.9	0	6	62	64	41	31	43.5	3
	9036264	36.52	-0.50	50.9	25.9	143	58	0	37.7	7.5	0	23	99	29	74	38	78.3	53
	9036272	36.63	-0.48	51.5	34.2	93.6	54	18.9	84.1	67.5	7.7	9.5	172	42	99	158	60	47
	9036281	36.45	-0.73	21.1	17.8	47.9	2.4	36.8	52.3	50.1	7.1	0	103	14	61	35	24.3	20.8
	9036308	36.90	-0.92	104	161	181	110	38.9	35.8	86.7	112	15	180	189	200	150	134	177
	9036310	36.03	-0.35	9.9	9.5	90.1	17	3	25.7	16.8	16.7	6.3	80	33	110	38	50.8	39.8
	9036312	36.53	-0.20	10.3	8.1	103	11	12.9	38	3.8	5	10	25	94	263	43	29.7	4.7
	9036322	36.32	-0.77	17.8	22.6	46.3	1.5	22.8	40.4	36.8	12.7	0	72	15	62	28	12.2	19.1
	9036323	36.82	-0.70	111	134	253	96	61.6	202	172	28.9	39	143	153	358	157	179	97.5
	9036336	36.28	-0.27	2.4	19.5	102	-99	-99	-99	13.2	8.4	33	29	31	128	36	49.1	114
	9036337	36.03	-0.58	25	38	77.5	37	7	119.5	57.2	9.5	0	101	24	63	51	45.5	28.5
	9036343	36.49	-0.52	-99	-99	-99	68	9.3	70.1	28.6	1.7	0	115	27	55	13	75.9	0
May	**ID**	**LON**	**LAT**	**H5X**	**H5Y**	**H5Z**	**I5X**	**I5Y**	**I5Z**	**J5X**	**J5Y**	**J5Z**	**K5X**	**K5Y**	**K5Z**	**L5X**	**L5Y**	**L5Z**
	9036002	36.43	-0.72	13.9	8.2	37.9	52	21.8	6.3	5.1	16.8	18	5.3	35	0	44	8.3	41.9
	9036025	36.63	-0.58	40.2	17.7	138	81	19.2	10	20.5	26.8	13	28	1.6	0	138	63.3	77.2
	9036034	36.33	-0.50	22.5	18.2	25.3	13	14.9	0	14.1	30.7	5.3	23	0	3.8	169	148	45
	9036061	36.63	-0.98	145	88	69.8	63	63.1	39.8	25.9	50.7	77	43	70	2	146	60.8	57.4
	9036072	36.25	-0.35	65.8	93.5	0	40	116	17.7	9.6	78.2	21	61	25	25	174	49.3	19.1
	9036076	36.02	-0.30	-99	-99	-99	21	29.6	26.5	12.3	20.1	39	13	8.3	19	115	86.8	5.8
	9036081	36.42	-0.65	47	4.6	18.8	21	7.7	23.6	0.7	49.1	5.9	9.9	6.5	0	61	41.6	44.1
	9036085	36.77	-0.13	8.4	1.6	0.3	30	20	2	0	37.5	5	35	31	0	109	36	29
	9036109	36.38	-0.65	-99	-99	-99	35	5.4	32.4	3.9	32.6	6.6	7.8	0	0	64	63	71.5
	9036147	36.20	-0.47	51.5	0	41.5	5	18.2	20.5	8.5	38.2	12	17	11	0	88	17.3	66
	9036151	36.17	-0.03	47.9	85.5	22.4	91	18.4	18.3	13.9	79.2	63	24	4.1	0	104	41.5	47.8
	9036152	36.65	-0.72	69	64.3	72.5	91	27	33.4	27.5	65.5	39	56	19	4.5	173	58.1	34.3
	9036164	36.68	-0.72	-99	-99	-99	149	147	48.2	-99	-99	-99	-99	-99	-99	165	28	41.7
	9036243	36.23	-0.25	43.8	68.8	24.1	26	25.5	62	31.7	63.5	60	38	0	20	183	40.6	38.8
	9036252	36.08	-0.25	39.2	0.5	44.1	24	67.7	49.4	1.5	24.3	45	23	16	16	88	87.5	0
	9036257	36.70	-0.92	44.8	64	21.5	58	49.6	47.8	-99	-99	-99	37	16	0	80	26	8
	9036259	36.77	-0.72	201	208	59.3	206	115	89.7	77.2	183	91	218	92	35	253	58.8	113
	9036261	36.10	-0.27	50.7	4.7	45.4	9.9	27.2	50.3	6.1	23.3	52	28	12	15	91	84.6	11.9
	9036262	36.45	-0.65	25.8	5.9	20.7	32	20.8	6.4	8.3	45.4	17	30	10	0	63	52.4	65.7
	9036264	36.52	-0.50	94.5	12.6	35.8	37	32.3	24	35.1	71.2	7.3	32	0	10	117	80.4	62.2
	9036272	36.63	-0.48	65.8	38.6	51.4	96	49.7	14	-99	-99	-99	19	19	5	228	81	50
	9036281	36.45	-0.73	10.1	9.7	50.6	63	27.9	5.7	0	15	22	38	49	0	56	11.3	39.3
	9036308	36.90	-0.92	55.7	56.6	21.3	64	90.3	28.5	59.8	64.5	68	67	192	17	173	151	204
	9036310	36.03	-0.35	12	27.5	40	9.8	16	46	17.5	28.4	29	20	26	12	74	87	6.2
	9036312	36.53	-0.20	25.9	57.6	32.6	40	40	10.5	2.5	72	11	71	17	12	169	87	7.5
	9036322	36.32	-0.77	6.6	9.1	29.7	49	13.8	2.3	8.4	7.6	46	26	12	0	84	13.3	61.6
	9036323	36.82	-0.70	212	209	67.1	219	184	72.6	101	81.6	73	50	77	14	200	111	67.5
	9036336	36.28	-0.27	51.5	49.3	7.8	-99	-99	-99	-99	-99	-99	57	34	1.1	215	54.2	12.6
	9036337	36.03	-0.58	40	0	16	35	25	5	34.7	37.5	10	72	2	13	64	21	15.5
	9036343	36.49	-0.52	38.3	42.3	78.8	34	8.6	6.6	7.6	64.3	19	34	13	0	150	56	28.4

June	ID	LON	LAT	H6X	H6Y	H6Z	I6X	I6Y	I6Z	J6X	J6Y	J6Z	K6X	K6Y	K6Z	L6X	L6Y	L6Z
	9036002	36.43	-0.72	6.4	30.8	16.4	1.5	21.9	18.6	36.5	54.2	1.9	0	72	13	45	40.5	0
	9036025	36.63	-0.58	19.8	66.6	20.8	19	44.2	76.5	95.4	24.4	18	-99	-99	-99	129	5	40.6
	9036034	36.33	-0.50	19.4	52.2	8.3	6.6	28.4	28.6	51.1	16.5	1.4	6	15	17	50	46.4	0
	9036061	36.63	-0.98	31.2	6.2	28.8	-99	-99	-99	40.5	55.1	5	6.5	11	4	50	4.5	0
	9036072	36.25	-0.35	4.5	18.8	17.5	-99	-99	-99	48.8	42.2	0	5.6	23	5.6	36	0	2.9
	9036076	36.02	-0.30	26.2	50.7	39	-99	-99	-99	40	44.6	3.5	11	8.1	9	118	17.7	40.1
	9036081	36.42	-0.65	9	31.8	23.2	-99	-99	-99	96.5	42.6	0	0	0.7	19	33	9.1	5.4
	9036085	36.77	-0.13	4	42.2	15.5	0	5.4	4.5	55	24.7	0	0	11	14	11	0	5
	9036109	36.38	-0.65	10.8	43.8	12.3	1.5	46.5	34.2	60.4	40.3	12	0	1.5	31	29	5.5	15
	9036147	36.20	-0.47	44.2	54.6	22.9	11	51.8	78.7	136	72.5	6.5	7.3	15	7.6	23	7.3	26.1
	9036151	36.17	-0.03	49	69.5	49.9	2	23.8	64.4	139	143	6.5	23	25	87	62	12.4	63.5
	9036152	36.65	-0.72	79	59.8	31.7	7.8	61	22.2	-99	-99	-99	0	45	14	7	13.2	0
	9036164	36.68	-0.72	-99	-99	-99	-99	-99	-99	81.5	30	5.1	-99	-99	-99	104	16.1	4
	9036243	36.23	-0.25	10.6	57.8	24.3	-99	-99	-99	112	30.2	0	26	59	14	65	73.9	54.6
	9036252	36.08	-0.25	77.2	28.9	44.9	14	30.8	79.2	108	12.2	16	11	26	23	22	37.7	6
	9036257	36.70	-0.92	0.2	1.6	14.6	2.5	11.6	20.5	-99	-99	-99	-99	-99	-99	-99	-99	-99
	9036259	36.77	-0.72	23.2	34.8	51.7	64	33.5	34.6	-99	-99	-99	56	82	60	141	17.5	13
	9036261	36.10	-0.27	49.5	32.3	35.8	13	30.1	35.8	15.8	0	0	11	31	30	40	39.9	27.8
	9036262	36.45	-0.65	13.1	26.2	31.7	6.3	61.8	9.8	37.1	61.5	6.8	0	47	9.4	60	7.7	12.9
	9036264	36.52	-0.50	43.8	84.1	46.5	22	2	45.6	65.2	105	0	14	57	29	64	82.2	2.1
	9036272	36.63	-0.48	28.1	96.8	11.8	44	56.4	53.5	154	73.5	30	7	47	31	60	27	4
	9036281	36.45	-0.73	2.5	30	25.3	2	16.1	18.6	35.8	49.7	1	1.1	49	16	39	31.9	0
	9036308	36.90	-0.92	5.8	4.7	9	13	11	9.7	0	0	0	-99	-99	-99	210	11.5	1.7
	9036310	36.03	-0.35	26.9	18.5	14.7	26	35	86.9	80.7	17	11	25	34	24	50	24.9	10
	9036312	36.53	-0.20	34	73.2	15.9	15	20.5	34.8	64	16.1	0	28	39	24	24	19	16.8
	9036322	36.32	-0.77	12.7	49.6	26.3	2.8	14.7	21	30.3	13.8	2.5	0	3.6	12	35	26.9	0
	9036323	36.82	-0.70	10.9	45.7	30.5	88	15.4	34.3	111	48.3	21	31	50	36	117	4.1	17.5
	9036336	36.28	-0.27	64.4	48	7.9	-99	-99	-99	211	15	0	0	70	32	69	85.6	84
	9036337	36.03	-0.58	14	26.5	12.5	30	40.5	46.5	111	53	2.5	9.5	32	31	-99	-99	-99
	9036343	36.49	-0.52	29	21.9	27.9	20	17.6	13.7	41.2	12.3	0	0	7.2	26	33	3.7	0
Oct	**ID**	**LON**	**LAT**	**HAX**	**HAY**	**HAZ**	**IAX**	**IAY**	**IAZ**	**JAX**	**JAY**	**JAZ**	**KAX**	**KAY**	**KAZ**	**LAX**	**LAY**	**LAZ**
	9036002	36.43	-0.72	16.2	26.9	52.7	-99	-99	-99	1	22.3	53	32	54	25	0	29.8	29.1
	9036025	36.63	-0.58	3.2	55.6	66.4	-99	-99	-99	12.8	45.1	30	28	87	55	22	15.3	36
	9036034	36.33	-0.50	0	13.2	32.8	-99	-99	-99	12.3	11.7	4.7	13	18	27	5.1	20.7	18.4
	9036061	36.63	-0.98	9.5	126	142	-99	-99	-99	0	0	8.6	64	89	142	0	0	0
	9036072	36.25	-0.35	0	38.6	61.1	-99	-99	-99	4.5	45.9	11	63	133	93	14	3.4	8.9
	9036076	36.02	-0.30	0	21.4	23.8	-99	-99	-99	25.9	16.6	23	-99	-99	-99	58	22.4	2.8
	9036081	36.42	-0.65	6.8	22.8	44	-99	-99	-99	0	0	33	37	47	16	0	5.9	10.5
	9036085	36.77	-0.13	0	14.7	34.5	-99	-99	-99	8	8	1.5	16	61	12	47	6.5	15.5
	9036109	36.38	-0.65	0	25.5	23.2	-99	-99	-99	29.1	0	0	38	46	21	-99	-99	-99
	9036147	36.20	-0.47	0	23.2	10.3	-99	-99	-99	11.9	10.2	14	4.6	41	7.7	4.8	43.6	21
	9036151	36.17	-0.03	3.7	8.5	0	-99	-99	-99	0	33.5	29	25	69	47	-99	-99	-99
	9036152	36.65	-0.72	15.8	14.9	40	-99	-99	-99	4	15.3	0	53	124	68	-99	-99	-99
	9036164	36.68	-0.72	-99	-99	-99	-99	-99	-99	0	0	38	-99	-99	-99	37	12.8	0
	9036243	36.23	-0.25	0	17.1	22.4	-99	-99	-99	13	8.7	30	68	84	121	69	47.8	61
	9036252	36.08	-0.25	3.5	31	23	-99	-99	-99	13	11.8	9.7	0	54	87	-99	-99	-99
	9036257	36.70	-0.92	-99	-99	-99	-99	-99	-99	-99	-99	-99	0	47	40	-99	-99	-99
	9036259	36.77	-0.72	8.9	142	198	-99	-99	-99	11.3	57.6	48	86	297	170	7.5	91.2	3.9
	9036261	36.10	-0.27	8.9	17	17.6	-99	-99	-99	10.6	36.1	17	18	38	123	9.6	34.3	3.5
	9036262	36.45	-0.65	6.2	28.4	46.8	-99	-99	-99	10	0.6	6.6	31	46	5.8	0	18.5	6.5
	9036264	36.52	-0.50	5	15.7	37.4	-99	-99	-99	28.5	59.6	59	12	45	15	5.9	12.6	22
	9036272	36.63	-0.48	32.4	48.9	62.9	-99	-99	-99	19	73	21	64	117	138	64	41	55
	9036281	36.45	-0.73	13.2	34.6	24.4	-99	-99	-99	1.8	16	53	31	48	6.4	4.4	43	18.4
	9036308	36.90	-0.92	0	135	74.8	-99	-99	-99	0	0	0	237	104	115	37	0	0
	9036310	36.03	-0.35	0	22.7	2.1	-99	-99	-99	5	6	0	9.2	32	58	16	36.7	0
	9036312	36.53	-0.20	18.2	16	30	-99	-99	-99	3.5	2	24	10	48	30	30	61.6	15.2
	9036322	36.32	-0.77	21.1	21.8	19.7	-99	-99	-99	15.8	7.9	29	24	26	23	8.4	45.7	19.8
	9036323	36.82	-0.70	7.8	112	221	-99	-99	-99	7.5	38.6	32	72	183	145	-99	-99	-99
	9036336	36.28	-0.27	-99	-99	-99	-99	-99	-99	15.2	36	1.5	36	44	124	33	54.9	60
	9036337	36.03	-0.58	-99	-99	-99	-99	-99	-99	7	8.5	15	29	27	17	49	17.5	40
	9036343	36.49	-0.52	5.2	26.9	27.1	-99	-99	-99	8.5	0	14	5.4	54	23	0	1.5	0

Nov	ID	LON	LAT	HBX	HBY	HBZ	IBX	IBY	IBZ	JBX	JBY	JBZ	KBX	KBY	KBZ	LBX	LBY	LBZ
	9036002	36.43	-0.72	38.9	0	0	1.9	43.3	7.5	28.3	3.5	27	67	52	37	15	6.1	2
	9036025	36.63	-0.58	111	42	63.3	30	78.1	14.6	29.1	18.6	48	78	98	16	15	23.2	31.4
	9036034	36.33	-0.50	23.7	71.7	13	0	27.4	11.2	19.3	5.9	68	49	81	55	30	17.9	0
	9036061	36.63	-0.98	161	144	30.1	66	64.2	12	-99	-99	-99	198	84	40	37	21.5	14.5
	9036072	36.25	-0.35	70.5	34	27	23	29.9	6.8	9.5	75.9	32	130	52	24	51	18.8	5.7
	9036076	36.02	-0.30	34.9	48.3	30.8	-99	-99	-99	32.7	27	27	-99	-99	-99	36	15.7	4.7
	9036081	36.42	-0.65	60.2	70	42	4.2	27.4	1.1	6.9	5.4	31	60	54	36	10	17.4	10.8
	9036085	36.77	-0.13	83	88.5	21.5	9	35	36.1	31.5	20.5	43	65	77	58	31	17.8	4
	9036109	36.38	-0.65	41.7	54.7	12.3	6.1	38.5	18.9	9.6	0	68	74	68	48	-99	-99	-99
	9036147	36.20	-0.47	30.6	45.9	0	0	39.6	7.9	10.4	6.1	58	85	63	28	6.8	8	0
	9036151	36.17	-0.03	115	46.4	28.7	92	22.9	3.7	3	9.5	32	30	101	50	9	25.5	0
	9036152	36.65	-0.72	92.3	102	35.3	28	39.4	3.2	34	12.5	46	117	122	56	-99	-99	-99
	9036164	36.68	-0.72	125	111	23.4	-99	-99	-99	59.1	33.5	129	-99	-99	-99	53	36.9	51.8
	9036243	36.23	-0.25	109	53.4	71.9	143	81.5	10.5	12.1	7.1	73	58	131	62	56	27	31.9
	9036252	36.08	-0.25	58.9	21.5	39	26	35.2	10	12.8	2.5	81	120	68	61	-99	-99	-99
	9036257	36.70	-0.92	-99	-99	-99	18	24.3	0	-99	-99	-99	-99	-99	-99	-99	-99	-99
	9036259	36.77	-0.72	272	178	76	86	108	39.5	96	104	144	306	160	96	163	93.6	61
	9036261	36.10	-0.27	43	27.6	22.9	29	34.8	15.2	15.7	7.1	73	77	80	65	58	11.8	12.4
	9036262	36.45	-0.65	52.4	62.8	34.7	1.8	17.8	7	16	0	42	44	92	52	13	22	14.2
	9036264	36.52	-0.50	57.9	51.3	68.2	46	62.1	14.9	28.8	4.5	55	60	90	28	22	36.8	13.6
	9036272	36.63	-0.48	-99	-99	-99	63	93.4	18.6	29.5	14	88	194	99	63	34	62.5	44
	9036281	36.45	-0.73	91.9	82.2	31.2	6.2	17	5	46.4	4.3	40	75	44	63	-99	-99	-99
	9036308	36.90	-0.92	194	151	68.2	47	184	129.5	77.1	94.8	128	269	95	120	-99	-99	-99
	9036310	36.03	-0.35	33.5	58	18.8	33	12	20.5	26	10.5	67	59	82	28	58	29.2	6.5
	9036312	36.53	-0.20	85	55.5	62.5	55	59	11.3	25.5	5.3	26	110	69	58	18	38.5	12.5
	9036322	36.32	-0.77	78.7	59.5	56.4	2.3	19.6	3.5	25.5	0	20	58	29	44	25	15.5	0
	9036323	36.82	-0.70	326	191	164	140	140	150.6	57.7	81.6	106	247	129	46	-99	-99	-99
	9036336	36.28	-0.27	-99	-99	-99	85	119	22.5	20	0	8.1	66	65	39	63	48.8	25.5
	9036337	36.03	-0.58	-99	-99	-99	27	25	14.1	7.3	8.3	75	84	108	106	15	1.5	3
	9036343	36.49	-0.52	40	87.8	29.6	9.2	66.6	18	15.3	5.8	34	67	60	29	-99	-99	-99
Dec	**ID**	**LON**	**LAT**	**HCX**	**HCY**	**HCZ**	**ICX**	**ICY**	**ICZ**	**JCX**	**JCY**	**JCZ**	**KCX**	**KCY**	**KCZ**	**LCX**	**LCY**	**LCZ**
	9036002	36.43	-0.72	16.3	2.1	0	-99	-99	-99	3.4	0	3.3	49	15	34	12	1	0
	9036025	36.63	-0.58	25.7	3.6	0	-99	-99	-99	2	7.4	3	46	42	29	1.8	0	15.3
	9036034	36.33	-0.50	0	0	2.4	6.5	36.4	19.2	0	7.2	0	51	8.4	16	15	4.1	0
	9036061	36.63	-0.98	18.3	6	10	13	49.9	4	0	0	3	83	104	53	27	0	0
	9036072	36.25	-0.35	102	3.3	9.9	16	52.6	6.2	94.4	31.6	68	83	28	59	4.6	8.9	0
	9036076	36.02	-0.30	10.3	0	0	-99	-99	-99	7.4	2.4	1.1	-99	-99	-99	1.6	2.5	0
	9036081	36.42	-0.65	12.2	1.4	3.4	29	3.1	0	0	10.8	3.2	33	13	51	17	5	0
	9036085	36.77	-0.13	30.2	0.5	0.7	6.5	36.4	5	24	0.2	13	32	0	44	0	0	0
	9036109	36.38	-0.65	-99	-99	-99	7.2	10.8	0	-99	-99	-99	72	16	42	-99	-99	-99
	9036147	36.20	-0.47	42.6	0	0	20	41.6	3.2	9.7	0	0	27	6.1	36	3.6	4.6	0
	9036151	36.17	-0.03	7	0	0	5.2	22	2.8	5.5	0	0	19	3.5	0	0	0	0
	9036152	36.65	-0.72	8.2	3.5	0	6.7	32.2	5.1	34	25	36	61	111	43	2.1	0.4	10.7
	9036164	36.68	-0.72	-99	-99	-99	11	40	10	7.7	40.9	0	-99	-99	-99	11	11.1	3.2
	9036243	36.23	-0.25	18.6	0	0	52	51.5	0	26.4	0	11	55	16	7.6	0	0	0
	9036252	36.08	-0.25	2.5	0	0	14	44.5	0	0	0	0	46	5.2	24	-99	-99	-99
	9036257	36.70	-0.92	-99	-99	-99	-99	-99	-99	-99	-99	-99	-99	-99	-99	-99	-99	-99
	9036259	36.77	-0.72	102	11.7	2.9	23	87.2	4.7	45.2	28.4	0	156	56	136	4.2	20.9	25.8
	9036261	36.10	-0.27	7.7	0	0	13	27.3	3.6	2.8	1.6	0	43	4.7	15	1.4	0.3	2.6
	9036262	36.45	-0.65	7.7	0.5	0	6.3	7.2	6.5	3.9	7.6	2.6	46	24	23	0	3.4	0
	9036264	36.52	-0.50	0	0	0.3	8.5	9.2	28.5	7.3	0	2	-99	-99	-99	0	1	3
	9036272	36.63	-0.48	14.1	8.8	8.9	18	38.5	5.8	55.8	20	2	52	39	34	0	8	2
	9036281	36.45	-0.73	12.7	1.5	1.6	13	8.1	5.1	9.1	1.8	0.8	63	21	28	0	0	0
	9036308	36.90	-0.92	84.4	0	0	38	144	5.4	48.7	15	0	161	28	116	10	33.3	2.2
	9036310	36.03	-0.35	4.5	0	5.5	11	16	0.7	0	0	4.5	52	3.7	5	2.5	0	0
	9036312	36.53	-0.20	43.6	22.7	11.9	9.5	16	23.6	8	0	0	65	21	29	0.5	9	2.5
	9036322	36.32	-0.77	26.4	0	4.1	0	6.9	5.1	6.1	0	0	58	25	14	0	0	0
	9036323	36.82	-0.70	103	29	11.5	26	126	16.6	55.7	29.2	0	98	33	102	-99	-99	-99
	9036336	36.28	-0.27	-99	-99	-99	-99	-99	-99	0	0	0	33	4	55	0	1.8	0.6
	9036337	36.03	-0.58	-99	-99	-99	39	93.3	7.3	2	1	2.8	92	25	31	0	0	1
	9036343	36.49	-0.52	12.9	0	0	1.6	9.3	7.9	11.2	10.8	18	82	50	29	-99	-99	-99

APPENDIX C Determination of optimum threshold Tt (daily and decadal data) including contingency table

CCD30

			March							April				
			Ir=0	Ir=1						Ir=0	Ir=1			
		Ic=0	2551	597					Ic=0	1275	658			
R >	0mm	Ic=1	596	586			R >	0mm	Ic=1	346	837			
h =	0	2	4	6	8	10	h=	0	2	4	6	8	10	
PC	0.72	0.74	0.75	0.75	0.74	0.74	PC	0.68	0.66	0.64	0.62	0.59	0.60	
Bias	1.00	0.74	0.55	0.46	0.37	0.31	Bias	0.79	0.61	0.49	0.40	0.32	0.27	
HR	0.50	0.39	0.31	0.27	0.22	0.19	HR	0.56	0.45	0.36	0.31	0.25	0.22	
FAR	0.19	0.13	0.09	0.07	0.06	0.05	FAR	0.21	0.14	0.11	0.09	0.06	0.05	
KSS	0.31	0.26	0.22	0.20	0.16	0.14	KSS	0.35	0.31	0.25	0.22	0.19	0.17	

			May							June				
			Ir=0	Ir=1						Ir=0	Ir=1			
		Ic=0	2063	1124					Ic=0	2015	846			
R >	0mm	Ic=1	431	753			R >	0mm	Ic=1	321	466			
h=	0	2	4	6	8	10	h =	0	2	4	6	8	10	
PC	0.64	0.64	0.63	0.62	0.60	0.60	PC	0.68	0.68	0.68	0.67	0.65	0.65	
Bias	0.63	0.44	0.32	0.24	0.17	0.13	Bias	0.60	0.44	0.32	0.21	0.13	0.09	
HR	0.40	0.30	0.23	0.18	0.14	0.10	HR	0.36	0.28	0.21	0.14	0.09	0.06	
FAR	0.17	0.10	0.06	0.05	0.03	0.02	FAR	0.14	0.09	0.06	0.04	0.02	0.01	
KSS	0.23	0.20	0.17	0.14	0.11	0.08	KSS	0.22	0.19	0.15	0.10	0.07	0.05	

			October							November				
			Ir=0	Ir=1						Ir=0	Ir=1			
		Ic=0	1614	789					Ic=0	1458	1282			
R >	0mm	Ic=1	267	289			R >	0mm	Ic=1	396	794			
h=	0	2	4	6	8	10	h =	0	2	4	6	8	10	
PC	0.64	0.65	0.65	0.64	0.64	0.64	PC	0.57	0.55	0.53	0.52	0.49	0.50	
Bias	0.52	0.28	0.14	0.07	0.04	0.02	Bias	0.57	0.41	0.29	0.21	0.15	0.10	
HR	0.27	0.15	0.08	0.05	0.03	0.01	HR	0.38	0.28	0.20	0.15	0.11	0.08	
FAR	0.14	0.07	0.03	0.01	0.01	0.00	FAR	0.21	0.15	0.09	0.07	0.04	0.03	
KSS	0.13	0.08	0.05	0.03	0.02	0.01	KSS	0.17	0.13	0.11	0.08	0.06	0.05	

			December			
			Ir=0	Ir=1		
		Ic=0	2752	712		
R >	0mm	Ic=1	174	258		
h=	0	2	4	6	8	10
PC	0.77	0.78	0.77	0.76	0.75	0.75
Bias	0.45	0.24	0.13	0.08	0.06	0.04
HR	0.27	0.17	0.10	0.06	0.04	0.02
FAR	0.06	0.02	0.01	0.01	0.00	0.00
KSS	0.21	0.15	0.09	0.06	0.04	0.02

1.Daily data.

			March							April				
			Ir=0	Ir=1						Ir=0	Ir=1			
		Ic=0	14	20					Ic=0	4	17			
R >	0mm	Ic=1	56	263			R >	0mm	Ic=1	8	143			
h =	0	2	4	6	8	10	h =	0	2	4	6	8	10	
PC	0.78	0.78	0.67	0.59	0.50	0.50	PC	0.85	0.87	0.78	0.65	0.48	0.48	
Bias	1.13	0.86	0.67	0.55	0.46	0.42	Bias	0.94	0.89	0.78	0.63	0.53	0.44	
HR	0.93	0.79	0.63	0.52	0.44	0.40	HR	0.89	0.88	0.77	0.63	0.53	0.44	
FAR	0.80	0.27	0.16	0.11	0.09	0.09	FAR	0.67	0.25	0.08	0.00	0.00	0.00	
KSS	0.13	0.52	0.48	0.41	0.35	0.31	KSS	0.23	0.63	0.69	0.63	0.53	0.44	

			May							June				
			Ir=0	Ir=1						Ir=0	Ir=1			
		Ic=0	13	68					Ic=0	15	58			
R >	0mm	Ic=1	10	332			R >	0mm	Ic=1	9	238			
h=	0	2	4	6	8	10	h=	0	2	4	6	8	10	
PC	0.82	0.69	0.52	0.42	0.34	0.34	PC	0.79	0.61	0.53	0.43	0.30	0.30	
Bias	0.86	0.69	0.49	0.39	0.33	0.31	Bias	0.83	0.59	0.50	0.40	0.28	0.25	
HR	0.83	0.68	0.49	0.39	0.33	0.31	HR	0.80	0.58	0.50	0.39	0.28	0.25	
FAR	0.43	0.13	0.00	0.00	0.00	0.00	FAR	0.38	0.08	0.04	0.04	0.04	0.04	
KSS	0.40	0.55	0.49	0.39	0.33	0.31	KSS	0.43	0.50	0.45	0.35	0.24	0.21	

			October							November				
			Ir=0	Ir=1						Ir=0	Ir=1			
		Ic=0	8	30					Ic=0	9	68			
R >	0mm	Ic=1	17	162			R >	0mm	Ic=1	5	310			
h=	0	2	4	6	8	10	h=	0	2	4	6	8	10	
PC	0.78	0.58	0.41	0.34	0.23	0.24	PC	0.81	0.73	0.61	0.51	0.31	0.31	
Bias	0.93	0.61	0.37	0.28	0.20	0.14	Bias	0.83	0.73	0.62	0.51	0.39	0.29	
HR	0.84	0.57	0.35	0.27	0.19	0.14	HR	0.82	0.72	0.61	0.50	0.39	0.29	
FAR	0.68	0.32	0.16	0.08	0.08	0.00	FAR	0.36	0.21	0.21	0.21	0.14	0.07	
KSS	0.16	0.25	0.19	0.19	0.11	0.14	KSS	0.46	0.51	0.39	0.29	0.24	0.22	

			December			
			Ir=0	Ir=1		
		Ic=0	48	98		
R >	0mm	Ic=1	28	163		
h=	0	2	4	6	8	10
PC	0.63	0.49	0.42	0.40	0.36	0.36
Bias	0.73	0.39	0.27	0.23	0.20	0.18
HR	0.62	0.36	0.26	0.23	0.20	0.18
FAR	0.37	0.08	0.03	0.01	0.01	0.01
KSS	0.26	0.29	0.23	0.21	0.19	0.16

2.decadal data.

CCD40

			March							April				
			Ir=0	Ir=1						Ir=0	Ir=1			
		Ic=0	26	68					Ic=0	11	38			
R >	0mm	Ic=1	48	240			R >	0mm	Ic=1	1	122			
h=	0	2	4	6	8	10	h=	0	2	4	6	8	10	
PC	0.70	0.57	0.50	0.46	0.45	0.45	PC	0.77	0.59	0.51	0.45	0.40	0.40	
Bias	0.94	0.55	0.43	0.38	0.36	0.35	Bias	0.77	0.58	0.47	0.41	0.39	0.35	
HR	0.78	0.51	0.41	0.36	0.34	0.34	HR	0.76	0.57	0.47	0.41	0.39	0.35	
FAR	0.65	0.16	0.11	0.09	0.08	0.07	FAR	0.08	0.08	0.00	0.00	0.00	0.00	
KSS	0.13	0.35	0.30	0.26	0.26	0.27	KSS	0.68	0.49	0.47	0.41	0.39	0.35	

			May							June				
			Ir=0	Ir=1						Ir=0	Ir=1			
		Ic=0	18	112					Ic=0	22	109			
R >	0mm	Ic=1	5	288			R >	0mm	Ic=1	2	187			
h=	0	2	4	6	8	10	h=	0	2	4	6	8	10	
PC	0.72	0.51	0.38	0.33	0.28	0.28	PC	0.65	0.49	0.37	0.28	0.14	0.14	
Bias	0.73	0.48	0.34	0.29	0.25	0.24	Bias	0.64	0.47	0.32	0.23	0.16	0.08	
HR	0.72	0.48	0.34	0.29	0.25	0.24	HR	0.63	0.46	0.32	0.22	0.15	0.08	
FAR	0.22	0.00	0.00	0.00	0.00	0.00	FAR	0.08	0.08	0.04	0.04	0.04	0.04	
KSS	0.50	0.48	0.34	0.29	0.25	0.24	KSS	0.55	0.38	0.28	0.18	0.11	0.04	

			October							November				
			Ir=0	Ir=1						Ir=0	Ir=1			
		Ic=0	18	91					Ic=0	10	107			
R >	0mm	Ic=1	7	101			R >	0mm	Ic=1	4	272			
h =	0	2	4	6	8	10	h=	0	2	4	6	8	10	
PC	0.55	0.31	0.24	0.18	0.14	0.14	PC	0.72	0.44	0.30	0.20	0.12	0.12	
Bias	0.56	0.24	0.17	0.07	0.04	0.03	Bias	0.73	0.43	0.27	0.17	0.13	0.09	
HR	0.53	0.23	0.16	0.07	0.04	0.03	HR	0.72	0.43	0.27	0.17	0.13	0.09	
FAR	0.28	0.08	0.08	0.00	0.00	0.00	FAR	0.29	0.14	0.00	0.00	0.00	0.00	
KSS	0.25	0.15	0.08	0.07	0.04	0.03	KSS	0.43	0.28	0.27	0.17	0.13	0.09	

			December			
			Ir=0	Ir=1		
		Ic=0	67	156		
R >	0mm	Ic=1	9	105		
h=	0	2	4	6	8	10
PC	0.51	0.38	0.36	0.31	0.23	0.23
Bias	0.44	0.21	0.18	0.11	0.04	0.00
HR	0.40	0.20	0.18	0.11	0.04	0.00
FAR	0.12	0.01	0.01	0.00	0.00	0.00
KSS	0.28	0.19	0.16	0.11	0.04	0.00

1.Decadal data.

APPENDIX D Monthly variogram and model fitting

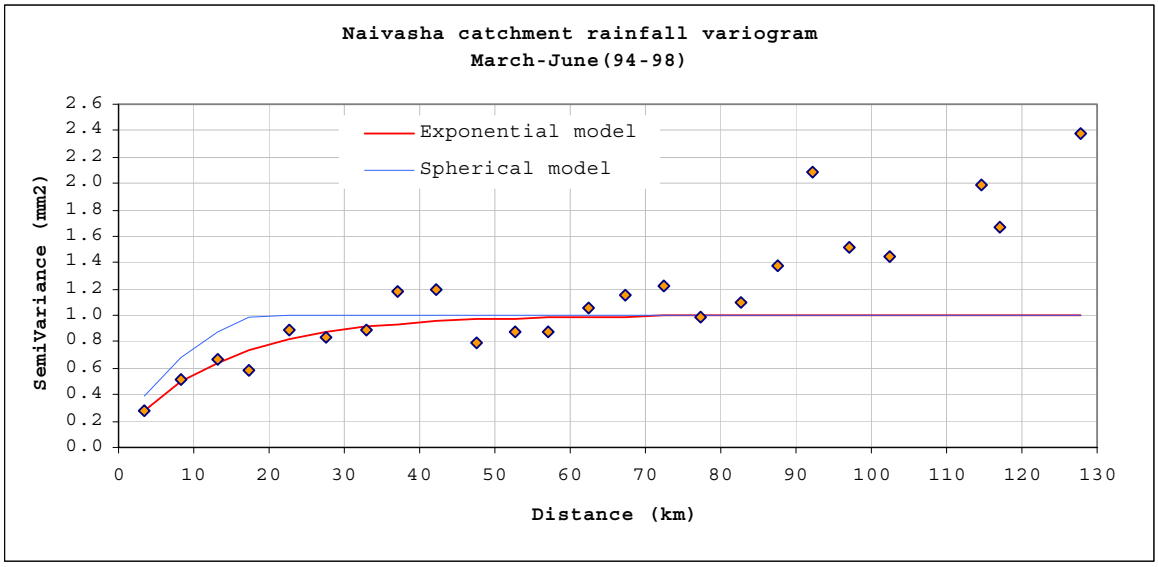

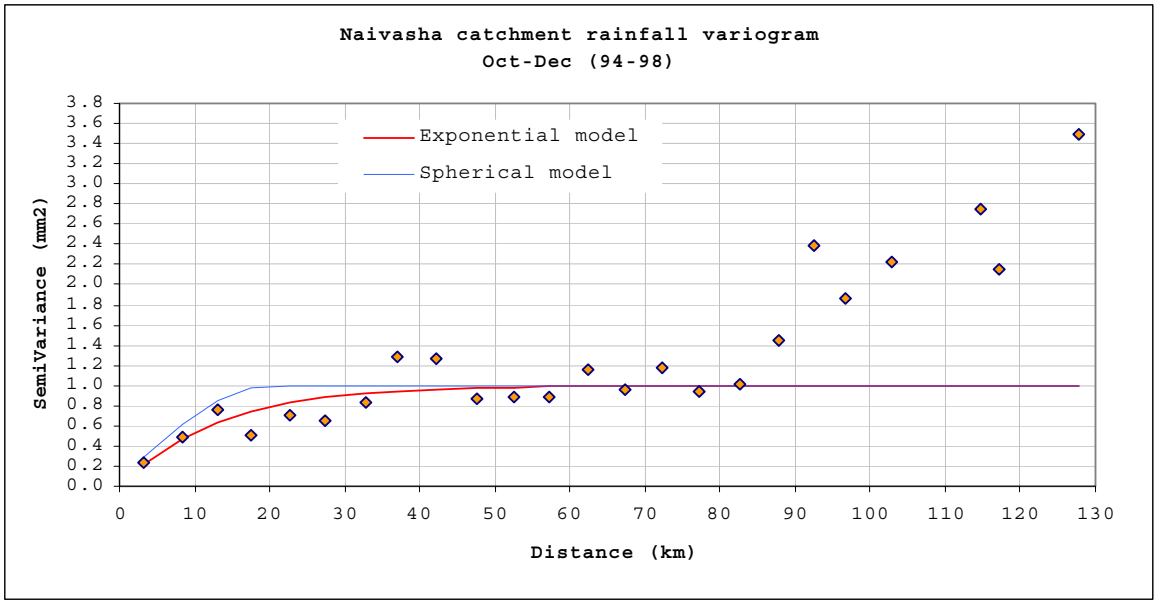

Monthly variogram, decadl data for the year 94 to 98 with lag spacing 5km, for long (march to june) and short (october to November) rainy season.

APPENDIX E Calibration plot calculation for decadal data

	P=	0.21						P	0.35	est		
Date	CCD30cat	Box cox	Fc	KR	Sqrtrain	estsqrt	EstR	Residuals	box-cox	box-cox	EstR	Residuals
H3Y	2.55	1.03	0.91	14.23	3.77	4.79	22.93	8.70	4.38	5.55	21.83	7.60
H3Z	21.48	4.31	1.00	31.52	5.61	6.11	37.38	5.85	6.70	8.37	49.94	18.42
H4X	5.58	2.07	1.00	29.70	5.45	5.00	25.00	-4.69	6.51	6.44	29.13	-0.56
H4Y	5.60	2.07	0.99	22.06	4.70	5.00	25.02	2.96	5.58	6.45	29.18	7.12
H4Z	27.40	4.78	1.00	96.06	9.80	6.53	42.61	-53.44	11.26	8.78	55.33	-40.73
H5X	2.56	1.04	0.93	38.86	6.23	4.79	22.93	-15.93	7.43	5.55	21.85	-17.01
H5Y	2.22	0.87	0.61	31.72	5.63	4.77	22.71	-9.01	6.72	5.40	20.77	-10.94
H5Z	0.61	-0.46	0.43	41.28	6.42	4.65	21.65	-19.63	7.65	4.26	13.54	-27.73
H6X	6.75	2.35	1.00	26.42	5.14	5.08	25.83	-0.60	6.13	6.68	31.34	4.92
H6Y	6.91	2.38	0.97	52.38	7.24	5.09	25.94	-26.44	8.56	6.71	31.63	-20.75
H6Z	6.17	2.22	1.00	21.38	4.62	5.04	25.42	4.04	5.49	6.57	30.28	8.90
HAZ	1.50	0.42	0.79	36.66	6.05	4.71	22.23	-14.43	7.22	5.02	18.14	-18.52
HBX	12.76	3.37	1.00	70.99	8.43	5.50	30.29	-40.70	9.84	7.56	40.32	-30.67
HBY	9.81	2.93	1.00	60.90	7.80	5.30	28.06	-32.85	9.18	7.19	36.29	-24.62
HBZ	10.01	2.96	1.00	42.99	6.56	5.31	28.20	-14.79	7.80	7.21	36.58	-6.42
HCX	1.80	0.63	0.86	22.30	4.72	4.74	22.43	0.13	5.61	5.20	19.32	-2.98
HCZ	0.09	-1.86	0.09	3.54	1.88	4.62	21.31	17.78	1.59	3.05	7.96	4.43
I3X	31.42	5.06	1.00	59.99	7.75	6.81	46.36	-13.63	9.12	9.02	58.65	-1.34
I5X	5.30	2.00	0.99	47.61	6.90	4.98	24.81	-22.80	8.19	6.38	28.59	-19.03
I5Y	11.63	3.21	1.00	29.68	5.45	5.42	29.42	-0.26	6.50	7.43	38.84	9.16
I5Z	1.72	0.57	0.77	15.78	3.97	4.73	22.38	6.60	4.65	5.15	19.01	3.23
I6Y	5.94	2.16	0.98	30.61	5.53	5.03	25.26	-5.35	6.61	6.52	29.85	-0.76
I6Z	1.38	0.33	0.66	31.33	5.60	4.71	22.15	-9.18	6.68	4.94	17.62	-13.71
IBX	0.56	-0.55	0.23	28.99	5.38	4.65	21.61	-7.37	6.43	4.18	13.13	-15.85
IBY	6.24	2.23	1.00	50.49	7.11	5.05	25.47	-25.02	8.42	6.58	30.41	-20.08
IBZ	5.09	1.94	1.00	11.24	3.35	4.97	24.67	13.42	3.81	6.33	28.15	16.91
ICX	0.12	-1.70	0.12	11.51	3.39	4.62	21.33	9.82	3.86	3.19	8.53	-2.98
ICY	2.30	0.91	0.63	22.64	4.76	4.77	22.76	0.12	5.66	5.44	21.05	-1.59
ICZ	1.20	0.18	0.74	9.64	3.10	4.69	22.03	12.39	3.46	4.82	16.82	7.18
J3X	4.44	1.75	1.00	7.89	2.81	4.92	24.22	16.32	3.03	6.17	26.74	18.85
J3Y	3.37	1.38	0.82	20.45	4.52	4.85	23.48	3.03	5.36	5.85	24.14	3.69
J3Z	34.48	5.25	1.00	54.95	7.41	7.02	49.33	-5.62	8.76	9.19	61.04	6.09
J4Z	0.45	-0.73	0.25	8.07	2.84	4.64	21.54	13.48	3.08	4.03	12.33	4.27
J5X	4.12	1.65	1.00	13.73	3.71	4.90	24.00	10.27	4.29	6.08	26.01	12.28
J5Y	10.65	3.06	1.00	45.10	6.72	5.36	28.68	-16.41	7.98	7.30	37.49	-7.60
J5Z	0.76	-0.27	0.34	22.42	4.74	4.66	21.74	-0.68	5.63	4.42	14.47	-7.95
J6X	4.80	1.86	0.77	73.63	8.58	4.95	24.47	-49.17	10.01	6.26	27.54	-46.09
J6Y	12.19	3.29	1.00	36.01	6.00	5.46	29.85	-6.16	7.16	7.50	39.58	3.57
JAX	6.14	2.21	1.00	12.30	3.51	5.04	25.40	13.10	4.02	6.56	30.23	17.93
JAY	1.48	0.41	0.69	21.81	4.67	4.71	22.22	0.41	5.55	5.01	18.07	-3.74
JAZ	0.56	-0.55	0.42	21.40	4.63	4.65	21.61	0.21	5.49	4.18	13.14	-8.26
JBX	5.38	2.02	1.00	23.91	4.89	4.99	24.86	0.95	5.82	6.40	28.74	4.82
JBY	0.16	-1.52	0.16	8.96	2.99	4.62	21.36	12.40	3.30	3.34	9.15	0.19
JBZ	6.90	2.38	1.00	43.08	6.56	5.09	25.94	-17.15	7.81	6.71	31.61	-11.47
JCX	1.45	0.39	0.75	15.39	3.92	4.71	22.20	6.81	4.58	4.99	17.94	2.55
JCY	0.89	-0.12	0.73	7.53	2.74	4.67	21.83	14.30	2.93	4.55	15.23	7.70
JCZ	0.70	-0.35	0.54	8.18	2.86	4.66	21.71	13.52	3.11	4.36	14.11	5.93
K3X	1.02	0.02	1.00	0.86	0.93	4.68	21.91	21.05	-0.14	4.67	15.94	15.08
K3Y	1.34	0.30	0.76	1.85	1.36	4.70	22.13	20.28	0.69	4.92	17.46	15.61
K3Z	60.84	6.52	1.00	31.90	5.65	8.87	78.66	46.76	6.74	10.29	78.26	46.36
K4X	106.60	7.93	1.00	84.40	9.19	12.07	145.74	61.34	10.64	11.50	#####	16.40
K5X	27.20	4.77	1.00	35.37	5.95	6.51	42.43	7.06	7.10	8.77	55.16	19.79
K5Y	2.58	1.05	0.85	14.97	3.87	4.79	22.95	7.98	4.51	5.56	21.91	6.94
K5Z	0.10	-1.86	0.04	4.71	2.17	4.62	21.31	16.61	2.06	3.05	7.98	3.28
K6X	0.86	-0.15	0.67	5.90	2.43	4.67	21.81	15.92	2.46	4.53	15.08	9.18
K6Y	4.79	1.85	0.99	33.69	5.80	4.94	24.45	-9.24	6.93	6.26	27.50	-6.19
K6Z	8.25	2.65	1.00	20.02	4.47	5.19	26.91	6.89	5.30	6.95	33.88	13.87

KAX	3.74	1.52	0.98	30.74	5.54	4.87	23.73	-7.01	6.62	5.97	25.08	-5.66
KAY	2.34	0.93	0.85	59.41	7.71	4.77	22.79	-36.62	9.08	5.46	21.18	-38.23
KBX	9.77	2.92	1.00	82.88	9.10	5.29	28.03	-54.85	10.55	7.18	36.23	-46.64
KBY	70.64	6.88	1.00	72.29	8.50	9.55	91.30	19.01	9.93	10.60	83.66	11.37
KBZ	9.68	2.91	1.00	45.45	6.74	5.29	27.96	-17.50	8.01	7.17	36.09	-9.36
KCX	12.51	3.33	1.00	58.81	7.67	5.49	30.09	-28.72	9.03	7.53	39.99	-18.82
KCY	15.55	3.71	1.00	31.02	5.57	5.70	32.47	1.45	6.65	7.86	43.69	12.67
KCZ	3.54	1.45	0.97	30.66	5.54	4.86	23.60	-7.07	6.61	5.91	24.58	-6.08
L3X	7.95	2.60	1.00	20.00	4.47	5.17	26.69	6.69	5.30	6.90	33.41	13.41
L3Y	0.76	-0.26	0.48	10.16	3.19	4.66	21.75	11.58	3.58	4.43	14.52	4.36
L3Z	4.14	1.66	1.00	15.13	3.89	4.90	24.01	8.88	4.54	6.09	26.05	10.92
L4Z	6.82	2.37	0.99	31.65	5.63	5.09	25.88	-5.76	6.72	6.70	31.48	-0.16
L5X	29.70	4.94	1.00	136.14	11.67	6.69	44.74	-91.40	13.10	8.92	57.26	-78.88
L5Y	32.27	5.12	1.00	60.43	7.77	6.87	47.19	-13.24	9.15	9.07	59.33	-1.09
L5Z	3.08	1.27	0.97	43.44	6.59	4.83	23.28	-20.15	7.84	5.75	23.36	-20.08
L6Y	1.30	0.27	0.70	30.85	5.55	4.70	22.10	-8.75	6.63	4.89	17.29	-13.55
LAX	5.05	1.93	1.00	17.21	4.15	4.96	24.63	7.43	4.88	6.32	28.06	10.85
LAY	8.23	2.65	1.00	31.10	5.58	5.19	26.89	-4.21	6.66	6.94	33.85	2.75
LBX	5.59	2.07	1.00	27.41	5.24	5.00	25.02	-2.39	6.25	6.45	29.17	1.76
LBY	0.58	-0.52	0.48	27.25	5.22	4.65	21.63	-5.62	6.23	4.21	13.28	-13.97
LBZ	0.30	-1.06	0.28	13.62	3.69	4.63	21.45	7.83	4.27	3.74	10.94	-2.68
LCZ	1.32	0.29	0.54	2.41	1.55	4.70	22.11	19.71	1.03	4.90	17.38	14.98

APPENDIX F Deviation assessment for decadal data

Date	EstR	Act.rain	ErrActu	AbsRes	Err Ratio
H3Y	21.82	14.23	1.78	7.59	4.27
H3Z	49.70	31.52	5.76	18.18	3.16
H4X	29.09	29.70	4.77	0.61	0.13
H4Y	29.13	22.06	2.66	7.08	2.66
H4Z	55.02	96.06	3.66	41.04	11.21
H5X	21.84	38.86	5.66	17.02	3.01
H5Y	20.77	31.72	6.37	10.95	1.72
H5Z	13.54	41.28	7.80	27.73	3.56
H6X	31.28	26.42	4.90	4.86	0.99
H6Y	31.57	52.38	5.09	20.81	4.09
H6Z	30.23	21.38	2.26	8.85	3.92
HAZ	18.14	36.66	3.58	18.52	5.17
HBX	40.19	70.99	6.48	30.81	4.76
HBY	36.19	60.90	5.85	24.71	4.22
HBZ	36.48	42.99	5.33	6.52	1.22
HCX	19.32	22.30	5.98	2.98	0.50
HCZ	7.94	3.54	0.97	4.41	4.57
I3X	58.30	59.99	7.17	1.70	0.24
I5X	28.55	47.61	5.75	19.07	3.31
I5Y	38.72	29.68	6.18	9.04	1.46
I5Z	19.01	15.78	3.73	3.23	0.87
I6Y	29.80	30.61	5.32	0.81	0.15
I6Z	17.62	31.33	5.00	13.71	2.74
IBX	13.13	28.99	8.68	15.85	1.83
IBY	30.36	50.49	6.66	20.14	3.02
IBZ	28.12	11.24	1.43	16.87	11.80
ICX	8.52	11.51	5.92	3.00	0.51
ICY	21.05	22.64	2.27	1.60	0.70
ICZ	16.82	9.64	4.20	7.18	1.71
J3X	26.71	7.89	1.71	18.82	10.98
J3Y	24.13	20.45	2.73	3.67	1.34
J3Z	60.66	54.95	7.88	5.70	0.72
J4Z	12.33	8.07	2.20	4.26	1.94
J5X	25.98	13.73	2.77	12.25	4.43
J5Y	37.39	45.10	5.69	7.71	1.35
J5Z	14.47	22.42	3.93	7.96	2.03
J6X	27.50	73.63	6.25	46.13	7.38
J6Y	39.45	36.01	6.11	3.44	0.56
JAX	30.18	12.30	1.99	17.88	9.01
JAY	18.07	21.81	5.17	3.74	0.72
JAZ	13.14	21.40	4.28	8.27	1.93
JBX	28.69	23.91	2.34	4.78	2.04
JBY	9.14	8.96	4.05	0.18	0.04
JBZ	31.55	43.08	4.76	11.53	2.42
JCX	17.94	15.39	5.92	2.55	0.43
JCY	15.23	7.53	2.27	7.70	3.39
JCZ	14.11	8.18	4.20	5.93	1.41
K3X	15.94	0.86	0.58	15.08	26.04
K3Y	17.46	1.85	0.93	15.61	16.73
K3Z	77.59	31.90	5.96	45.70	7.66
K4X	99.69	84.40	10.04	15.29	1.52
K5X	54.85	35.37	4.36	19.49	4.47
K5Y	21.90	14.97	3.28	6.93	2.11
K5Z	7.96	4.71	1.76	3.26	1.85
K6X	15.08	5.90	2.16	9.18	4.25
K6Y	27.46	33.69	5.75	6.23	1.08
K6Z	33.81	20.02	1.98	13.79	6.96
KAX	25.06	30.74	4.31	5.68	1.32
KAY	21.17	59.41	7.66	38.24	4.99
KBX	36.14	82.88	8.55	46.74	5.47
KBY	82.89	72.29	6.24	10.60	1.70
KBZ	36.00	45.45	3.32	9.46	2.85
KCX	39.86	58.81	3.39	18.95	5.59

KCY	43.52	31.02	5.86	12.50	2.13
KCZ	24.56	30.66	3.37	6.10	1.81
L3X	33.34	20.00	3.60	13.34	3.70
L3Y	14.52	10.16	2.26	4.35	1.93
L3Z	26.03	15.13	3.28	10.89	3.32
L4Z	31.42	31.65	6.39	0.22	0.04
L5X	56.93	136.14	13.60	79.21	5.82
L5Y	58.97	60.43	7.60	1.46	0.19
L5Z	23.34	43.44	4.59	20.09	4.38
L6Y	17.29	30.85	6.40	13.55	2.12
LAX	28.02	17.21	5.45	10.81	1.98
LAY	33.78	31.10	4.73	2.67	0.57
LBX	29.13	27.41	4.36	1.72	0.39
LBY	13.27	27.25	3.88	13.97	3.60
LBZ	10.93	13.62	3.46	2.69	0.78
LCZ	17.38	2.41	1.07	14.97	13.98

APPENDIX G Comparison of kriged rainfall estimate with arthemetic mean and Thiessen polygon method

Dekade	CCD30	Kriging	Thiessen	Arthemetic
J3X	4.443	8.777	7.798	9.753
J3Y	3.369	20.299	21.031	20.024
J3Z	34.481	54.578	51.210	54.959
K3X	1.019	0.777	1.582	1.018
K3Y	1.339	1.320	1.264	1.812
K3Z	60.840	32.994	31.199	29.100
L3X	7.953	25.193	18.925	20.659
L3Y	0.764	10.976	9.737	9.947
L3Z	4.142	20.705	12.600	14.241
J4Z	0.452	8.361	9.601	7.824
K4X	106.604	86.868	86.305	86.324
L4Z	6.824	35.803	33.002	30.241
K5X	27.198	36.797	35.999	35.741
K5Y	2.575	19.386	15.129	14.265
K5Z	0.095	4.496	4.012	5.535
L5X	29.698	129.795	128.966	126.465
L5Y	32.274	59.127	60.147	54.635
L5Z	3.076	45.462	47.844	42.041
H6X	6.745	25.041	26.749	23.594
H6Y	6.908	46.619	55.041	48.112
H6Z	6.170	22.808	24.266	21.194
JAX	6.142	11.123	13.115	10.941
JAY	1.482	20.131	22.196	20.741
JAZ	0.557	21.757	27.084	22.529
KAX	3.736	32.642	29.925	33.806
KAY	2.340	60.458	55.621	61.641
IBX	0.556	28.515	27.913	31.171
IBY	6.236	50.024	51.141	49.676
IBZ	5.094	13.394	11.419	11.100
JBX	5.377	24.904	24.814	21.359
JBY	0.160	10.263	6.734	10.065
KBX	9.774	86.432	81.420	81.859
KBY	70.642	72.403	73.681	77.235
KBZ	9.679	47.822	47.803	47.882

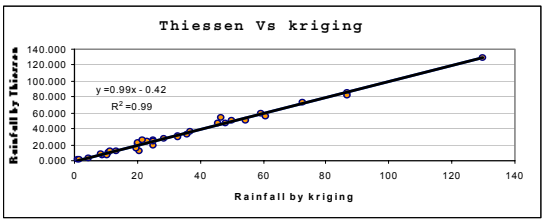

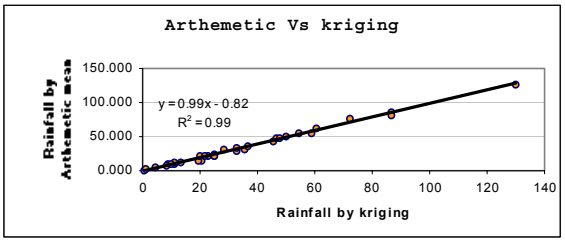

APPENDIX H Pixel calibration for decadal data

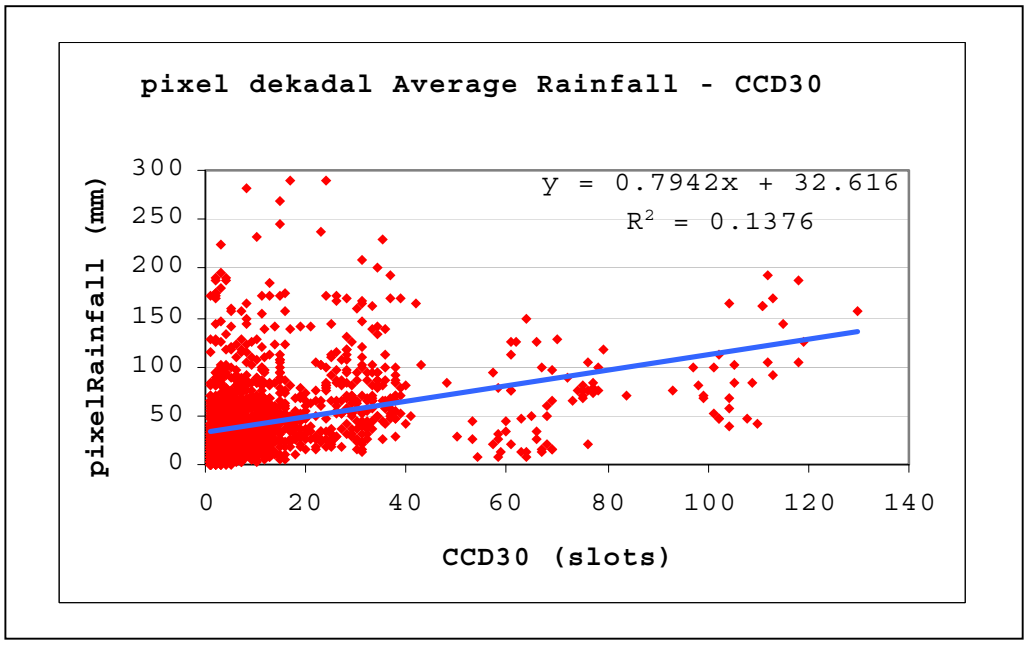

pixel calibration for the dekadal data.

APPENDIX I Annual rainfall and altitude relationship

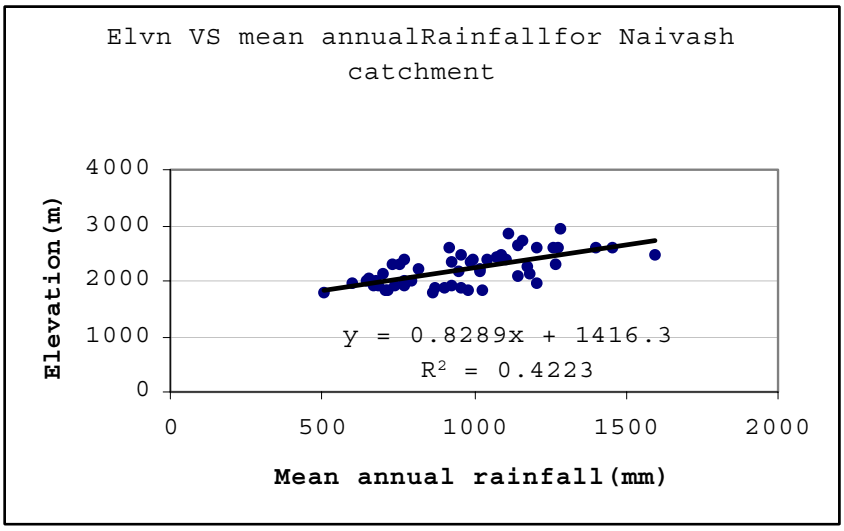

Graph,which shows the relation between elevation and mean annual rainfall for Naivasha catchment (source: thesis report by Kwacha).

APENDIX J Listing of the program

Windowing:

AWK.

```
BEGIN{
REGION = "Na"
MET_COORDS = "-565 1378 -309 1122"
LL_COORDS  = "32 5 42 -5"
}
{
af_file = substr($1,1,8)
metfile = REGION substr(af_file,3,6)
llfile  = substr(metfile,1,4) "l" substr(metfile,6,3)
print "c:\\idrisi\\window x", af_file, metfile, "2", MET_COORDS
print "c:\\bin\\met2ll", metfile, "templl 0.05"
print "c:\\idrisi\\window x templl", llfile, "2", LL_COORDS
print "del templl.*"
print ""
}
```

bat

```
dir %1.img /on/b > list.txt
c:\bin\gawk -fmyprog.awk list.txt > job.bat
call job.bat
del job.bat
del list.txt
```

Unzip file

AWK

```
BEGIN{
        REGION = "Na"
        MET_COORDS = "-565 1378 -309 1122"
        LL_COORDS  = "32 5 42 -5"
        ZIPDRIVE   = "c:\\"
}
{
#       this program
        af_file = substr($1,1,3) "3" substr($1,5,4)
        metfile = REGION substr(af_file,3,6)
        llfile  = substr(metfile,1,4) "l" substr(metfile,6,3)
        print "c:\\bin\\pkunzip", ZIPDRIVE $1, af_file".*"
        print "c:\\idrisi\\window x", af_file, metfile, "2", MET_COORDS
        print "c:\\bin\\met2ll", metfile, "templl 0.05"
        print "c:\\idrisi\\window x templl", llfile, "2", LL_COORDS
        print "del", af_file".*"
        print "del templl.*"
        print ""
}
```

bat

```
rem dir %1.zip /on/b > list.txt
```

```
c:\bin\gawk -fafzip2ll.awk list.txt > jobwin.bat
call jobwin.bat
del jobwin.bat
del list.txt
```

Spliting the data

Splitds.awk

```
# AWK script to split a table file in "row-date/column-station" format into
# as many individual time step files as exist. The output name is derived
# from the rwo header which is a date in DD/MM/YY
BEGIN{
        EXT    = ".TXT"
        NHEAD  = 1      # Number of row headers, usually 1
                        # First data column is (NHEAD+1)th column.
}
{
        if (NR==1){
                nstatn = $1     # first row of file has this quantity
                region = substr(FILENAME,1,2)
                param  = substr(FILENAME,3,2)
       geog   = substr(FILENAME,5,1)
        }
        else if (NR == 2){
                for (i = 1; i <= nstatn+NHEAD; i++) id[i] = $i
        }
        else if (NR == 3){
                for (i = 1; i <= nstatn+NHEAD; i++) lon[i] = $i
        }
        else if (NR == 4){
                for (i = 1; i <= nstatn+NHEAD; i++) lat[i] = $i
        }
        else{
                DATE = ZAMIS_date($1)
            outfile = region param geog DATE EXT
                print "1", nstatn > outfile
                for (i = 1; i <= nstatn+NHEAD; i++){
                        print id[i], "   ", lon[i], "   ", lat[i], "  ", $i  >> outfile
                }
                print "generated file", outfile
        }

}
```

```
function ZAMIS_date(date){
        # date is in the date format DD/MM/YY
        # alphabetic date code
        date_code = "123456789ABCDEFGHIJKLMNOPQRSTUVWXYZ"

        # extraction of year - subtract 77 from year so 87=10, 88=11, ...
        # then retrieve the year code from the date code string
        yy    = substr(date,7,2) - 77
        year  = substr(date_code,yy,1)

        # extraction of month - subtract 0 for MM to become a number (1-12)
        # then retrieve the month code from the date code string
        mm    = substr(date,4,2) - 0
        month = substr(date_code,mm,1)

        # extraction of day - subtract 0 for DD to become a number (1-31)
        # then retrieve the day code from the date code string
        dd    = substr(date,1,2) - 0
        day   = substr(date_code,dd,1)

        zamis_date = year month day
        return zamis_date
}
```

Splitds.bat

```
@echo off
rem Runs the table splitting awk script. Output files generated within the script
\bin\gawk -fsplitds.awk %1
```

Variogram Derivation:

glsvario.bat

```
rem NOTE  :  Amend the data table name and the vario .dat files before using !!!!!
rem runs VARIOT to derive the experimental variogram
\bin\variot -s -t -z Nargp0%31.txt %2 > vg_%3%2.txt

rem converts to format used by EP GLS program AVAMCP
\bin\gawk -fvg2ls.awk vg_%3%2.txt > vtemp
rem prepares input file to AVAMCP and runs it
echo vtemp > infile
echo %1 >> infile
echo 1 >> infile
echo 1 >> infile
echo 2 >> infile
echo coeff1 >> infile
```

```
echo coeff2 >> infile
\bin\avamcp < infile
del infile
rem converts the output coefficient file from AVAMCP into
rem TAMSAT standard variogram coefficients format
\bin\gawk -fgls2dat.awk coeff2 >  Navcl0%31.dat
rem clean up
del vtemp
del coeff1
del coeff2
```

Kriging (KRIGOPOL):

AWK

```
BEGIN {
        area = "Namask"
        output = "krig.txt"
}
{
        Rfile = $1
        region = substr(Rfile,1,2)
        month = substr(Rfile,7,1)
        if (NR==1) to = "> "
       else       to = ">>"
        varfile = region "vcl0" month "1.dat"
        print "c:\\bin\\krigopol",Rfile,varfile,area,to,output
}
```

bat

```
@echo off
dir %1.txt /on/b > kr.txt
c:\bin\gawk -fkrig1.awk kr.txt > assign.bat
call assign.bat
rem  del assign.bat
rem  del kr.txt
```

Merging of satellite and gauge data (GET_STN):

AWK

```
BEGIN{  PATH = "c:\\bin\\"
        height = "8"
        output = "stn.txt"
}
{
      gauge = $1
```

```
        ccd = substr(gauge,1,2) "c3M" substr(gauge,6,3)
       if(NR==1) to = ">"
       else      to = ">>"
      print PATH"get_stn -m -p", height, gauge, ccd, to, output
}
```

bat

```
@echo off
dir %1.txt /on/b > mes.txt
c:\bin\gawk -fgetstn.awk mes.txt > jobstn.bat
call jobstn.bat
del jobstn.bat
del mes.txt
Where :
-m   convert the rain gauge stn (lon, lat) to meteosat co-ordinate
-p   parallax correction
 8   is height of cloud in parallax correction
```

Derivation average CCD over the catchment (MEANPOL)

AWK

```
BEGIN{
        PATH  = "c:\\bin\\"
        mask  = "Namask2"
        thresh["a"] = 0
        thresh["b"] = 0
        thresh["c"] = 0
        thresh["3"] = 1
        thresh["4"] = 0
        thresh["5"] = 0
        thresh["6"] = 0
        if (output == "") output  = "outmpol"
        output = output ".txt"
}
{
        image = substr($1,1,8)
        month = tolower(substr(image,7,1))
          t   = thresh[month]
        if (NR==1) to = "> "
        else       to = ">>"
        print PATH"meanpol -x", t, mask, image, to, output
}
```

bat

```
@echo off
```

```
rem USAGE : MEANPOL IMGSPEC OUTPUT
rem where OUTPUT is the name of the output text file
dir %1.img /on/b > datalist
\bin\gawk -fmeanpolk.awk -voutput=%2 datalist > jobmean.bat
call jobmean.bat
del  jobmean.bat
del datalist
```

APPENDIX K Naming convention for files (data+image)

1.The file should have eight characters and three-file extension (idrisi extension)

2.The characters should be in the form of RRTTGYMT.

Where: RR: Region code
TT: Type codes (data type)
G: Geography code
YMT: Date code (Y=year, M=month and T= time step)

For the year the METEOSAT data archive starts at 1987, it is agreed to have:

Year	87	88	89	90	91	92	93	94	95	96	97	98	99	2000
Code	A	B	C	D	E	F	G	H	I	J	K	L	M	N

Month

Month	Jan	Feb	March	Apr	May	June	July	Aug	Sept	Oct	Nov	Dec
Code	1	2	3	4	5	6	7	8	9	A	B	C

Decade

Decade	First decade	Second decade	Third decade
Code	X	Y	Z

Time step (day)

Day	1	2	3	4	5	6	7	8	9	10	11	12	13	14	15	16	17	18	19	20	21	22	23	24	25	26	27	28	29	30	31
Code	1	2	3	4	5	6	7	8	9	A	B	C	D	E	F	G	H	I	J	K	L	M	N	O	P	Q	R	S	T	U	V

APPENDIX L File locations

The following table refers to the location of file used in the report.

Data type	Data location	Description
CCD images	C:\Kenya\Data\kec3l	CCD images with threshold -30°C (Latitude-Longitude coordinate
	C:\Kenya\Data\kec3t	CCD images with threshold -30°C (METEOSAT coordinate)
	C:\Kenya\Data\kec4l	CCD images with threshold -40°C (Latitude-Longitude coordinate
	C:\Kenya\Data\kec4t	CCD images with threshold -40°C (METEOSAT coordinate)
Rain gauge data	C:\Kenya\Data\Kergp	Rain gauge station location and row data
XLS data	C:\Kenya\Result\Daily	Data arrangement, variogram derivation,calibaeration plot,regression and deviation assessement
	C:\Kenya\Result\dekadal	Data arrangement, variogram derivation,calibaeration plot, regression pixel caliberation, deviation assessement and comparison of CCD to Thiessen polygon and arthemetic mean.
	C:\Kenya\Result\Comparison	Discharge row data and Discharge Response to event CCD and kriged rainfal
Program file	C:\bin	All the program that are used in this thesis
Word document	C:\Kenya\Document	Thesis reporat
ILWIS image	C:\Kenya\Process	Selected CCD image imported from IDRISI to evaluate discharge response
IDRISI Mask Image	C:\Kenya\Process	Mask image of Naivasha and Malewa which are used for kriging and determination of average CCD over the catchment